UNIVERSITY OF COPENHAGEN

Universität für Bodenkultur Wien
University of Natural Resources and Life Sciences, Vienna

GLOF hazard associated with glacier retreat in the Cordillera Blanca, Peru: a case study on Laguna 513

Master thesis:

Celia Sancho de Pablo

EnvEuro MSc programme in Environmental Science

Main supervisor: Herbert Formayer, Assoc. Prof. Mag. Dr. (*Universität für Bodenkultur Wien, BOKU*)

Co-supervisor: Daniel Ortiz Gonzalo, Postdoc and Lecturer (*Københavns Universitet, KU*)

External co-supervisor: José Úbeda Palenque, Assoc. Prof. Dr. (*Universidad Complutense de Madrid, UCM*)

Affidavit - Declaration of Authorship

I, Celia Sancho de Pablo, hereby declare that I am the sole author of this work. No assistance other than that permitted has been used and all quotes and concepts taken from unpublished sources, published literature or the internet in wording or in basic content have been identified with precise source citations.

Celia Sancho

Date: 17/05/2021

Signature: Celia Sancho de Pablo

Table of contents:

LIST OF FIGURES

LIST OF TABLES

ABSTRACT

ENGLISH

High-mountain environments with snow and ice are particularly sensitive to climatic changes, especially in the tropics. Glacier hazards threaten societies in mountain regions worldwide. Of special concern are cascading mass movement processes impacting glacier lakes and triggering glacier lake outburst floods (GLOFs). The Cordillera Blanca in the Peruvian Andes is the most glaciated mountain range in the tropics. The risk of GLOFs from lakes that have formed at the base of retreating glaciers is very high in these areas. In this mountain range, the glacier lake Laguna 513 was formed in the late 1960s due to the glacier Cochca retreat and was declared highly dangerous in 1988. This study includes an analysis of the glacier Cochca evolution from 1962 to 2015, a research of the climate on the study area including the past data trends, spatial variability, correlation of the temperature with ENSO phenomenon and projections of future climate trends under different scenarios. The work also incorporates simulations of a scenario of a GLOF from the glacier Cochca into the lake Laguna 513 that affects the city of Carhuaz, through the tools *r.avaflow*® and *ArcGIS*®. The study concludes that the glacier Cochca retreated during the studied period and according to future temperature trends, it is expected to continue retreating; the climate in the area is determined by a strong seasonal variation in precipitation with the rainy season in southern hemisphere summer and reduced seasonal temperature variability; a warming is expected in the area according to regional climate scenarios and precipitation is predicted to increase too, especially during the rainy season. And as a final conclusion according to the *r.avaflow*® simulation performed, if a GLOF event of the studied dimensions happens, the event would take a short time to reach the city of Carhuaz and would pose a high risk for the population downstream.

GERMAN

Vergletscherte Hochgebirgsregionen reagieren besonders empfindlich auf Klimaveränderungen, ganz besonders in den Tropen. Durch Gletscher induzierte Naturkatastrophen bedrohen weltweit Siedlungsräume in Gebirgsregionen. Von besonderer Bedeutung sind hierbei kaskadische Sturzprozesse in Verbindung mit Gletscherseen, welche Seeausbrüche „glacier lake ourburst floods“ (GLOFs) verursachen. Das Risiko von GLOFs in neu entstandenen Gletscherseen an den Zungen sich zurückziehender Gletscher ist besonders hoch. In einem derartigen Rückzugsgebiet des Gletscher Cochca hat sich der Gletschersee Laguna 513 in den späten 1960er Jahren gebildet und 1988 wurde er als extrem gefährlich eingestuft. Diese Studie beinhaltet eine Analyse der Entwicklung des Gletscher Cochca von 1962 bis 2015, eine Untersuchung des Klimas der Region einschließlich historischer Trends, räumlicher Variabilität, dem Zusammenhang zwischen der regionalen Temperaturanomalie und dem ENSO – Phänomen, sowie Klimaszenarien basierend auf verschiedene Emissionsszenarien. Die Arbeit beinhaltet die Modellierung eines GLOFs des Gletschers Cochca am Gletschersee Laguna 513, welche die Stadt Carhuaz erreicht. Hierzu wurden die Programme r.avaflow® und ArcGIS® verwendet.

Die Studie ergab, dass der Glescher Cochca während der Untersuchungsperiode weiter zurückgeschmolzen ist und aufgrund der fortschreitenden Erwärmung sich auch in Zukunft weiter zurückziehen wird. Das lokale Klima ist von einer hohen saisonalen Variabilität im Niederschlag geprägt mit einer Regenzeit im südhemisphärischen Sommer, während der eine reduzierte Temperaturvariabilität auftritt. Die regionalen Klimaszenarien zeigen einen weiteren

Anstieg der Temperatur, sowie eine Zunahme der Niederschläge, speziell während der Regenzeit. Die Ergebnisse der *r.avaflow*® Modellierung eines GLOF Ereignisses zeigen, dass die Flutwelle die Stadt Carhuaz erreichen würde und auch die Bevölkerung in weiter stromabwärts gelegenen Regionen noch betroffen wären.

SPANISH

Los ecosistemas de alta montaña con nieve y hielo son particularmente sensibles a los cambios climáticos, especialmente en los trópicos. Los riesgos de los glaciares amenazan a las sociedades de las regiones montañosas de todo el mundo. De especial preocupación son los procesos de movimiento masivo en cascada que impactan los lagos glaciares y provocan inundaciones repentinas de lagos glaciares (GLOF en inglés). La Cordillera Blanca en los Andes peruanos es la cadena montañosa con más glaciares de los trópicos. El riesgo de GLOF de los lagos que se han formado en la base de los glaciares en retroceso es muy alto en estas áreas. En esta cordillera, el lago glaciar Laguna 513 se formó a fines de la década de 1960 debido al retroceso del glaciar Cochca y fue declarado altamente peligroso en 1988. Este estudio incluye un análisis de la evolución del glaciar Cochca de 1962 a 2015, una investigación del clima en el área de estudio, incluidas las tendencias de datos pasadas, la variabilidad espacial, la correlación de la temperatura con el fenómeno ENOS y las proyecciones de las tendencias climáticas futuras en diferentes escenarios. El trabajo también incorpora simulaciones de un escenario de un GLOF desde el glaciar Cochca hasta la Laguna 513 que afecta a la ciudad de Carhuaz, a través de las herramientas r.avaflow® y ArcGIS®. El estudio concluye que el glaciar Cochca retrocedió durante el período estudiado y de acuerdo con las tendencias futuras de temperatura, se espera que continúe retrocediendo; el clima de la zona está determinado por una fuerte variación estacional de las precipitaciones con temporada de lluvias en el verano del hemisferio sur y una escasa variabilidad estacional de temperatura; se espera un calentamiento en el área de acuerdo con los escenarios climáticos regionales y también se prevé un aumento de las precipitaciones durante la temporada de lluvias. Y como conclusión final de acuerdo con la simulación r.avaflow® realizada, si ocurre un evento GLOF de las dimensiones estudiadas, el evento tardaría poco tiempo en llegar a la ciudad de Carhuaz y supondría un alto riesgo para la población aguas abajo.

1 INTRODUCTION AND OBJECTIVES

Glacier lake outburst floods (GLOFs) are frequently a cascading mass movement processes that start by avalanches impacting on a glacier lake that end up triggering a significant inundation and destruction downstream. The risk of GLOFs from lakes that have formed at the base of retreating glaciers in high mountain areas, like the Cordillera Blanca in Peru, is very high. Cordillera Blanca is the most glaciated mountain range in the tropics and has been the scene of rapid deglaciation for many decades. High-mountain environments with snow and ice are particularly sensitive to climatic changes, especially in the tropics, and there is an increasing scientific and policy interest in detecting the climate change impacts on these natural areas.

The introduction of this master thesis provides some background information on the topic. It presents general information about effects of climate change on the cryosphere, also about climatic patterns as El Niño, that influence the climate of the study area. Other significant topics are GLOFs, glaciers and glacier lakes. Specific information about the study area - the Peruvian Andes, the Cordillera Blanca, glacier lake Laguna 513 and the city of Carhuaz - is also provided. It includes its history and past events, the risk management and the population relationship with glaciers, as various populations are established in these areas due to the strong dependency on water resources from glacier melt because the pronounced dry season on the area. This section also includes the objectives and hypothesis of this master thesis, the main studies on which it is focused and the justification of the chosen software.

1.1 CLIMATE CHANGE AND THE CRYOSPHERE IN THE TROPICS

1.1.1 Climate change effects on the cryosphere

Climate change is affecting and will affect the cryosphere in the high mountain areas and more specifically the glaciers and glacier lakes (Hock *et al.*, 2019).

According to the Chapter 2 “High Mountain Areas” of the Intergovernmental Panel on Climate Change (IPCC) Special Report on “the Ocean and Cryosphere in a Changing Climate” (2019), there is high confidence that snow cover, glaciers and permafrost are projected to remain decreasing in size in almost all regions during the 21st century. There is also high confidence that the number and extent of glacier lakes will continue to increase in most regions in the near-term decades, and new lakes will develop in areas that are closer to steep and potentially unstable mountain walls where lake outbursts can be more easily triggered by the impact of landslides and ice avalanches.

Observations with satellites and in situ of changes in area, length and mass of glaciers demonstrate a globally largely coherent picture of mountain glacier recession in the last decades (Zemp *et al.*, 2015), although with very high confidence the annual and regional variability is large (Hock *et al.*, 2019).

1.1.2 Climate change effects on the tropics

On decadal and longer timescales, climate models predict that greenhouse-gas-forced warming will drive temperatures to rise faster at higher elevations and that this vertical amplification will be greatest in the tropics due to upper-tropospheric humidity and water-vapor feedback (David A. Randall, 2007; IPCC, 2007). Data from general circulation models (GCMs) indicate that the mixed water-vapor/lapse-rate feedback provides the biggest positive radiative feedback and that by itself it almost doubles the warming in response to forcing by greenhouse-gas increases. As a result, the projected changes in mean annual free-air temperatures show twice as much warming at higher elevations in the tropics as is predicted at the Earth's surface (Bradley *et al.*, 2006; Thompson *et al.*, 2011). Moreover, some high-elevation tropical glaciers seem to be already responding to these higher temperatures, which may explain the accelerating rate of glacier loss at some of these locations (Coudrain *et al.*, 2005; Thompson *et al.*, 2006, 2011).

As these processes occur and snow is removed, the less reflective exposed glacier ice melts. Once ongoing, melting requires 7.5 times less energy than sublimation. As the ice disappears and more of the darker land surface is exposed, absorption of the intense higher-elevation radiation increases, and therefore the changes happening get accelerated through positive feedbacks (Bradley *et al.*, 2006; Thompson *et al.*, 2011). These projections are consistent with the recently documented ascent of the freezing level height (FLH) in the tropical atmosphere (the free-air 0°C isotherm) across the tropics and a warming trend of ~0.1°C per decade over the last 50 years based on high-elevation surface temperatures and upper-air data (Bradley *et al.*, 2009).

1.1.3 Climate change effects on freshwater availability

The mountain cryosphere is an important source of freshwater in the mountains and the downstream regions. Fluctuations in the cryosphere due to climate change can alter freshwater availability and will have direct consequences for human populations and ecosystems. Glaciers supply water that supports human communities both close and far away from the glacier, for example, for agriculture or drinking water (Hock *et al.*, 2019).

The rising temperatures due to climate change cause mountain glaciers to melt and change the water availability. At the beginning, as glaciers melt faster and shrink in response to a warmer climate, water is released from long-term glacial storages and more water runs downhill from the glacier. Though, there will be a turning point after several years or decades, often called 'peak water' (Figure 1), after which glacier runoff, and as a consequence its contribution to river flow downstream, will decline. Peak water runoff from glaciers can exceed the amount of initial yearly runoff by 50% or more. After the turning point, this additional water decreases gradually as the glacier continues to shrink, and eventually stops when the glacier has disappeared or retreated to higher elevations where the temperatures are low enough to maintain the glacier. As a result, communities, farms, villages and cities downstream lose this valuable water source. The total amounts of river runoffs will then mainly depend on rainfall, snowmelt, ground water and evaporation (Hock *et al.*, 2019).

Moreover, glacier decline can alter the timing in the year and day when most water is available in the rivers that collect water from glaciers. In mid or high latitudes, glacier runoff is highest in the summer, when the glacier ice remains melting after the disappearance of the winter snow, and highest during the day when air temperature and solar radiation are at their maxima (Figure 1). As peak water happens, more intense glacier melt rates also increase the daily runoff maxima considerably. In tropical areas, such as parts of the Andes, the seasonal air temperature variations are minor, and the variations between wet and dry seasons are the foremost control on the amount and timing of glacier runoff throughout the year. The effects of glaciers on river runoff further downstream depend on the distance from the glacier. Close to the glaciers (e.g., within several kilometres), initial increases in yearly glacier runoff until peak water followed by decreases can affect water supply considerably, and larger peaks in daily runoff from the glaciers can cause floods (Hock *et al.*, 2019).

Further from the glaciers the impact of glacier shrinkage on total river runoff have a tendency to become minor or negligible. Nevertheless, the melt water from glaciers in the mountains can be a significant source of water in hot and dry years or seasons when river runoff would otherwise be low. For the same reason it will reduce variability in total river runoff from year to year, even in areas located hundreds of kilometres away from the glaciers. Additional components of the water cycle such as rainfall, evaporation, groundwater and snowmelt can either compensate or strengthen the effects of changes in glacier runoff as the climate changes (Hock *et al.*, 2019).

In Figure 1 three different time scales are shown: annual runoff from the entire basin during a decade (upper panel); runoff variations over one year (middle panel) and variations during a sunny and a rainy summer day (lower panel). Note that seasonal and daily runoff variations are different before, during and after the peak water flow. The glacier's initial negative annual mass budget becomes more negative over time until eventually the glacier has completely melted away. Note that this is a simplified figure so permafrost is not addressed specifically and the exact partitioning between the different sources of water will vary between different river basins (Hock *et al.*, 2019).

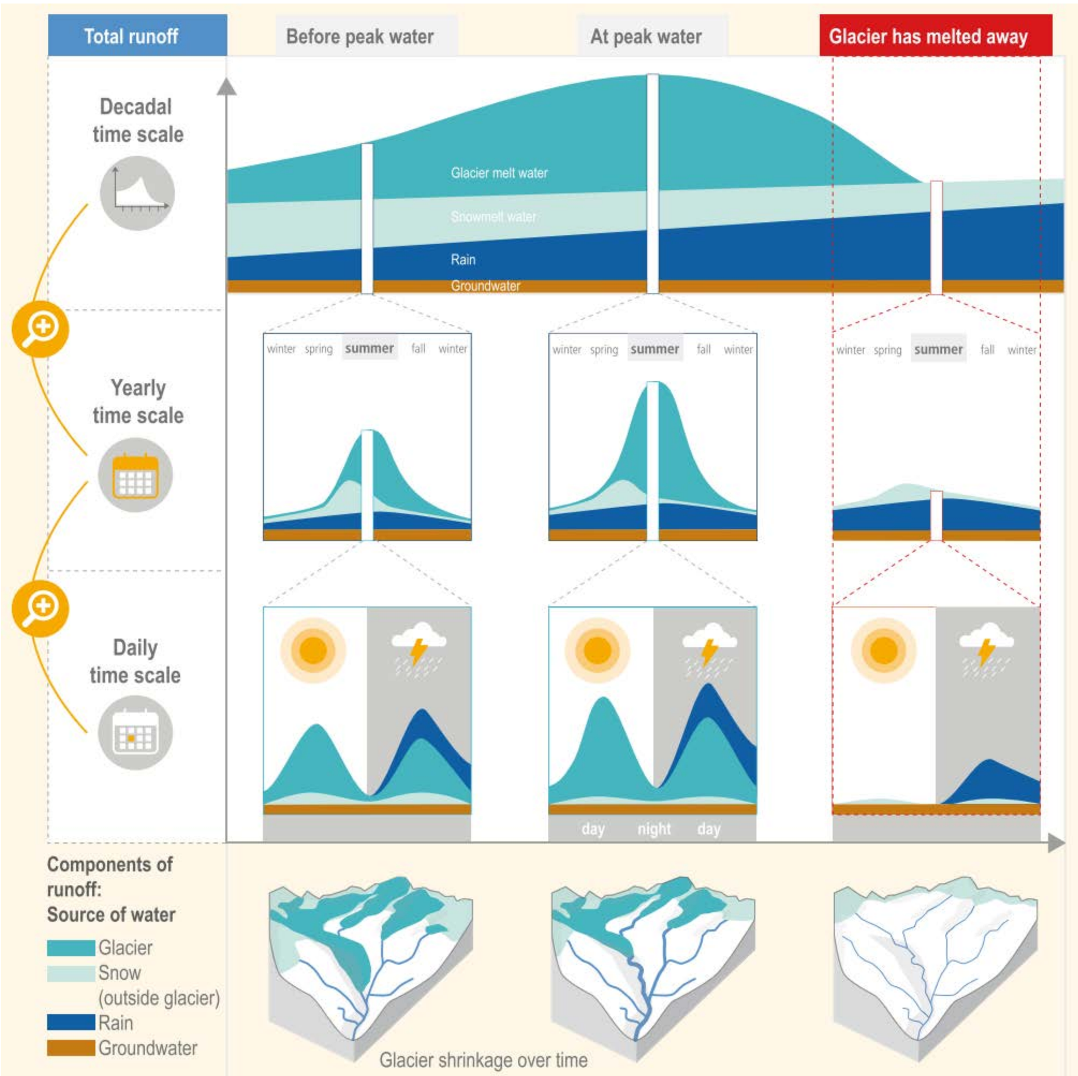

Figure 1. Simplified overview of runoff changes from a river basin with large (e.g., >50%) glacier cover as the glaciers retreat, showing the relative quantities of water from different sources: glaciers, snow (outside the glacier), rainfall and groundwater. (Hock *et al.*, 2019).

1.2 El Niño Southern Oscillation (ENSO) influence

El Niño Southern Oscillation (ENSO) is a naturally occurring fluctuation that originates in the tropical Pacific (Collins *et al.*, 2010). It is one of the most prominent coupled ocean–atmosphere phenomenon, source of seasonal and interannual global climate variability (Trenberth and Caron, 2000; Christie *et al.*, 2009; Wolter and Timlin, 2011). This phenomenon is globally associated with extreme weather conditions such as heavy snowstorms, floods, droughts and tropical cyclone activities. It creates large ecological (Holmgren *et al.*, 2001), social (Bouma *et al.*, 1997) and economic impacts (Chen *et al.*, 2001) worldwide (Christie *et al.*, 2009).

During the past few decades, the study of the ENSO influences on the climate of the tropical Central Andes in South America has become a major issue for the local and international scientific community due to the negative effects of El Niño events on water resources in this region (Vuille *et al.*, 2000; Garreaud and Aceituno, 2001; Francou *et al.*, 2003; Christie *et al.*, 2009). ENSO strongly modulates glacier mass balance, rain and snowfall variability in the Central Andes (Vuille *et al.*, 2000; Francou *et al.*, 2004).

Several studies (Francou *et al.*, 1995, 2003, 2004; Ribstein *et al.*, 1995; Arnaud *et al.*, 2001) of glacier mass balance in the tropics, specifically in the Andes, have proven that ENSO is an important influence. Even though the effect of the current warming trend on the frequency and intensity of future ENSOs is uncertain (Collins *et al.*, 2010), the accelerating retreat of the tropical Andean glaciers is almost certainly linked to the combined effects of the continual warming and the periodic occurrences of El Niño (Thompson *et al.*, 2011).

1.3 Glacier and glacier lakes behaviour studies

The rate at which a glacier responds to climate change is inversely proportional to its size. A large glacier will respond more gradually than a small glacier, taking longer time to shrink in a warmer/drier climate or to grow in a cooler/wetter climate (Thompson *et al.*, 2011).

Tropical glaciers are particularly sensitive to minor changes in ambient temperatures, as they already exist very close to the melting point (Thompson *et al.*, 2011).

Changes in the cryosphere due to climate change have an effect in the frequency and magnitude of hazards, the processes involved, and the locations exposed to the hazards. In general, natural hazards, and the caused disasters, are sporadic by nature, and vulnerability and exposure display geographic disparities. The assessment of risk changes is founded not only on direct evidence, but also on laboratory experiments, theoretical considerations and calculations, and numerical modelling (Hock *et al.*, 2019).

Multiple studies (Haeberli *et al.*, 2011; Emmer and Vilímek, 2013, 2014; Somos-Valenzuela *et al.*, 2016) recommended to evaluate the glacier lake hazards based on systematic and scientific analysis of the following aspects:

- lake type,
- moraine dam characteristics,
- outburst mechanisms,
- down-valley processes,
- possible cascades of processes.

Future changes in climate patterns are likely to increase the frequency of avalanches because of reduced stability of permafrost, bedrock and steep glacier slopes in the mountain glaciers and specifically in Cordillera Blanca, Peru (Fischer *et al.*, 2012; Somos-Valenzuela *et al.*, 2016). With the change in these conditions, avalanches are expected to be a potential trigger of Glacier Lake Outburst Floods (GLOFs) (Emmer and Cochachin, 2013; Emmer and Vilímek, 2013; Somos-Valenzuela *et al.*, 2016)

1.3.1 Lake type classification

Emmer *et al.*(2015) organized the types of lakes into a seven classes system:

(1) Ice-dammed: Embedded on the glacier surface or confined by part of the glacier tongue
(2) Moraine or periglacial debris-dammed
    a. Close to recent glaciers: confined by fresh moraines (younger than Little Ice Age (LIA) - most recent glacier advance peak) which may still contain some ice, glacier till, active rock glaciers or undefined boulder and debris material
    b. Far from recent glaciers: confined by LIA or older moraines or glacier till, inactive/fossil rock glaciers or undefined boulder and debris material
(3) Bedrock-dammed
    a. Close to recent glaciers: confined by a solid rock mass exposed younger than the LIA
    b. Far from recent glaciers: confined by a solid rock mass exposed since the LIA or longer
(4) Landslide-dammed: confined by the deposit of a mass movement such as a rock fall, landslide or debris flow

1.3.2 Temporal analysis

The general life cycle of lakes in high mountains with retreating and advancing glaciers may be divided into three phases: glacier advance, glacial retreat (sub-phases ‘proglacial’ and ‘glacier-detached’) and nonglacial (Emmer *et al.*, 2015, 2016). Firstly, during the glacier advance phase, depressions in bedrock are intensively modelled (over-deepened), massive moraines are built, and ice-dammed lakes occupying tributary valleys blocked by advancing glaciers may form in the main valley. During the initial phase of glacier retreat, the proglacial subphase, new lakes form (the phases of the formation of these lakes are shown in Table 1) in the elevation zone close to the retreating glacier tongues, replacing retreating glacier tongues behind terminal moraines and filling glacially modelled depressions in the bedrock. The overall number of lakes as well as the overall number of lake outburst floods generally increase in this phase (Emmer *et al.*, 2015). During the final phase of glacier retreat, glacier detached subphase, when the majority of glaciers are already melted away, lakes whose catchments are no longer occupied by glaciers may turn into seasonal or endorheic lakes, or may become extinct in a non-catastrophic way as a result of basin filling by sedimentation and/or losing their main source of water. The last phase is a completely deglaciated catchment of the lakes. The areal extent of the lakes (not necessary the volume) in the final phase of glacier retreat suggests that lake extinction represented by lake area reduction is considerably delayed with respect to glacier retreat (Emmer *et al.*, 2015, 2016).

Table 1. Characteristics of the three phases of bedrock-dammed lake evolution. Adapted from (Emmer *et al.*, 2015)

Phase of lake evolution	Typical duration[c]	Lake-glacier interaction	Lake volume	Susceptibility to GLOF	Hazard	Example
Phase I. (Proglacial)	10^0–10^1 years	Lake is in direct contact with glacier	Increasing (lake growth)	Stagnant (high)	Increasing from zero to high	Currently forming proglacial lakes
Phase II. (Glacier-detached)	10^1–10^2 years	Lake is no more in direct contact with the glacier, but part of its catchment is still glacierized	Constant[a]	Decreasing (from high to low)	Decreasing (from high to low)	Lakes in currently deglaciating valleys
Phase III. (Nonglacial)	>10^2 years	Entire lake catchment is completely deglaciated	Constant[a,b]	Stagnant (low)	Stagnant (low)	Lakes in already deglaciated valleys

[a] Lake filling by sediments is not considered here.

[b] Seasonal fluctuation of lake level is not considered here.

[c] The durations are regional settings of Austrian Alps, might differ in the Andes.

1.3.3 Equilibrium-Line Altitude of glaciers

The equilibrium-line altitude (ELA) marks the area or zone on a glacier where accumulation is balanced by ablation over a 1-year period, so it represents the boundary altitude separating the accumulation zone from the ablation zone. The ELA is sensitive to several meteorological factors, such as variations in winter precipitation, summer temperature, and wind transport of dry snow. When the annual net mass balance is negative, the ELA rises, and when the annual net mass balance is positive, the ELA declines. Fluctuations in the ELA result in a change in thickness and the advance or retreat of the glacier and they provide an important indicator of glacier response to climate change (Singh *et al.*, 2011; Nesje, 2014; Zemp *et al.*, 2015).

For the majority of mountain glaciers in the temperate regions of the world, there exists a close linear relationship between the ELA of the glacier and the precipitation and temperature controls on glacier mass. To keep the same ELA elevation on a glacier, it is predicted that roughly 300 mm of supplementary precipitation per degree of warming would be required. Projections from regional climate models in the Alps (Christensen *et al.*, 2002; Singh *et al.*, 2011) propose that warming will provoke an average reduction of annual precipitation, with strong reductions in summer that any local increases in winter will not compensate for. As a consequence, there will be a rapidly glacier retreat until a new equilibrium at much higher elevations is obtained, with substantially reduced volume and surface area and smaller accumulation zone; some may disappear entirely when the deglaciation is complete as the ELA may ultimately end up above the glacier catchment area (David A. Randall, 2007; Singh *et al.*, 2011).

The freezing level height (FLH, also called freezing height or free air 0°C isotherm) has been suggested as an approximation of the ELA of glaciers (Schauwecker *et al.*, 2017).

The FLH is defined as the lowest level in the free atmosphere with a temperature of 0°C. Since melting of solid precipitation starts approximately where air temperature is over 0°C, the FLH during precipitation events is closely related to the snowfall level height (SLH) - also called snow/rain transition height or melting level (Schauwecker *et al.*, 2017).

The SLH is a critical variable in precisely defining mass balance and runoff for tropical glaciers. The SLH is defined as the top of the melting layer during precipitation events, which is the altitude throughout solid precipitation melts as it descends. Consequently, for the research on glaciers, it is decisive to study the seasonal and regional variabilities of the FLH, past and future changes, and how the FLH during precipitation events is linked to the SLH (Schauwecker *et al.*, 2017).

1.4 GLOFs

High-mountain environments with snow and ice are particularly sensitive to climatic changes, especially in the tropics. Glacier hazards threaten societies in mountain regions worldwide. Special concern is cascading mass movement processes: e.g. rock or ice avalanches, impacting glacier lakes and triggering Glacier Lake Outburst Floods (GLOFs) (Schneider *et al.*, 2014; Emmer *et al.*, 2016).

The major mountain disasters in terms of reach, damage and lives lost concerning ice, snow and permafrost happened through a combination or chain or cascades of processes, which includes GLOFs (Evans and Delaney, 2015; Iribarren Anacona *et al.*, 2015; Hock *et al.*, 2019). Glacier-related floods, including GLOFs, are documented for most mountain ranges with glaciers and are part of the most far-reaching glacier hazards. Past events affected areas up to hundreds of kilometres downstream (Carrivick and Tweed, 2016; Hock *et al.*, 2019).

Retreating glaciers produced lakes at their fronts in many high mountain regions in recent decades (Frey *et al.*, 2010; Gardelle *et al.*, 2011; Loriaux and Casassa, 2013). There is high confidence that current global glacier shrinkage caused new lakes to form and existing lakes to grow in most regions, for example in South America (Loriaux and Casassa, 2013; Paul and Mölg, 2014; Zhang *et al.*, 2015; Buckel *et al.*, 2018; Hock *et al.*, 2019).

The risk of GLOFs from lakes that have formed at the base of retreating glaciers is very high in these mountain areas. GLOFs were in many mountain regions and over recent decades documented to have been triggered by impact waves from snow-, ice- or rock-avalanches, landslides, iceberg calving events falling into glacial lakes, initiating a chain of processes that may culminate in significant inundation and destruction in the settlements downstream (Benn *et al.*, 2012; Somos-Valenzuela *et al.*, 2016; Narama *et al.*, 2017; Hock *et al.*, 2019). Additionally, GLOF processes can be negatively affected by a temporary blockage of surface or subsurface drainage channels (Hock *et al.*, 2019).

Comprehensive risk assessments for GLOFs are rare (Allen *et al.*, 2016) and complex because GLOFs are typically the consequence of a cascade of triggering and propagating mass flow processes instead of an individual process (Schneider *et al.*, 2014; Westoby, Glasser, Brasington, *et al.*, 2014; Huggel *et al.*, 2020). Few studies have attempted to simulate an entire GLOF hazard process chain in a single modelling environment, and they generally limit the number of processes considered. For instance, Worni *et al.* (2014) excluded avalanche simulations from their modelling framework. Worni *et al*. (2014) and Westoby, N. F. Glasser, *et al.* (2014) review typical modelling approaches for GLOFs that involve land or ice masses falling into glacial lakes (Somos-Valenzuela *et al.*, 2016). The predominant approach separately simulates individual processes, where different processes are connected by applying the results of one model as the input for the simulation of the subsequent model (Schneider *et al.*, 2014; Westoby, Glasser, Hambrey, *et al.*, 2014; Worni *et al.*, 2014).

To better understand how a GLOF process works, following it is described the typical process chain of a GLOF, it consists of: first, an impulse-wave generated by mass flow of rock or ice impact on a glacier lake, next the moraine dam overtopping and/or breaching, and ultimately the lake emptying and the downstream flood propagation with the inundation of riverine populated areas (Figure 2) (Clague and Evans, 2000; Westoby, Glasser, Brasington, *et al.*, 2014; Worni *et al.*, 2014; Somos-Valenzuela *et al.*, 2016).

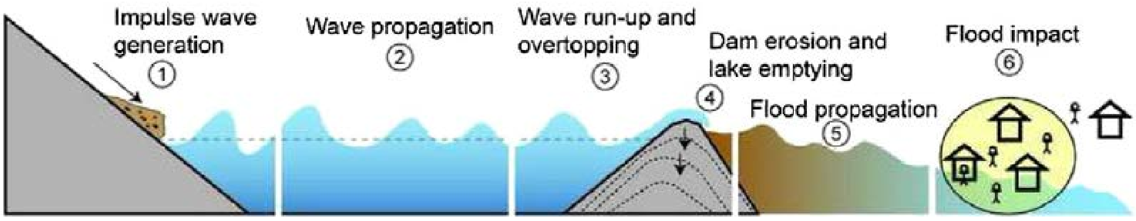

Figure 2. Simplified representation of a characteristic GLOF process chain. The process starts when (1) a landslide falls into a lake, producing (2) an impact wave that (3) overtops and (4) incises the dam, resulting in (5) a flood that travels downstream and (6) eventually impacts population settlements or infrastructures (Worni *et al.*, 2014).

A more detailed representation of a GLOF process, including the potential triggers, the conditioning factors for dam failures and the key stages of a hazardous moraine-dammed glacial lake outburst, is detailed in Figure 3 below (Westoby, Glasser, Brasington, *et al.*, 2014).

The potential triggers include (Westoby, Glasser, Brasington, *et al.*, 2014):

(A) contact glacier calving
(B) icefall from hanging glaciers
(C) rock/ice/snow avalanches
(D) dam settlement and/or piping
(E) ice-cored moraine degradation
(F) rapid input of water from supra-, en-, or subglacial (including subaqueous) sources
(G) seismicity

The conditioning factors for dam failure include (Westoby, Glasser, Brasington, *et al.*, 2014):

(a) large lake volume
(b) low width-to-height dam ratio
(c) degradation of buried ice in the moraine structure
(d) limited dam freeboard.

The key stages of a GLOF include (Westoby, Glasser, Brasington, *et al.*, 2014):

(1) propagation of displacement or seiche waves in the lake, and/ or piping through the dam
(2) breach initiation and breach formation
(3) propagation of resultant flood wave(s) down-valley.

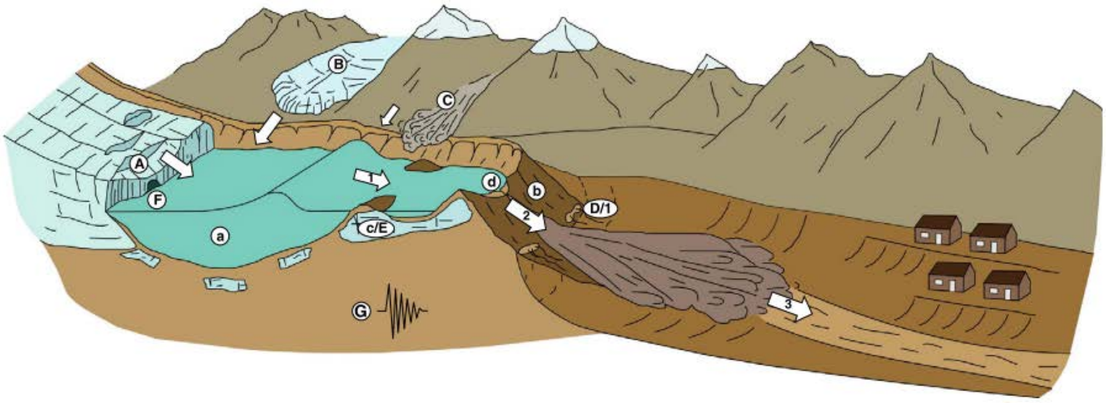

Figure 3. Representation of a hazardous moraine-dammed glacial lake. See text for a description (Westoby, Glasser, Brasington, *et al.*, 2014).

1.5 TROPICAL GLACIERS, PERU AND CORDILLERA BLANCA

The high mountain areas in Peru are especially vulnerable to, and affected by, impacts from climate change. The Andes has a length of 7000 km approximately with a maximum elevation of 6960 m a.s.l. and it is divided into 3 areas: Northern, Central and Southern Andes. The Peruvian Andes are located in the central part along with the Bolivian Andes. Peru has a long and fairly well documented history of natural disasters. It is probable that significant glacial retreats during the medieval warming period (800 to 1200 A.D.) also produced avalanches and floods whose traces are visible on many slopes around the Cordillera Blanca (Portocarrero Rodríguez *et al.*, 2014).

Cordillera Blanca (Spanish, for “white mountain range” due to the abundance of glaciers it presents) is located in the western part of the Peruvian Andes. The Cordillera Blanca runs approximately 180 km north-south in Central Peru, at 8˚30’S-9˚40’S. It contains more than 60 mountains above 5700 m. The glacier-covered area of the Cordillera Blanca has decreased from a Little Ice Age (LIA) peak (the peak LIA advance in Cordillera Blanca occurred between 1590 and 1720 (Solomina *et al.*, 2007)) of 900 km^2 to about 700 km^2 in 1970, 528 km^2 in 2003, and further decreased to 482 km^2 in 2010 (Burns and Nolin, 2014; Somos-Valenzuela *et al.*, 2016). Official numbers of Unidad de Glaciología y Recursos Hídricos (UGRH) (Glaciology Unit) and Autoridad Nacional del Agua (ANA) reported 472 km^2 in 2012 (Emmer *et al.*, 2016). It accounts for approximately 25% of the world’s tropical ice, making the Cordillera Blanca the most glaciated mountain range in the Tropic (Emmer and Vilímek, 2014; Schneider *et al.*, 2014).

The Cordillera Blanca presents very steep summits that are undergoing a long-term slope destabilization due to warming and permafrost degradation (Haeberli, 2013). Ice and rock avalanches falling from retreating glaciers are especially dangerous in relation with glacial lakes forming or increasing at the foot of steep mountain slopes because they can trigger large waves in the lakes and potentially lead to GLOF events (Carey *et al.*, 2012; Haeberli, 2013; Somos-Valenzuela *et al.*, 2016).

An inventory (Glaciology Unit, 2009) indicates there are 830 glacial lakes in the Cordillera Blanca, with 514 of them draining into the Río Santa watershed and on to the Pacific Ocean (the east side of the Cordillera Blanca drains to the Atlantic). All 514 present surface areas larger than 5000 m^2 and volumes between 100000 m^3 and 79 million m^3. Five of these glacial lakes have caused natural disasters in the past, including lake Laguna 513. Several may pose substantial current threats. Over the past three decades, increased climate variability has reduced glacier stability and created conditions unlike from those studied prior to the 1970s. Prevention measures need to comprise new criteria such as water management (smaller glaciers contribute to increased stress on water supplies) and disaster risk analyses (warmer temperatures can lead to increased frequency of ice avalanches) (Portocarrero Rodríguez *et al.*, 2014).

A more recent study from Emmer *et al.* (2016) detected 882 lakes in Cordillera Blanca conducting a manual analysis of high resolution optical images that was verified with field surveys. From those, a total of 357 lakes (40.5%) currently have some glaciers in their catchments, of which 75 lakes (8.5% of all lakes) are in direct contact with the glaciers ('proglacial' sub-phase). 450 lakes were detected (51.0% of all lakes) whose catchments are currently completely without glaciers (Table 2) (Emmer *et al.*, 2016).

Table 2. Characteristics of the lakes present in Cordillera Blanca, including type of lake (see section1.3.1) and relation to glacier. Adapted from(Emmer et al., 2016)

Lake type	Number	Lake-glacier relation		
		Direct contact	Some glaciers in the catchment	No glaciers
Cordillera Blanca overall	882	75 (8.5%)	357 (40.5%)	450 (51.0%)
Landslide-dammed lakes	23 (2.6%)	0	10 (43.5%)	13 (56.5%)
Ice-dammed lakes	31 (3.5%)	31 (100%)	0	0
Moraine-dammed lakes	311 (35.3%)	13 (4.2%)	179 (57.5%)	119 (38.3%)
Bedrock-dammed lakes	276 (31.3%)	25 (9.0%)	102 (37.0%)	149 (54.0%)
Combined-dam lakes	140 (15.9%)	6 (4.3%)	49 (35.0%)	85 (60.7%)
Not specified lake	101 (11.4%)	0	17 (16.8%)	84 (83.2%)

1.6 History and past major events in Cordillera Blanca

There are many examples in the Cordillera Blanca of glacier-associated incidents and catastrophes (Lliboutry *et al.*, 1977; Portocarrero Rodríguez *et al.*, 2014; Somos-Valenzuela *et al.*, 2016). The beginning of the glacier risks studies was on account of a catastrophic GLOF originated from lake Palcacocha, on 13 December 1941, that killed about 1800 people in the city of Huaraz, Peru (Somos-Valenzuela *et al.*, 2016).

During the 1940s, risk reduction measures were undertaken at the most unstable glacier lakes. However, current changes are rapidly evolving beyond historical experience and pose increasingly large challenges to local communities and institutions (Schneider *et al.*, 2014).

The most deadly glacier disaster was the 1970 avalanche that killed an estimated 6,000 people and buried the city of Yungay. The avalanche was triggered by a massive earthquake that killed 55,000 people. The 1970 earthquake and Yungay's avalanche inspired the first systematic studies of Mount Hualcán glaciers and led to the innovative but failed hazard zoning plans to reduce future exposure to potential glacier avalanches and GLOFs (Carey *et al.*, 2012).

One of the most recent events in the Cordillera Blanca occurred on 11 April 2010, when an ice-rock avalanche from the top of Mount Hualcán NE of the town of Carhuaz entered the glacier lake Laguna 513, the targeted study area of this project. The avalanche triggered a flood wave that transformed into a debris flow and impacted downstream areas as it reached the city of Carhuaz (Schneider *et al.*, 2014; Huggel *et al.*, 2020).

1.7 Lake Laguna 513 history

The glacier lake Laguna 513 that is located at 4428 m a.s.l., is a relatively young lake that has been formed in the late 1960s-early 1970s (Figure 4) due to glacier retreat, before the basin was filled with glacier ice (Portocarrero Rodríguez *et al.*, 2014; Huggel *et al.*, 2020). Once the lake starts forming, the presence of liquid water accelerates the glacier retreat and consequently the lake formation. The lake finished forming in the late 1980s and immediately experienced various reduced GLOF events derived from falling ice from hanging glaciers (Portocarrero Rodríguez *et al.*, 2014). The pictures correspond to: Top left: Aerial photo of Laguna 513 as a puddle on the surface of the glacier in 1962; the yellow circle marks the approximate size of the developing lake. Top right and middle left: Emerging ponds in the early 1970s, these ponds would combine into Laguna 513. Middle right: Laguna 513 almost totally formed in the late 1980s. Bottom: Laguna 513 showing the hanging receding glacial tongue and Mount Hualcán in 2010.

Figure 4. Chronology of the formation of the emerging glacial lake Laguna 513. Black and white photos: Glaciology Office Archives, Color photos: César Portocarrero (Portocarrero Rodríguez *et al.*, 2014).

Laguna 513 was already declared highly dangerous in 1988 and subjected to exhaustive security works to artificially lower the water´s level around 20 m by 1994. The remoteness of the place and the lack of resources available for a major project prompted the Glaciology Unit to place temporary siphons with financial help from the British and Austrian governments. These 2 siphons installed in 1989 and 1990, were plastic pipes, of 254 mm and 305 mm diameter, and were used to lower the water level by about 6 meters in total (Portocarrero Rodríguez *et al.*, 2014). First, to prevent an imminent outburst flood, engineers installed a siphon that pumped approximately 1 million m^3 of water out of Laguna 513. But the lake level and freeboard did barely reduce because new water came into the lake during the 1988-1989 wet season. After this, engineers thus installed a second siphon that lowered the lake's water level 5 m by June 1990. A proposal to further lower the lake level was planned, but before these measures were implemented, Laguna 513 produced a GLOF in 1991. The flood was alarming but relatively small thanks to previous engineering efforts that averted catastrophe. The GLOF undoubtedly would have been significantly larger if engineers had not already partially drained the lake (Carey *et al.*, 2012).

This GLOF in Laguna 513 in 1991 motivated authorities to finance the final stage of the Laguna 513 security. Starting in 1992 and financed by the Peru's Civil Defense Institute, engineers drilled four tunnels through the Laguna 513 moraine dam and bedrock beneath it. By April 1994, the Laguna 513 security project was completed with 4-6 million m^3 of water removed and the final 155 m long tunnel brought the lake level down, so it was dammed behind bedrock with 20 m of freeboard left to the basin's natural rock rim in order to contain potential wave flows created by ice avalanches falling into the lake (Carey *et al.*, 2012; Portocarrero Rodríguez *et al.*, 2014).

The reason to drill four tunnels instead of one was that the engineers in charge of the process understood that drilling a single tunnel 20 m below Laguna 513 water surface would have created a dangerous situation: upon opening the tunnel to drain the lake, the flowing water could have generated enough hydrostatic pressure to create a catastrophic flood (Carey *et al.*, 2012).

This did not reduce GLOFs risk to zero, though the probability of occurrence and magnitude of GLOFs was substantially lowered. From 1994 to April 2010, Laguna 513 was categorized as safe, with a low probability of producing a GLOF event (Carey *et al.*, 2012) and in 2004, authorities and specialists produced a report indicating that the lake could be considered safe due to the infrastructure in place (Huggel *et al.*, 2020). Nevertheless, Laguna 513, like other Cordillera Blanca glacial lakes, was monitored to ensure its stability (Carey *et al.*, 2012). However, as the event in 2010, previously mentioned, showed us, there is still a considerable risk in the lake that has to be addressed, which it is one of the reasons why this lake is the issue of the study.

This major event in lake Laguna 513 on 11 April 2010 was caused from ice falling from a hanging glacier. The event was induced by an approximately 0.5 million m^3 of ice-rock avalanche falling from the summit of Nevado Hualcán that fell into Laguna 513 causing a hydrodynamic surge and a wave higher than 20 m that overtopped the natural rock dam and flooded the Chucchun River for approximately 30 hours and produced debris flows that reached the town of Carhuaz (Carey *et al.*, 2012; Schneider *et al.*, 2014).Communities settled in the valley below suffered from damage to households, the riverbed, the access road, agricultural fields, and to the La Merced thermal baths in Hualcán. There is still a considerable risk of ice avalanches striking the lake in the future(Portocarrero Rodríguez *et al.*, 2014).

International experts were contacted to examine the lake (Prof. Wilfried Haeberli from the Institute of Geography at the University of Zurich and Prof. Stephen Evans of Waterloo University in Canada). They confirmed the success of the safety measures that had been constructed into Laguna 513, which prevented a much larger flood that would have damaged the Chucchun River course more severely (Portocarrero Rodríguez *et al.*, 2014).

Before the event in 2010, in 1997 an independent report from INAGGA, Instituto Andino de Glaciología y Geo Ambiente, (Carey *et al.*, 2012) reiterated the previous assessment of the stability of the lake dam but suggested that climate change, with the subsequent effect on glacier retreat and ice stability, will increase the probability of glacier avalanches on Mount Hualcán. Because avalanches were impossible to forecast, the report concluded that the only possible way of protecting the city of Carhuaz and its residents was through hazard zoning. Nevertheless, this suggestion was never implemented in the area (Carey *et al.*, 2012).

1.8 Population dependency on glaciers

Despite the risks mentioned above, populations have established in the vicinity of icy mountain peaks and thus in potentially hazardous regions, the reason of this, is the local inhabitants´ strong dependence on water resources from glacier melt because of the pronounced dry season (~May to September) in this geographical area (Schneider *et al.*, 2014).

Almost 10% (671 million people) of the global population lived in high mountain regions in 2010, based on gridded population data (Jones and Neill, 2016) and at a distance of less than 100 km from glaciers or permafrost located in mountains areas. This population is expected to grow to between 736 and 844 million people across the shared socioeconomic pathways by 2050 (Gao, 2019). Many people living outside of mountain areas and not included in these numbers are also affected by changes in the mountain cryosphere (Hock *et al.*, 2019).

The high mountain areas have maintained agricultural livelihoods for centuries. Rural communities living in these areas are dependent on suitable levels of soil moisture at planting time, derived in part from irrigation water which includes glacier and snowmelt water; as a result, they are exposed to risk associated to cryosphere changes. This glacier runoff variability will generate significant direct and indirect socio-economic impacts. Community livelihoods in rural mountain areas can be vulnerable to small-scale environmental changes due to the interdependence among water, biodiversity, and livelihoods (Carey *et al.*, 2017). The vulnerability to the impacts of these cryosphere changes of many mountain communities is increased by the relative poverty of their inhabitants. (Hock *et al.*, 2019)

The local people's behaviour and culture also suffer the impacts associated with glacier runoff variability. The traditions in which people imagine causality shape their responses to water scarcity, and these understandings, local knowledge, and cultural beliefs can differ noticeably from scientific representations of the runoff problem. Globally, glaciers and the mountains that sustain them have spiritual and cultural value for societies and the changes to glaciers, snow, lakes, and rivers could affect these local beliefs and practices (Carey *et al.*, 2017). Boelens (2014) explained how different social groups in the Andes have different perspectives on glacier runoff: engineers have a technical vision with biophysical features; non-governmental organizations work through socio-legal frameworks; and residents understand it through, among other ways, historical and cultural perspectives. In many places in Peru, climate change and glacier runoff variability have caused some residents to change their spiritual relationships because they believe that their religious offerings are no longer ensuring freshwater availability, and others report that glacier and snow loss demonstrates reduced power of their Apus (a powerful mountain deity that controls water and consequently origin and persistence of life). More research is needed to study how these cultural factors affect water use and management (Boelens, 2014; Carey *et al.*, 2017).

In the Andes, the glacial-fed streams are essential for hydroelectric production, irrigation and municipal water supplies. The larger-scale impacts haven't happened yet, and already people who live in areas affected by the changes in these glaciers are already beginning to experience the consequences. The lives and livelihoods of Quechua people, who already live at a basic subsistence level, are being adversely impacted by a dynamic and rapidly changing landscape as a result of the melting ice cap and its outlet glaciers, specifically, their lives are endangered when glacial lake dams are breached.(Thompson *et al.*, 2011).

1.9 DISASTER RISK REDUCTION AND ADAPTATION

1.9.1 General perspective

Adaptation actions have been recognised in several countries with glacier covered mountain ranges, mostly reactive responses (rather than anticipatory plans) to high mountain hazards (McDowell *et al.*, 2019; Xenarios *et al.*, 2019). But still, scientific literature reflecting on lessons learned from adaptation efforts generally remains scarce. Some adaptation strategies applied include (Hock *et al.*, 2019):

- engineering solutions such as lowering of glacier lake levels, channel engineering, or slope stabilisation that reduce the hazard potential;
- nature-based solutions such as revegetation efforts to stabilise hazard prone slopes or channels;
- hazard and risk mapping as a basis for land zoning and early warning systems that would reduce potential exposure;
- various community level interventions to develop disaster response programmes, build local capacities and reduce vulnerability.

The engineered responses to reduce glacier flood risk have been mostly developed in the mid-20th century in Peru (Haeberli *et al.*, 2001). And there is no published evidence that avalanche risk management, through defence structures design and norms, control measures and warning systems, has been modified as an adaptation to climate change, over the past decades. Projected changes in avalanche character bear potential reductions of the effectiveness of current approaches for infrastructure design and avalanche risk management (Ancey and Bain, 2015; Hock *et al.*, 2019).

Early warning systems require strong local engagement and capacity building to ensure affected communities know how to prepare for and respond to emergencies, and to ensure the long-term sustainability of the project (Hock *et al.*, 2019).

Regions affected by floods, avalanches and landslides related with the cryosphere, generally call for multi-pronged approaches (plans of action consisted of several separate elements or methods from several points of view or directions and taking multiple-entry points) personalised to local circumstances, with the integration of Indigenous and local knowledge together with enhanced scientific understanding and technical capacities; they should include a strong local participation and early engagement in the process, a high-level communication and exchange between all actors involved. Particularly for mountain regions, there is high confidence that the integration of knowledge and practices across natural and social sciences, and the humanities, is the most efficient way to address the complex underlying components of hazard, exposure and vulnerability of risks related to glaciers, snow, and permafrost (Carey *et al.*, 2014; McDowell and Koppes, 2017; Allen *et al.*, 2018; Hock *et al.*, 2019; Vaidya *et al.*, 2019).

1.9.2 Measures in the Andes

More specifically, adaptation measures have been undertaken in the Andes. These actions haven't been established in the same way through the region. For example, there are some differences between the northern (or low latitude) and southern Andes (Figure 5). The number of adaptations undertaken has been larger on the Northern part and the predominant sectors addressed have been agriculture, followed by water sector in the north part and water and undefined sector (adaptation where no clear classification to a specific sector could be allocated) in the south part. In the northern part, formal policies and autonomous actions present a similar number of actions; on the other hand, in the southern Andes formal policies are predominant (Hock *et al.*, 2019).

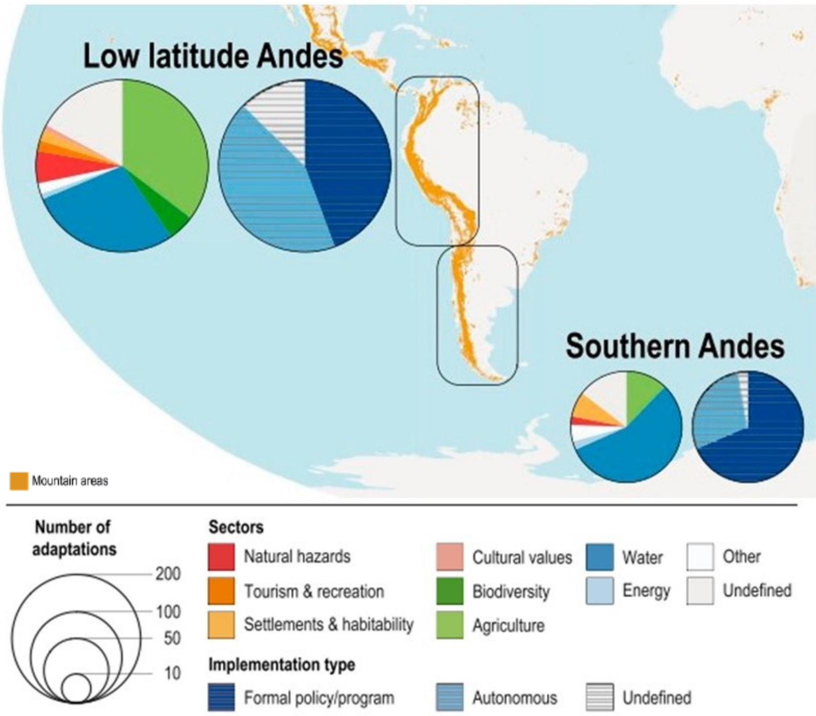

Figure 5. Documented number of individual adaptation actions in the 2 high mountain regions of the Andes with pie charts indicating the number of adaptation measures for sectors. Adapted from (Hock *et al.*, 2019).

1.9.3 Measures in the study area

More specifically, in Laguna 513 mitigation plans for reducing the risk were also developed. After the 2010 major event in the glacier lake Laguna 513, the local and national authorities, as well as Peruvian and international experts, met to discuss ways to implement protection measures for local populations and resources in future events. The outcome was plans for a GLOF Early Warning System (EWS) that originated in 2011 and implemented within three years. The GLOF EWS, the first in the Andean region that has become the model for several other EWS in the Peruvian Andes (e.g. Huaraz- Palcacocha, Urubamba-Chicón), was established in the framework of the Glacier Project (Swiss Agency for Development and Cooperation (SDC) *et al.*, 2020) in Huaraz (Huggel *et al.*, 2020). In Figure 6, the stations and the receiving centre of Laguna 513 EWS are shown.

The EWS stations were equipped with the following instruments (Huggel *et al.*, 2020):

1. Data centre Carhuaz (2640 m a.s.l.): real-time data access and infrastructure for launching alarms.

2. Repeater station (3189 m a.s.l.): receiving and sending antenna.

3. Station Laguna 513 (4491 m a.s.l.): to detect potential mass movements impacting the lake. Receiving and sending antenna and data logger.

4. Station Pampa Shonquil (3600 m a.s.l.): river discharge station and meteorological station with sensors for measuring air temperature and humidity, precipitation, wind speed, and solar radiation. Sending antenna and data logger.

5. Information receiving and warning station at Pariacaca (3138 m a.s.l.): the monitoring system informs the local population about events at Laguna 513 and sirens activation from the Data Centre Carhuaz to facilitate evacuation.

Figure 6. Early Warning System established in Laguna 513 and Carhuaz after the 2010 event comprises two stations - a main station at the Laguna 513 dam (1st picture from the left) and a station in the Pampa Shonquil (2nd), which includes meteorological measuring instruments – a repeater station for transferring the signal from the lake to the data centre (3rd), a data centre in the municipality of Carhuaz (4th), and a warning station in the community of Pariacaca (not in the picture) (Huggel *et al.*, 2020).

1.10 FACTORS THAT INFLUENCE RISK MANAGEMENT OF GLACIER LAKES

To prevent GLOFs, first it is necessary to identify the risk. To identify the real risk, it would require visiting each lake subject of study which would take a huge amount of time and resources. Since the start of the last decade, it has become possible to use satellite images to produce glaciological inventories, but sometimes these images have been proven to be unreliable for the identification of dangerous lakes as they are out of date. Therefore, on-site verification must be conducted on a frequent basis. Taking just sporadic or occasional glacial monitoring decreases the likelihood of noticing critical changes as dangerous lakes develop over time (Portocarrero Rodríguez *et al.*, 2014).

The following factors need to be considered when assessing the risks of glacial lakes (Portocarrero Rodríguez *et al.*, 2014) :

- The glacier characteristics: such as slope, the magnitude of crevasse (a deep crack or fissure in, e.g., the ice of a glacier), the magnitude of fragmentation, and estimated thickness.
- The slope of the bedrock: the average slope helps to determine the maximum travel distance, describing the angle of the horizontal with a line from the starting point to the farthest point of the deposition. In the Swiss Alps, a minimum average slope of 11° has been observed for debris flows from GLOFs (Haeberli, 1983; Huggel *et al.*, 2002). Scientists at the University of Zurich (Huggel *et al.*, 2004) have developed empirical

relationships based on glacier studies in the Alps that help to determine the slope at which slippage might occur depending on temperature (Figure 7).

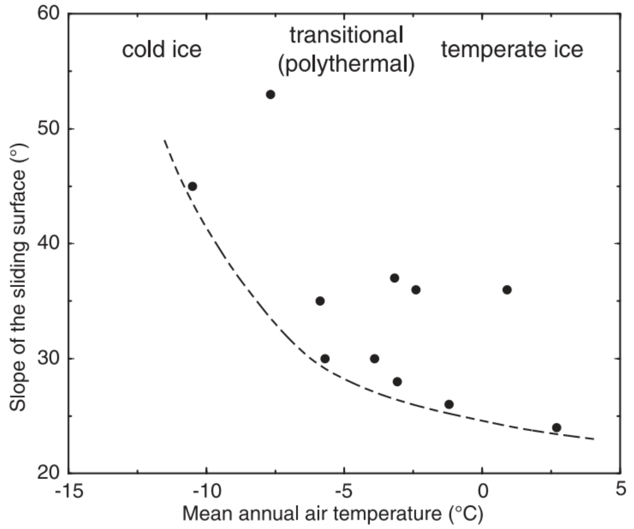

Figure 7. Relation between mean annual air temperature and critical slope for failure on ramp-type glaciers (Huggel *et al.*, 2004)

- The geometry and structure of the moraine forming the lake basin: since many GLOFs are a consequence from moraine material sliding into the lake, the composition and slope of the moraine can determine the stability of the basin.
- The length and slope of the downstream valley: when a GLOF happens, the destruction that it will cause downstream is strongly determined by its volume and kinetic energy. A flood's kinetic energy will depend on the physical characteristics of the path of the downstream flow. A long path with a gentle slope will dissipate some of the flood's energy. By contrast, the flood's velocity can increase when it travels through a steep downstream gradient.
- The presence of hanging glaciers: Masses of ice on very steep slopes without support from below are termed hanging glaciers. The combined effects of their large volume and gravity can cause huge avalanches that may result in dangerous surges if it falls into a lake. Decreasing adherence between the ice and the basal rock because of warming temperatures, especially in tropical glaciers, creates unstable conditions for glaciers on steep, rocky slopes.
- The process of glacier tongues undermined by glacial lakes (calving): as glaciers retreat, it frequently leaves behind empty spaces that are progressively filled with meltwater and ultimately form lakes. As these lakes are still in direct contact with the glacier tongue, the temperature difference between the water and the glacier produces an eroding effect that finally causes the ice to break off and cascade into the lake and can create a dangerous surge wave, depending on the mass of the ice falling and the volume and shape of the lake.
- The volume of the lake: multiple factors can create surge waves and other disturbances that trigger GLOFs. The magnitude and destructive potential of the flood is partly dependant on the volume of the lake. Decades of preventive work in Peru have discovered that the most effective preventive measure is to reduce the volume of dangerous lakes.
- The presence of seismic and tectonic factors: although the relationship between seismic activity and glacier stability is still unclear, some examples in the lakes Lazo Huntay and

Chuspicocha, which flooded the town of Huancayo in central Peru, demonstrates that earthquakes can result in glacial avalanches.

- The discharge rates: engineers and decision makers have the necessity to know the magnitude and variation of discharge rates from a glacial lake to correctly design pipelines and overflow channels that can prevent the lake's surface from rising to unsafe levels. These measurements should determine a value where water can be transported easily through the pipeline even during periods of heavy rainfall and abrupt inflows into the lake.
- The determination of the potential GLOF trigger: all GLOF occurrences are triggered by a mixture of locally specific variables. Contributing factors include lake volume, large impacts from above (rock or icefall), and moraine collapse due to its shape or internal weaknesses. These factors often change over time which complicates the identification and monitoring of a GLOF. Thus, understanding potential triggers for each lake is critical for evaluating risk. Potential triggers can be deduced based on history, statistics, or models; however, field verification is critical to their determination.

However, the probability of occurrence is difficult to estimate due to the rapid changes in the nature of glacial systems, the low frequency of GLOF events, and the significant complexity of the involved processes (Huggel *et al.*, 2004). According to Fell (1994) there are four ways to determine the probability of land sliding: (1) probabilistic analysis (Mostyn and Li, 1993); (2) use of historic data (Morgan *et al.*, 1992); (3) relationship to rainfall (Fell *et al.*, 1991); and (4) use of geomorphological and geotechnical information (Hungr *et al.*, 1984). The first three approaches cannot be applied for GLOFs due to a lack of frequency and historical data and the fourth one is most subjective but allows to assign a qualitative, or relative (within a study region), probability (Huggel *et al.*, 2004).

1.11 Social problematic issues

There are problems to fund the long-term maintenance of the EWS as it is dependent on long-standing national and international expertise and requires regular presence on-site and permanent joint capacity building and exchange with local people and authorities. Small municipalities with a limited budget usually have other priorities like investing in health and education services (Huggel *et al.*, 2020).

Other problems may arise from cultural traditions and misbeliefs. One example was the destruction of one of the stations accomplished by local inhabitants. In 2016, a large area of the central tropical Andes was affected by a strong drought. Usually, after a long dry Austral winter season, there is rainfall season in October. But in 2016, no rainfall was recorded in October and November. Farmers got desperate and rumours started to spread that the lack of water was caused by the antennas of the EWS at lake 513. A large number of locals from neighbouring areas gathered at lake 513 on 24 November and decided to dismantle the EWS station at the lake (Huggel *et al.*, 2020).

It must be kept in mind that the relation between local (risk exposed) people to their natural environment and their perceptions of different risks strongly determines their attitude towards risk reduction efforts. Local people can have intimate relations with mountains, glaciers and lakes as places of spirituality and the origin of life. Hence, a GLOF may be understood as a reaction of, for example, a glacier (as a mountain spirit) and a lake (as a being) to human disturbance or inappropriate human behaviour (Huggel *et al.*, 2020).

1.12 OBJECTIVES

The main objectives of this study are:

- Assess the risk of GLOFs associated with glacier retreat coming from the glacier lake Laguna 513 and impacting the city of Carhuaz downstream.
- Simulate different GLOF scenarios.
- Find the most important processes, and their speed, causing catastrophic events.
- Assist policymakers to develop adequate mitigation measures including information for early warning systems.

1.13 HYPOTHESIS

Climate change is expected to increase the occurrence and magnitude of GLOF events in the area in the short term and create troubles for water supply for the local populations in the long term.

1.14 LITERATURE REVIEW

For the purpose of the study, the two most relevant studies in the area, in which the GLOF simulation of this master thesis is being based on, and the reasons why these studies have been chosen, are:

Schneider, D., Huggel, C., Cochachin, A., Guillén, S., & García, J. (2014). Mapping hazards from glacier lake outburst floods based on modelling of process cascades at Lake 513, Carhuaz, Peru. *Advances in Geosciences*, *35*(April 2010), 145–155. https://doi.org/10.5194/adgeo-35-145-2014

- It covers the same study area
- It modelled the 2010 avalanche and GLOF event in Laguna 513
- It modelled the cascade of mass movement processes observed using the numerical models RAMMS and IBER

Mergili, M., Pudasaini, S. P., Emmer, A., Fischer, J. T., Cochachin, A., & Frey, H. (2020). Reconstruction of the 1941 GLOF process chain at Lake Palcacocha (Cordillera Blanca, Peru). *Hydrology and Earth System Sciences*, *24*(1), 93–114. https://doi.org/10.5194/hess-24-93-2020

- It is located in a near area with similar conditions, the moraine-dammed glacier lake Palcacocha
- It modelled the 1941 GLOF in lake Palcacocha
- It uses the same hydrological simulation methodology followed by this master thesis: *r.avaflow*®

2 METHODOLOGY

This study is located in Peru, in the most glaciated mountain range in the Tropic, more specifically in a glacier lake object of past GLOF disaster events, the glacier lake laguna 513. The methodology followed consists of 3 parts which are related with each other: (1) a study of the evolution of the nearest glacier during the last decades, (2) a climatological study with past and future data to make future climate projections in the area, (3) and a mass flow simulation of a GLOF event in Laguna 513.

2.1 STUDY AREA

The study area comprehends the lake Laguna 513 (Figure 8), the vicinity glacier and the city of Carhuaz downstream, including the watershed. In Figure 9 the location of the study area is shown, starting from its location in South America, following by the location of the Peruvian glaciers until a closer view showing the area between Carhuaz and the Laguna 513 and a closer view on the lake and the vicinity glacier. The Laguna 513 has an altitude of 4428 m a.s.l., it is located at the south side of the glacier Cochca and its coordinates are 9° 12´ 50´´S and 77° 33´10´´W. The lake and the glacier are located in the south-west side of the mountain, receiving a larger influence from the Pacific Ocean than from Amazonia.

In Figure 10, a more specific view of the study area is shown. From the top Hualcán at 6125 m, the maximum altitude of the studied glacier, then lake Laguna 513, downstream the plain of Pampa (Quechua, for "flat place") Shonquil at around 3600 m a.s.l. and further the city of Carhuaz. The elevation profile is also shown, presenting the distance between the lake and the city of around 15 km with an elevation difference of around 2000 m.

This selected study area has been estimated to have a high risk for the populations downstream. A recent study in Cordillera Blanca by Barbadillo Jorge (2020) - that calculates the damage potential of the glacier lakes considering hazard, and vulnerability and exposure - has defined Laguna 513 as one of the top five lakes with the highest damage potential from a total of 40 glacier lakes studied by the author of this study, that have been selected according to size and population proximity from the 830 lakes inventoried in Cordillera Blanca in 2014 by ANA.

Figure 8. Picture of lake Laguna 513. Photography from Elisa Hernandez (2018).

Location maps of the study area

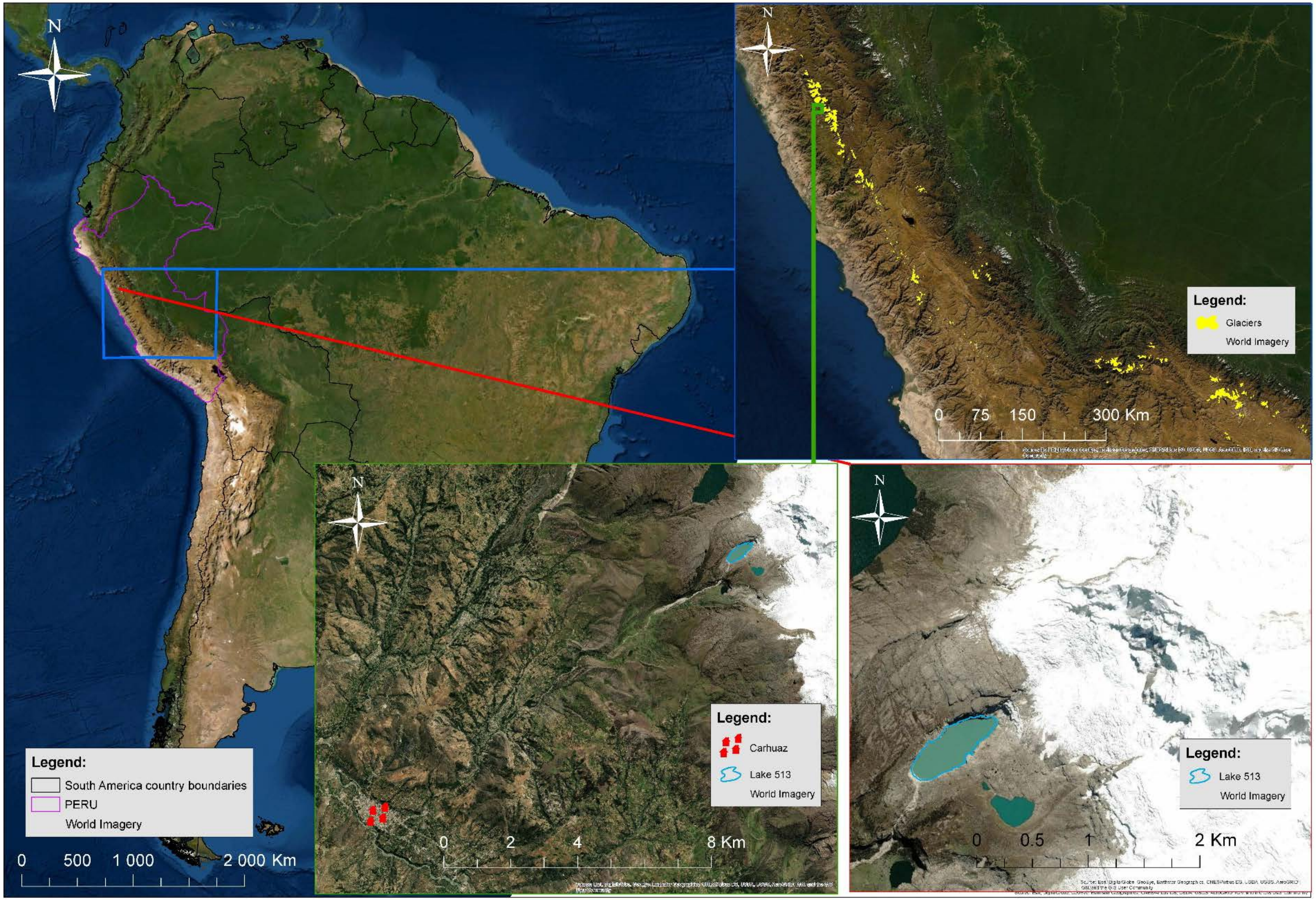

Figure 9. Location maps of the study area, showing the location in South America, Peru, the Peruvian glaciers distribution, the situation between the population and the glacier lake Laguna 513 and a closer view on the Laguna 513 and the nearest part of the glacier. Done in ArcGIS ArcMap® on ESRI world imagery and Peruvian glacier lakes distribution layer by Autoridad Nacional del Agua (ANA).

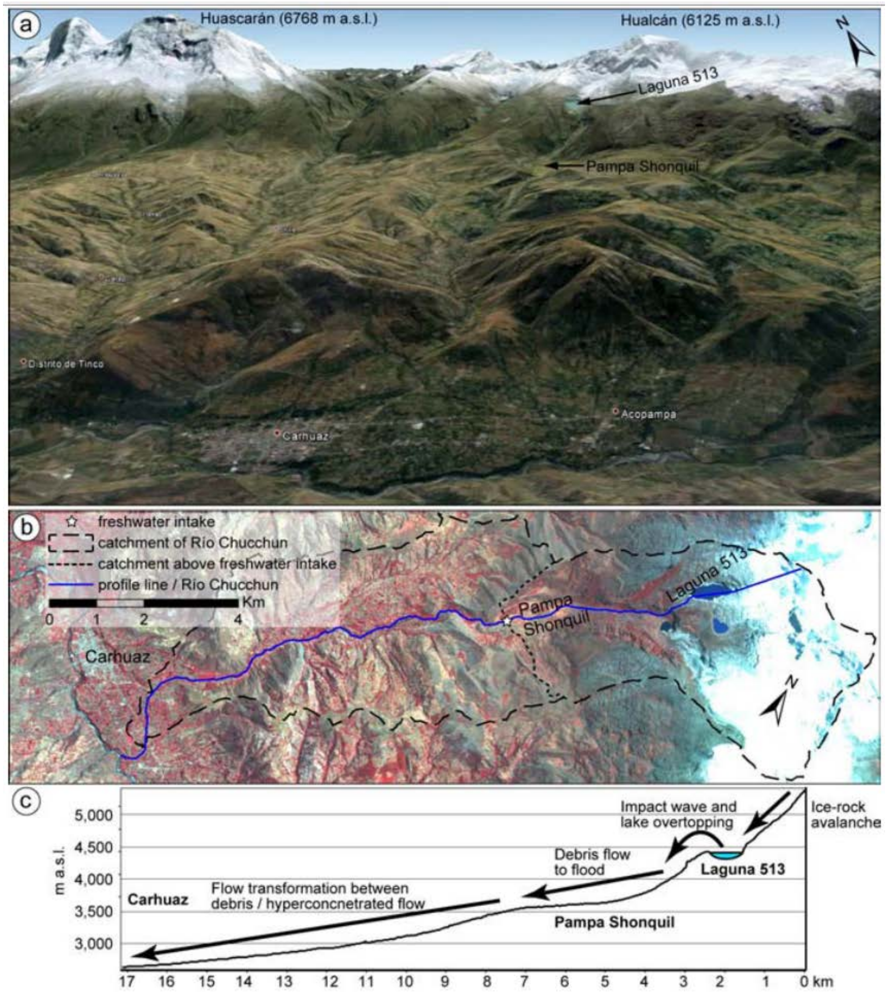

Figure 10. Overview of the area, from the Mount Hualcán until the city of Carhuaz including the Río Chucchun catchment above the City of Carhuaz and the glacier lake Laguna 513. (a)3-D view from Google Earth, (b) a SPOT satellite image from 2006 with the flow path (blue line) of the cascading mass movement processes, (c) the corresponding elevation profile (Schneider *et al.*, 2014).

2.1.1 Social and economic factors of Carhuaz: social vulnerability

The population of the district of Carhuaz – which includes the city of Carhuaz (Figure 11) and its surroundings - has approximately 15122 inhabitants with 52% of women and 48% of men (Instituto Nacional de Estadística e Informática (National Institute of Statistics and Informatics of Peru), 2018). The Human Development Index (HDI) is a summary measure of average achievement in key dimensions of human development from the United Nations measured from 0 (lowest) to 1 (highest).The HDI has three key dimensions: a long and healthy life, being knowledgeable and have a decent standard of living. According to the HDI, in 2012, all the districts of Cordillera Blanca, except one (Huaraz with a value of 0.53), were underneath the 0.5 value and specifically, Carhuaz had a value of 0.34, which is a low value that indicates reduced development within the area. The percentage of literacy in the population is 70% and the average monthly salary is 275.3 soles, it is very low even comparatively, considering that the minimum living wage in Peru is 930 soles (~ 240€). Additionally the adjacent districts in Cordillera Blanca are all beneath the minimum living wage too (Barbadillo Jorge, 2020).

These aspects together show that the population is predominantly vulnerable, which a low resilience to extreme events, unable to provide an effective response to disasters and taking months, even years or decades, to recover from an emergency event.

Figure 11. Photo of the city Carhuaz. Reference: https://sightisaright.org/missions/carhuaz-peru-2020/

2.2 Aspects to consider

Some aspects that have to be considered in order to assess the problematic subject of glacier retreat and associated phenomena. First, related to the physical aspects, it is important to know which is the process responsible for the risk, to assess where the snow and ice are coming from. It would be different if the snow and ice are coming from the top of Mount Hualcán (with an elevation of 6125 m a.s.l.), or from the nearest part of the glacier that is around 5000 m a.s.l.. In the first of the two cases, the ice and snow will accumulate every year and fall into the lake without large amounts of melting. In the second case, there will be a larger amount of melted ice and snow falling on to the lake that will increase with the years due to warming. This will influence the speed of the process in the short term, around one or two decades from now, and there will be an increase of flood risk due to warming from the lower parts of the glacier. In the long term, around 50 years from now, the snow line location will change with shifting to higher areas with the resulting glacier retreat, that will likely decrease the risk of flooding if the main process was forming in the nearest areas of the glacier but at the same time will create large problems of water supply in the vicinity populations. Additionally, it is relevant to estimate the state of the lake at the moment of the event, being aware of the seasonal fluctuations on precipitation distribution and melting period in the area. If high precipitation and melting periods coincide in time, the event will aggravate in size.

To assess the future changes in the glacier distribution along the years, a documentation of the previous changes is needed and can be obtained through high-quality orthophotos and used to calculate the velocity of the glacier retreat to acquire a linear extrapolation for future glacier retreat tendencies.

Secondly, the socio-economic aspects that have to be considered: the changes in distribution in the population of Carhuaz since the last major event in 2010 and the mitigation measures conducted to reduce future risks, both the development of new measures and the maintaining of the current infrastructure, the tunnels, in an adequate state.

2.3 SOFTWARE

A study like this requires multiple analysis with different kinds of software as there is not an integrated approached that can be used to analyse all the needed data.

For this project, open-source and available university licenses software were prioritized. Also, software with possible temporary licenses for students was used.

The software utilized in this project, in alphabetical order, is:

ArcGIS ArcMap® version 10.7.1,

ArcGIS ArcScene® version 10.7.1,

ArcMap® extension *ET GeoWizards®* version 12

AutoCAD Civil 3D® version 2019,

Google Earth Pro®

Klima 0.9®

Microsoft Excel®

r.avaflow® tool *r.lakerefill®*

r.avaflow® version 2.3

The coordinate system used for the spatial data in this project, selected for the adequacy of the location, is the World Geodetic System 1984 (WGS 84) / Universal Transverse Mercator (UTM) zone 18S (EPSG: 32718). It is a projected coordinate reference system with metric units and its area of use is between 78°W and 72°W, in the southern hemisphere between 80°S and the equator, both onshore and offshore (Geoscience Division Pacific Community (SPC), 2016)

A brief step by step methodology is presented in the sections below.

2.4 SOFTWARE JUSTIFICATION

The software available for this type of GLOF simulations was assessed and it was decided to utilize *r.avaflow®* for its multiple advantages, both in availability (open software) and in accuracy for the GLOFs predictions and simulations.

r.avaflow® represents an innovative open-source computational tool for routing rapid mass flows, avalanches, or process chains from a defined release area down an arbitrary topography to a deposition area. It was launched as an initiative to design, evaluate, and promote a comprehensive and innovative simulation model for the dynamics of various types of geomorphic mass flows.

This program applies an extended version of the approach of Pudasaini (2012) who introduced a general two-phase flow model including mixtures of solid particles and viscous fluid. It has been used for the simulation of computer-generated examples of sub-aqueous landslides and particle transport as well as GLOFs (Kafle *et al.*, 2016; Mergili, Pudasaini, *et al.*, 2020).

One of its main advantages of this program represents an integrated approach with multiphase models that can describe the interactions between the solid and the fluid phases, dynamic landslide–lake interactions and flow transformations. In contrast, most of the approaches used before for these GLOF events represent single-phase mixture models, like the simulation of a GLOF process chain in the Lake Palcacocha (Somos-Valenzuela *et al.*, 2016). In this simulation the process chain from avalanche to inundation was performed using four models: potential avalanches with *RAMMS*®, lake wave dynamics with *FLOW3D*®, the dynamic breaching process with *BASEMENT*® and the propagation of the flood wave downstream and inundation with *FLO2D*®.

The software *r.avaflow*® runs on *LINUX*® operating systems. It can be download for free in the *r.avaflow*® webpage (*https://www.avaflow.org/*). The current version used for this thesis is *r.avaflow*® 2.3. It is a module of *GRASS GIS*® and it relies on *GRASS GIS*® 7; it employs the programming languages *Python*® and *C*® along with the statistical software *R Project for Statistical Computing*® and it is most efficiently operated through shell scripting, not using the GUI of GRASS but working in the *LINUX*® terminal (Mergili *et al.*, 2017).

This software has been successfully used in many similar studies in the Cordillera Blanca area like in lake Palcacocha (Mergili, Pudasaini, *et al.*, 2020), in Nevado Huascarán (Mergili, Frank, *et al.*, 2018) in a multi-lake outburst flood in the Artizón and Santa Cruz valleys (Mergili, Emmer, *et al.*, 2018) and in other areas like Piz Cengalo, Switzerland (Mergili, Jaboyedoff, *et al.*, 2020). The studies developed in the Cordillera Blanca by Mergili *et al.* identified the capability of the tool to appropriately simulate the transformations at the boundary of individual processes, where one process transforms to the next, as one of the major challenges.

Other kinds of software - like Geographical Information Systems (GIS)- have been used to produce the data to import in the mass flow simulation and to analyse complementary information about the glacier and climate. This selected software has been chosen because its adequacy and efficiency.

2.5 Glacier morphology evolution

The 2 layers obtained from the Geomorphologic map of fluvioglacier forms west of Hualcán mountain peak (Concha, R., 2020), one from the year 1962 and the other from 2015, are used to assess the glacier evolution during these 53 years through a linear regression. The process is calculated in *ArcMap*®.

The area of the polygons of each year is calculated to obtain the trend of glacier shrinkage per decade in both layers. Some minor changes in the total area values are expected in the analysis of slope and elevation as a result of the change in resolution and conversion from vector to raster.

2.5.1 Slope

First dissolve into one individual polygon for each year with the tool "Dissolve". After, clip each glacier polygon with the layer with slope values (explained later in section 2.6.1) and produce an attribute table of the raster layer and export it to *Excel*® as dBase file (.dbf) format for analysis. This is produced with the tools "Build raster attribute table" and "Table to Excel"; note that the raster layer has to be integer type to produce an attribute table, it can be previously transformed with the tool "Int".

Once in Excel, the percentage of area occupied from the total glacier area for each slope value is calculated to assess the change of predominant slope values. Furthermore, the percentage of retreat area in relation to the area present in 1962 is calculated.

For a better representation, the slope values are categorized in 6 groups (Table 3): (1) areas flat or nearly flat, with a very reduced tilt; (2) areas under the minimum value for debris flow according to the study in the Swiss Alps (Huggel *et al.*, 2004) mentioned in the introduction, in section 1.10; (3), (4) and (5) three equidistant categories with medium and high values of tilt and (6) very high values with a slope of 45 degrees or 100%.

Table 3. Categorization of slope values of the glacier area.

Category	Slope percentage (degrees)
Nearly flat	0-5
Under the minimum for debris flow	6-11
Medium	12-22
Medium-high	23-33
High	34-44
Very high	≥45

A graphic showing the distribution, comparing the two different years, is produced. Additionally, a spatial representation is generated in *ArcMap®* comparing the glacier area at both periods of time, and their slope in degrees.

2.5.2 Elevation

The process is very similar as the previous one, instead of the layer of slope using the elevation data from the layer of the Digital Elevation Model (DEM) (also explained in in section 2.6.1). The same statistic values are calculated with the elevation values.

The categorization is made in eight equal intervals of 250 m from 4136 until 6135 m a.s.l., shown in Table 4.

Table 4. Categorization of elevation values of the glacier area.

Categories Elevation (m a.s.l.)
4136 - 4385
4386 - 4635
4636 - 4885
4886 - 5135
5136 - 5385
5386 - 5635
5636 - 5885
5886 - 6135

2.5.3 3D Distance:

The distance that the glacier retreated from 1962 to 2015 is obtained. Only the front line of the glacier retreat, the closest area from the lake Laguna 513, is considered for this study. Other minor areas of glacier retreat in the middle of the glacier are not considered.

The process is completed in *ArcMap®*. First, the front line of the glacier in both years has to be selected. The dissolved polygon layer of each year is converted to line with "Feature to Line" tool. From this line, with the editor open, the tool split and deleting the extra parts, the front line of the glacier is obtained. The starting and ending point of the front line have been selected in the intersection between the glacier shape in 1962 and 2015.

Secondly, as the distance is going to be true distance or 3D distance, the layers have to be transformed into layers with Z values obtained from the Digital Elevation Model of the area, mentioned before. This is done deriving the existing features' heights from a surface with the tools "Interpolate shape" to convert from 2D to 3D by interpolating z-values for input features from a surface (DEM) and "Add Surface Information" to interpolate heights for features, converting them to 3D, and then writing the property values as attributes to the input feature class.

Next the distance is calculated. One of the layers is converted into points, for example the layer from 1962, with the tool "Feature Vertices to Points" and utilized to estimate the distance to the nearest point of the line layer of 2015 with the tool "Near 3D". With the "Summary Statistics" tool, the minimum, mean and maximum distances are determined.

A few minor errors are assumed as there can be points that are closer to areas that are not in the expected retreat direction. But this is disregarded in favour of the difference of velocity of the automatization process compared to a manual analysis of each point (>1000).

2.6 CLIMATE DATA, SCENARIOS

2.6.1 Historical data

The data selected for the climatologic study is from Climatic Research Unit (CRU, 2020). The data covers the period from 1901 until the present. It is a global data set and for this analysis it is used a 5° x 5° grid of the study area and another eight 5° x 5° grids for the spatial variability study. The 3 variables studied are maximum temperature, minimum temperature and precipitation.

Even if there is data available from previous years, it is decided to use the data from 1961 that coincide with the period with available spatial glacier information. Thus, the time period used for the data is from 1961 until 2019.

A height correction is necessary for the data, as the CRU data of the study area grid is calculated for an altitude of 3841 m a.s.l., while the lake is located at 4450 m a.s.l. and the glacier even higher. For this height correction an estimation of 0.65 degrees decrease per 100 m of altitude gained is used. The height correction for the lake is accordingly 3.96 degrees of decrease in temperature. The height altitude correction is adopted for all temperature data.

Analysing the yearly data, a climate diagram is generated with the tool *Klima 0.9®* (Tobias Thrierer, 1999) and a temperature diagram with *Excel®* to analyse the evolution of the Tmax and Tmin through the year.

<u>Trends:</u>

The trends or evolution of annual temperature and precipitation are calculated for the studied time period. Including also the trends in the summer months (from October to March) that corresponds with the rainy season which evolution of precipitation is more significative. These trends are calculated yearly for the 4 variables: Tmax, Tmin, Tmean and Precipitation with the linear trendline and the R-squared value on the charts. The data includes the height correction previously mentioned.

<u>Spatial variability:</u>

The CRU data used includes the Tmax, Tmin and Precipitation of 9 grids including and surrounding the study area. The grid containing the study area and the one used for the previous analysis is the grid 5 or the middle grid, represented in Figure 12 along the others. Selecting the information for the time period (1961 until 2019) the average value is calculated for each grid and organised in a spatial distribution. The altitude values from the CRU data are obtained from a topography file and used to assess the variability according to elevation.

For a visualization of the spatial variability over a map and assess which topographic elements area influencing the data, 9 grids of 0.5 degrees are needed, this is produced in *ArcMap®*. A worldwide geographic information system is selected in the data frame properties coordinate system, in this case GCS_WGS_1984, to use longitude and latitude coordinate values as they are presented for the CRU data grids. Then the "Create Fishnet" tool in *ArcMap®* is used with fishnet origin coordinate: -78.5 (X) and -10.0 (Y), the Y axis orientated to the north (to -78.5, -8.5) and with a width and height of 0.5 degrees. The grids with coordinates from CRU data are represented in Figure 12.

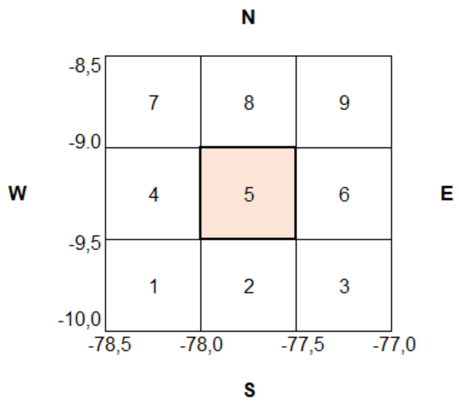

Figure 12. Fishnet of 9 grid with the 9 CRU data coordinates. Grid 5 contains the study area. Values of coordinates in latitude and longitude.

<u>ENSO correlation:</u>

To study the inter-annual variability, the correlation between El Niño Southern Oscillation (ENSO) and the mean temperature and precipitation, including summer precipitation, in the study area is analysed. The data used for this analysis corresponds to the Multivariate ENSO Index Version 2 (MEI.v2) and the CRU data explained above.

The MEI.v2 is a bi-monthly Multivariate ENSO index, the time series of the leading combined Empirical Orthogonal Function (EOF) which includes five different variables (sea level pressure (SLP), sea surface temperature (SST), zonal and meridional components of the surface wind, and outgoing longwave radiation (OLR)) over the tropical Pacific basin (30°S-30°N and 100°E-70°W) which included the study area (~9°S and ~77°W). The EOFs are calculated for 12 overlapping bi-monthly "seasons" or periods (Dec-Jan, Jan-Feb, Feb-Mar, ..., Nov-Dec) in order to take into account ENSO's seasonality, and reduce effects of higher frequency intra-seasonal variability. The MEI.v2 broadens upon the original MEI produced by Wolter and Timlin (1993) which was calculated using 6 variables for ENSO relevant atmosphere and ocean conditions. Large positive MEI values indicate the occurrence of El Niño conditions, while large negative MEI values indicate the occurrence of La Niña conditions. The ENSO data was obtained from the Physical Science Laboratory (2020). The time period used includes from 1979 to 2019, which has reliable data from both sources.

The positive/increase or negative/decrease of the temperatures variation due to ENSO variability is compared with the evolution of the mean temperature in the study area from CRU (after height correction), taking the average values of the time period considered as the reference value of increase or decrease. It is calculated both with annual and bimonthly data. The annual average of the CRU data is calculated. The bi-monthly Tmean is calculated with the two months average of the mean temperature starting from the data of December 1978 (to calculate 1979Dec-Jan data) until December 2019 (after height correction), to produce a more precise correlation with the ENSO data in the same time frame. The anomalies in the Tmean data are calculated in relation to the average mean temperature of the time period. The anomalies of mean temperature and ENSO data were plotted and a linear regression fitting was performed, obtaining the determination coefficient R-squared.

Additionally, the effect that ENSO phenomenon has in the temperature is analysed during the summer months which corresponds with the rainy season in the bimonthly periods: ON, ND, DJ, JF, FM and MA.

The same procedure is performed for the precipitation. And the analysis of the summer precipitation including the bimonthly periods ON, ND, DJ, JF, FM and MA, is also completed.

An additional method to assess the relationship between both variables is by computing the Pearson correlation coefficient and the corresponding p-value, with a level of significance $p=0.05$. The null hypothesis is that there is no relationship between the two observed phenomena. A small p-value (≤ 0.05) means that the observed results are unlikely to occur under the null hypothesis. Excel software with Real Statistics Resource pack was used for performing the correlation analysis.

2.6.2 Future scenario projections

Climate Change projections are needed to assess the availability of water resources, predict extreme events and consequently reduce risks and in general, manage socioeconomic impacts of possible future climate scenarios on ecosystems behaviour.

Climate is an extraordinary complex system with many physical processes intervening and an intricate network of interconnected variables involved. As a consequence, it is not valid to assume simply that the present trend of changes will continue in the future, and rigorous predictions based on computer models are needed, specially taking into account the uncertainty about the evolution of anthropogenic factors. GCMs are a representation of the climate at global scale, including detailed physical mechanisms and an exhaustive information about atmosphere, land, ice and oceans. They are under continuous improving, both in the representation of physical processes and the spatial and temporal resolution. In spite of their present limitations, GCM projections are able to capture the major features of the climate evolution in many areas of the world and are essential for future planning and adaptation to climate change.

The total data examined consists of: 7 (models) x 2 (Scenarios) x 3(variables) x 150(years) = 6300 years of data for analysis.

Models:

From the 31 available Global Circulation Models (GCMs) (see Appendix Table 8.1-1) (Almazroui *et al.*, 2020) 6 GCMs were selected based on resolution criteria. The 6 GCMs studied are:

- EC-Earth3
- MPI-ESM1-2-HR
- MRI-ESM2-0
- AWI-CM-1-1-MR
- BCC-CSM2-MR
- CNRM-CM6-1-HR

And as a 7th model, the ensemble mean of all the 31 models.

Future scenarios:

For future projections, an international team of climate scientists, economists and energy systems modellers have built a range of new “pathways” that examine how global society, demographics and economy might change over the next century. They are collectively known as the “Shared Socioeconomic Pathways” (SSPs). These include things such as population, economic growth, education, urbanisation and the rate of technological development. These SSPs look at five different ways in which the world might evolve in the absence of climate policy (Hausfather, 2018).

A group of researchers then developed the “Representative Concentration Pathways” (RCPs), describing different levels of greenhouse gases and other radiative forcing that might occur in the future. They developed four pathways, spanning a broad range of forcing in 2100 (2.6, 4.5, 6.0, and 8.5 W/m^2), but purposefully did not include any socioeconomic “narratives” to go alongside them (Hausfather, 2018).

The two efforts were designed to be complementary. The RCPs set pathways for greenhouse gas concentrations and, effectively, the amount of warming that could occur by the end of the century. While the SSPs set the stage on which reductions in emissions will, or will not, be achieved. The SSPs look on how different levels of climate change mitigation could be attained when the mitigation targets of RCPs are combined with the SSP. They include: a world of sustainability-focused growth and equality (SSP1); a “middle of the road” world where trends broadly follow their historical patterns (SSP2); a fragmented world of “resurgent nationalism” (SSP3); a world of ever-increasing inequality (SSP4); and a world of rapid and unconstrained growth in economy output and energy use (SSP5). (Hausfather, 2018).

The 2 future scenarios used are:

- mid-range SSP245: SSP2 (Middle of the Road - Medium challenges to mitigation and adaptation) and RCP4.5
- high-emission SSP585: SSP5 (Fossil-fuelled Development - High challenges to mitigation, low challenges to adaptation) and RCP8.5

Variables and data:

The 3 variables measured are:

- Precipitation on a monthly sum
- Maximum temperature in degree Celsius per month
- Minimum temperature in degree Celsius per month

The data is monthly, and the time period comprises from 1950 to 2100. The data of the models are remapped to the CRU grids in order to make the spatial distribution correspond with the CRU historical data distribution, mentioned in the previous chapter.

Height and Bias correction:

A height correction as explained for the historical data is performed in this data as first step. The second step is a Bias correction. The data used for this analysis is the ensemble of the 31 GCMs mentioned above.

Constructions of climate scenarios and modelling of climate change impacts are generally based on Global climate models (GCMs). However, these models cannot be directly used because of: i) limited spatial resolution at the regional scale (GCMs have coarse resolution, generally few hundreds kms) ii) insufficient knowledge of climate system dynamics, and iii) simplified modelling of the complex climate physics. The resulting biases can be very important for example, for estimation of temperature and precipitation extremes.

Over recent years, several studies and methods of bias correction have been developed. Fang *et al.* (2015) described the most important ones for temperature and precipitation projections, shown in Table 5. They range from the simplest Linear scaling LS method to the more complex statistical distribution approaches.

Table 5. Main Bias correction methods for Regional Climate Models (RCM)-simulated precipitation and temperature. Adapted from (Fang *et al.*, 2015)

Bias correction for precipitation	**Bias correction for temperature**
Linear scaling (LS)	Linear scaling (LS)
Local intensity scaling (LOCI)	Variance scaling (VARI)
Power transformation (PT)	Distribution mapping for temperature using Gaussian distribution (DM
Distribution mapping for precipitation using gamma distribution (DM)	
Quantile mapping (QM)	

All the bias correction methods have shown a positive effect compared to the raw GCM simulated data. Their performance is generally better for temperatures than for precipitations and shows to be case-dependent. We have chosen the simple LS to correct the GCM data. LS tries to match the mean of corrected values with that of observed ones. It applies a corrective additive term to temperature and a multiplier to precipitation (Equations. 1 and 2).

$$T_{corr} = T_{raw} + mean(T_{obs}) - mean(T_{raw}) \tag{1}$$

$$P_{corr} = P_{raw} \times \frac{mean(P_{obs})}{mean(P_{raw})} \tag{2}$$

where $\sigma(T_{obs})$ and $\sigma(T_{raw})$ are the standard deviations of observed and projected raw temperatures respectively and *mean*() symbolizes the monthly average value in the period.

The correction is performed for the monthly data for a more precise correction and once corrected; the annual averages are made. The precipitation is analysed just for the summer period, which is the rainy season, as the precipitations during the winter are already very scarce and the future trends will not affect in a great extent.

2.7 Mass flow simulation of a GLOF event

The input data for the simulation in *r.avaflow®* consist on: a Digital Elevation Model (DEM) of the area and rasters of the different release areas- both in the glacier and in the lake- and a set of parameters which have been defined after multiple simulations.

2.7.1 Digital Elevation Model

For the area, a Digital Elevation Model (DEM) from Alos Palsar (Dataset ASF DAAC, 2011) is used. Alos Palsar is a synthetic aperture radar (SAR) that obtains Radiometric Terrain Corrected GeoTIFF file for each polarization available in the Universal Transverse Mercator (UTM) system. The pixel spacing is 12.5 m for high-resolution (RT1). The SAR contains active remote sensors that provide their own artificial radiant energy source for illumination. Spaceborne Synthetic Aperture Radar (SAR) interferometry has been utilised to acquire high-resolution DEMs with wide coverage, particularly for persistently cloud-covered regions where stereophotogrammetry is hard to apply (Xiong *et al.*, 2017). The mission launched on 24th January 2006 and terminated in 2011. The DEM selected is the most recent available DEM, from the 3rd of July 2011 (ASF DAAC, 2011; Includes Material ©JAXA/METI, 2011). This DEM is reduced to the study area through the tool “Clip” in *ArcMap®* into a square of 192318000 m^2 that comprises the falling area of the glacier, Laguna 513 and the city of Carhuaz.

The slope in the area is calculated from the previously mentioned DEM in *ArcMap®* with the tool “Slope” in degrees. The orientation of each hillside is calculated with the tool “Aspect”.

A bathymetry of the Laguna 513 is obtained from Autoridad Nacional del Agua (ANA), from it, a Digital Elevation Model of the lake is created. The input file is a DraWinG 3D drawing file (.dwg) that it is analysed in *AutoCAD Civil 3D®* to obtain the elevation lines with 2 meters separation and to export them to a shapefile (.shp). The process starts with exporting the file to Drawing Exchange Format (.dxf), a data file format developed by *Autodesk®* for enabling data interoperability between *AutoCAD®* and other programs, and selecting all the layers with elevation line information in the same format (lines); then with the command “MAPEXPORT” the elevation lines are exported into a ESRI shapefile as a 3 dimension file and with the correct coordinate system. The elevation lines shapefile is further processed in *ArcMap®* to obtain a DEM through “Create TIN” and “TIN to raster” tools. The resulting pixel size is 0.7 m. Subsequent deposit in the lake after the bathymetry was obtained are not considered in this project.

The lake´s DEM obtained from the bathymetry has 2 purposes: the first one to calculate different scenarios of volume inside the lake, and the second one, to incorporate it in the DEM of the area. This process is done because the DEM from the bathymetry is more precise than the one obtained in the orthophoto. The reason of this precision reduction is the water response to energy waves from radar remote sensing, that suffer physical limitations in the dynamic water mass that can occasionally form major data gaps (Quadros *et al.*, 2008; Markert *et al.*, 2018).

For the first purpose: different scenarios of the water height of the lake are obtained. This process is conducted in *ArcScene®* calculating the desire elevation line and converting it into a polygon with an altitude value and, using these scenarios and the DEM previously mentioned, water volume is calculated using “Polygon Volume” tool.

For the second one: to produce just one DEM to introduce in the simulation, it is necessary to join both DEMs (lake’s DEM from bathymetry and DEM of the whole watershed) with the same pixel size, the pixel size chosen is 12.5 m which is the size of the DEM of the study area, the biggest pixel size from both DEMs. To change the pixel size of the lake´s DEM from 0.7 m to 12.5 m the TIN created from the bathymetry is exported to raster with a change in the pixel size. This is processed using *ArcMap®.* First, both DEMs are converted separately to points with altitude values applying “Raster to point” tool. Secondly, the points from the watershed’s DEM that coincide with lake’s DEM are removed with the tool “Erase” (it needs the ArcGIS for Desktop Advanced License or otherwise use the tool from the extension *ET GeoWizards®*). Consider that to cut a raster is necessary a polygon vector layer to select the area, which should be obtained previously, this can be done using the “Raster to Polygon”, “Reclass” and “Dissolve” tools from *ArcMap®.* The points from the lake’s DEM fill the space in the watershed’s DEM with the tool “Merge” into a new point dataset with altitudes of the whole watershed. Finally, this layer is transformed into a raster with “Topo to raster” tool, using the elevation of each point with the same pixel size as before, 12.5m, as with point elevation feature type.

The layers of the DEM have to be exported to Tagged Image File (.tif) format to work on *r.avaflow®* afterwards.

2.7.2 Release areas

The release areas define the initial distribution of the flow material in space and time. The simulation is a multiphase event with 2 solid phases falling from the glacier and one fluid phase inside the lake, filling it with water:

- 1st phase is formed by rock
- 2nd phase is formed by ice.
- 3rd phase is formed by water.

The layers of the release areas have to be exported to Tagged Image File (.tif) format to work on *r.avaflow®* afterwards.

<u>Solid release area:</u>

To select the area and the extend from where the glacier would fall into the lake, the following elements were taken into consideration:

- Previous disaster events in the same area: previous catastrophic events are considered, including the one in 2010, to analyse where the glacier detachments were produced before
- Kinetic energy: the nearest part of the glacier that is hanging onto the lake Laguna 513 has a high probability to fall into the lake in the short term but it wouldn´t fall with enough energy to create a very dangerous event for the population of Carhuaz. Nevertheless, from a higher point with a steep hillside, the kinetic energy would be bigger once it reaches the lake, creating a bigger wave that would overtop the dam and rapidly create a disaster event downstream
- Slope: the slope is considered to choose the location where the ice and rock wouldn't have any obstacle to reach the lake directly without losing energy. And also that they have high or medium high slope as it is easier to provoke landslides
- Glacier shape: using the layer of the glacier in 2015 and in 1962 analysed in a previous chapter to evaluate which areas have been suffering a bigger retreat and which areas still are part of the glacier
- Orthophotos: looking the state of the glacier in orthophoto in *ArcMap®* or in *Google Earth®* in 3D to analyse which area seems more likely to have a detachment.

Once the location is studied and decided, the release area is delimited in *ArcMap®*. First create polyline feature with the same spatial reference. Then, with the editor tool activated, draw elevation lines of the release area including the outside of the location area included for the simulation with "Create features" and "Edit vertices". In the attribute table, values of altitude are given to each elevation line, including zero values for the outside of the location area and the boundaries of the release area. As there is no possibility to know the glacier thickness in this area, the values are an approximation using the information mentioned above. Afterwards, with the tool "Create TIN", selecting the field with altitudes values for the "Height Field" a DEM of the release area is created. Final step, is the tool "Tin to raster" with natural neighbours and 12.5 m pixel size and then save the layer as .tif format to make it compatible with *r.avaflow®* and *GRASS GIS®.*

<u>Fluid release area:</u>

The third phase, the fluid release area, is the water level of the lake. To use the different scenarios of lake´s water level created in the previous subchapter in the *r.avaflow®* simulation, it is necessary to previously create the fluid release area in the lake. This is done with the r.lakerefill tool, a Python-based GRASS GIS 7 module for filling depressions in the terrain with water (Mergili, M., Pudasaini, S.P., 2014-2020).

The following parameters are required to run r.lakefill:

- Cellsize: raster cell size for computation. The same cellsize as for *r.avaflow®* simulations is applied. Otherwise, the lake surface might not be perfectly plane, which would result in numerical oscillations.
- Elevation: name of input GRASS raster map representing the terrain surface (usually in m a.s.l.) which is the 12.5 m DEM with bathymetry previously created.

- Lakedepth: name of output GRASS raster map of the computed lake depth (usually in metres). In *r.avaflow*®, this raster can be used as the fluid release height (parameter hrelease3).
- Level: lake level (usually in m a.s.l.). Note that the lake level has to be lower than or equal to the lowest point surrounding the depression to be filled in order to achieve the desired result. The scenario 1 and 2 levels are used to create the 2 different outputs
- Seedcoords: Two comma-separated values describing the x and y coordinates (usually in metres) of an arbitrary location within the depression to be filled. The point defined by these coordinates will be used as seed for filling the depression.

The module is executed through the terminal by calling its name along with the parameters. The script used for one of the scenarios is:

```
#Lake refill tool from r.avaflow®, 2 water level scenarios


#import dem and set region

r.in.gdal -o --overwrite input=dem_erbat.tif output=dem

g.region -s rast=dem


#lake refill scenario 1

r.lakefill cellsize=12.5 elevation=dem lakedepth=lakedepthscenario1 level=4.431
seedcoords=219894,8980688


#lake refill scenario 2

r.lakefill cellsize=12.5 elevation=dem lakedepth=lakedepthscenario2 level=4450
seedcoords=219894,8980688
```

2.7.3 Parameters

The parameters that have to be defined for the simulation are:

- Cellsize
- Phases
- Density
- Friction
- Viscosity
- Ambient
- Controls
- Thresholds
- Time

Explanations of each individual parameters and the values selected are defined in Appendix 8.2.

Additionally, there are some flags necessary to run the simulation:

- -a: for generation of output rasters and map plots of flow pressure and kinetic energy
- -e: enables the execution of the simulation model

- -k: keep the result GRASS raster maps
- -v: for evaluation and visualization of maps and profile plots

The values of these parameters have been defined studying the conditions of the area and past events, with the consultancy of experts in the field and with multiples tries to determine which conditions seem more realistic and adequate in this case.

2.7.4 *R.avaflow®* simulation

Once all the requirement software is installed and all the layers prepared, the first step is to launch GRASS with the desired Location and Mapset and then arguments can be typed directly into the command line of the terminal or utilize a shell script to run r.avaflow. The script used for this case is:

```
#Launching r.avaflow® computational experiments for the Laguna 513 process chain

#import DEM and set region

r.in.gdal -o --overwrite input=dem_erbat.tif output=dem

g.region -s rast=dem


#import release areas (glacier and lake)

r.in.gdal -o --overwrite input=TIN_sol_glac.tif output=releaseglacier

r.in.gdal -o --overwrite input=lakedepthscenario2 output=releaseph3


#convert the relase areas 1 and 2 from same raster (solid release)

r.mapcalc --overwrite "releaseph1 = releaseglacier*0.5"

r.mapcalc --overwrite "releaseph2 = releaseglacier*0.5"


#region: set from default and print

g.region -d

g.region -p


#Three phases simulation - solid, solid, liquid (3 phases 1: rock 2: ice 3: water) - with parameters

r.avaflow -a -e -k -v prefix=513 cellsize=12.5 elevation=dem phases=s,s,f
hrelease1=releaseph1 hrelease2=releaseph2 hrelease3=releaseph3
density=2700,1000,1000 friction=35,20,15,12,0,0 viscosity=9999,-9999,12.0,-9999,-
3.0,0,0.0 ambient=0.01,0.075,-7.0,0.0 controls=1,1,0,0,0,0
thresholds=0.5,10000,10000,0.01 time=30,2400
```

3 RESULTS

3.1 GLACIER EVOLUTION

According to the analysis performed in the glacier limit layers comparing the state of the glaciers in 1962 and in 2015, the glacier object of this study has reduced in size from 1055 ha in 1962 to 876 ha in 2015. This means a 17% reduction of the glaciated area in 53 years and a trend of reduction of 3.4 ha per year.

There have been changes in the slope of the terrain the glacier covers, the altitude it is located and the distance the glacier retreated. Table 6 presents a brief statistical summary of the three variables considered to assess the glacier evolution from 1962 to 2015, with the maximum, mean, minimum and standard deviation of the three variables. The slope of the terrain occupied by the glacier maintains the same extreme values, but the mean has been slightly reduced and the dispersion of the values has been reduced too. The glacier has retreated to higher elevations, 214 m higher, consequently a higher mean and lower dispersion values. The distance retreated of the glacier varies from 0 m or no shrink until 1039 m of retreat.

Table 6. Statistical summary of the glacier evolution variables.

		1962	2015
Area (ha)		1055	876
Slope (degrees)	Minimum	0	0
	Mean	25.7	25.3
	Maximum	73	73
	Standard deviation	12.5	11.7
Elevation (m a.s.l.)	Minimum	4136	4350
	Mean	5168.3	5241.8
	Maximum	6135	6135
	Standard deviation	407.8	355.8
Distance retreated (m)	Minimum	0	
	Mean	305.7	
	Maximum	1039	
	Standard deviation	260.2	

A more detailed study of the different variables is following in the next sections.

3.1.1 Slope

As mentioned before the slope values of the glaciated area, both in 1962 and 2015, vary from 0 to 73 degrees. The distribution of these values changes in both time frames. In Figure 13 it is shown the distribution of slope of the terrain that the glacier covered in 1962 and 2015, with a reduction in the area of all or almost all the slope values.

A better representation is obtained with slope categories, as in Table 7 and Figure 14, that shows that the extreme categories, almost flat and specially very high tilt have been reduced in 2015 in comparison with 1962: While the categories in the middle, specially the medium-high values, have increased in percentage in relation to the total change .Table 6 displays that the standard deviation of the slope value distribution in 2015 is lower than in 1962, showing that the dispersion of the values is lower, leading to the same result.

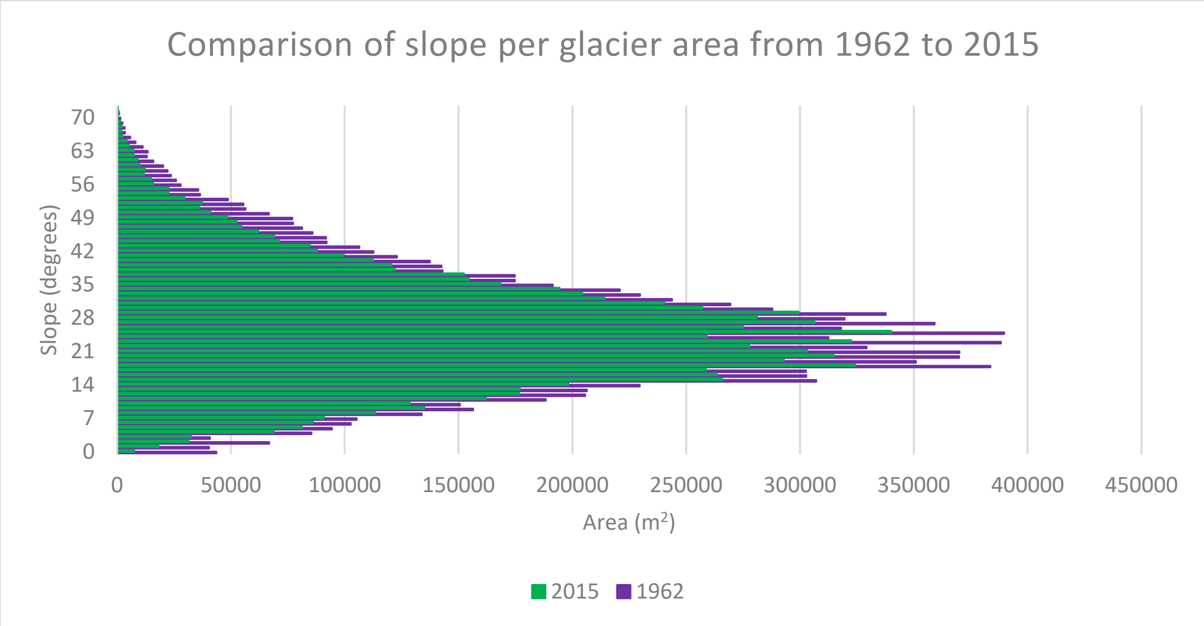

Figure 13. Comparison of the slope value distribution per glaciated area between 1962 (purple) and 2015 (green).

Table 7. Values of the 6 defined slope categories of area and percentage of area from the total comparing the glaciated area in 1962 and 2015.

Categories of Slope	Slope (degrees)	Area 1962 (m^2)	Area 2015 (m^2)	1962 % per total area	2015 % per total area	2015% - 1962%
Nearly flat	0-5	371293	239410	3.5	2.7	-0.8
Under the minimum for debris flow	6-11	836966	716213	7.9	8.2	+0.2
Medium	12-22	3357678	2852749	31.8	32.6	+0.8
Medium-high	23-33	3455485	2999375	32.7	34.2	+1.5
High	34-44	1618488	1367725	15.3	15.6	+0.3
Very high	≥45	911256	582466	8.6	6.7	-2.0
Sum:		10551166	8757938	100	100	

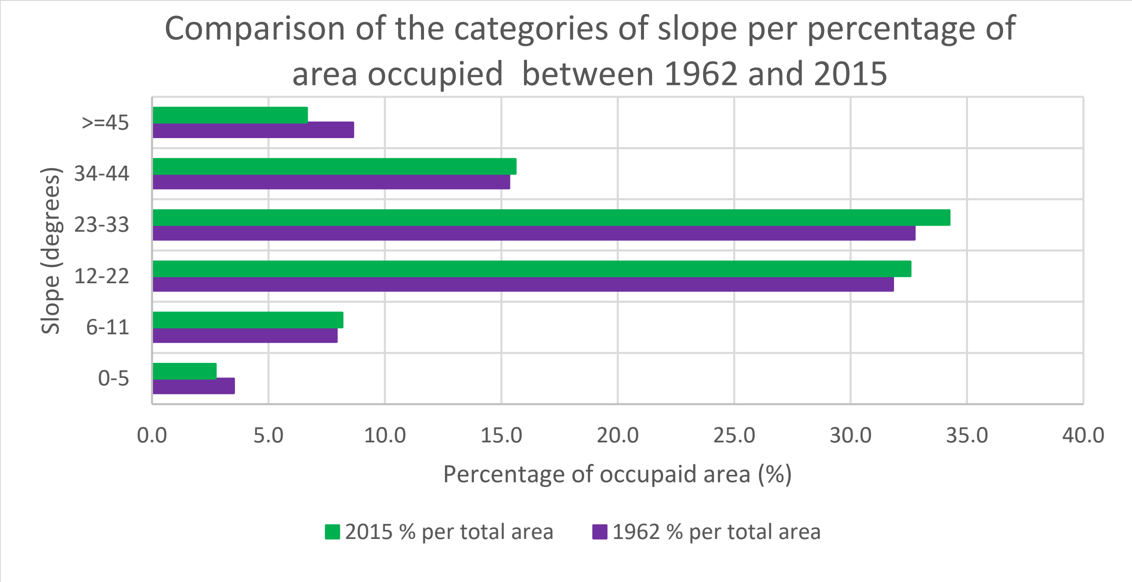

Figure 14. Comparison of the slope categories distribution in percentage of area occupied between 1962 (purple) and 2015 (green).

Taking a closer view, Figure 15 shows the area reduction of the glacier according to the slope values. The biggest reduction can be found in the 18-25 degrees interval approximately. Another large reduction is shown in the very low (approximately lower than 3 degrees) slope values. As it was shown before, the distribution of all the slope values is not uniform, so for a better understanding of the lost area, the percentage of area reduced from the glaciated area in 1962 is calculated. These results are shown in Table 8 and Figure 16. The highest reduction can be seen in both the very low and very high tilt values. The two categories that were less abundant also in 1962, both with a reduction of 36% in relation to 1962. While the intermediate categories have suffered a reduction between 13% and 16% of their glaciated areas.

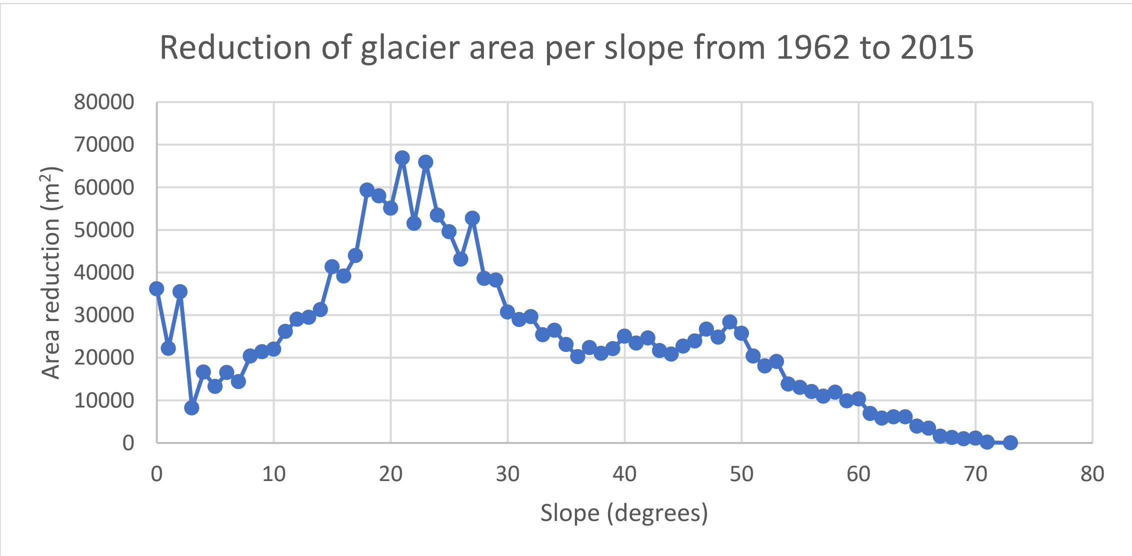

Figure 15. The reduction of glaciated area according to the slope values from 1962 to 2015.

Table 8. Values of the 6 defined slope categories of retreated area and percentage of area retreated from the area in 1962, until 2015.

Categories of Slope	Slope (degrees)	Area retreated (1962 -2015) (m^2)	% retreated from 1962
Nearly flat	0-5	131883	35.5
Under the minimum for debris flow	6-11	120753	14.4
Medium	12-22	504928	15.0
Medium-high	23-33	456110	13.2
High	34-44	250763	15.5
Very high	≥45	328790	36.1

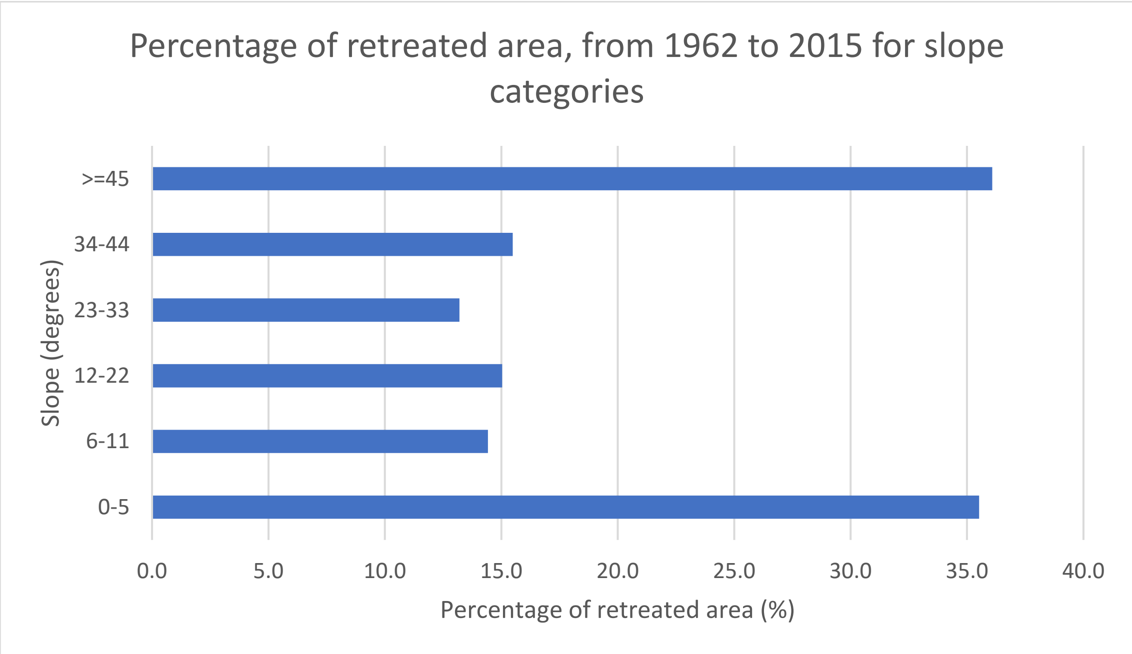

Figure 16. The percentage of retreated area in relation to the area glaciated in 1962 according to the categories of slope defined.

The spatial distribution of this reduction according to slope is presented in Figure 21. It is observed that the major reduction has appeared in the front line of the glacier, where there is a variability of the slopes present, highlighting the disappearance of the glacier in the area where the new lake developed. However there have been retreats of the glacier in other areas of higher altitude and these areas are distinct because they possess high or at least medium high slope values, that can provoke landslides that can lead to disasters downstream.

3.1.2 Elevation

Over the past years, the glacier has retreated to higher elevations. In 1962 it was occupying areas until 4136 m a.s.l. and in 2015, the minimum altitude was 4350. The difference in altitude is 214 m in 53 years, which means an increase in altitude of 4 m per year. The areas retreated have been mostly in low and medium-low altitudes but also some minor reductions in high altitudes as it is shown in the percentage distribution of altitudes in Figure 17 and Table 9. The medium altitudes that were already predominant have become more frequent as shown in Figure 18.

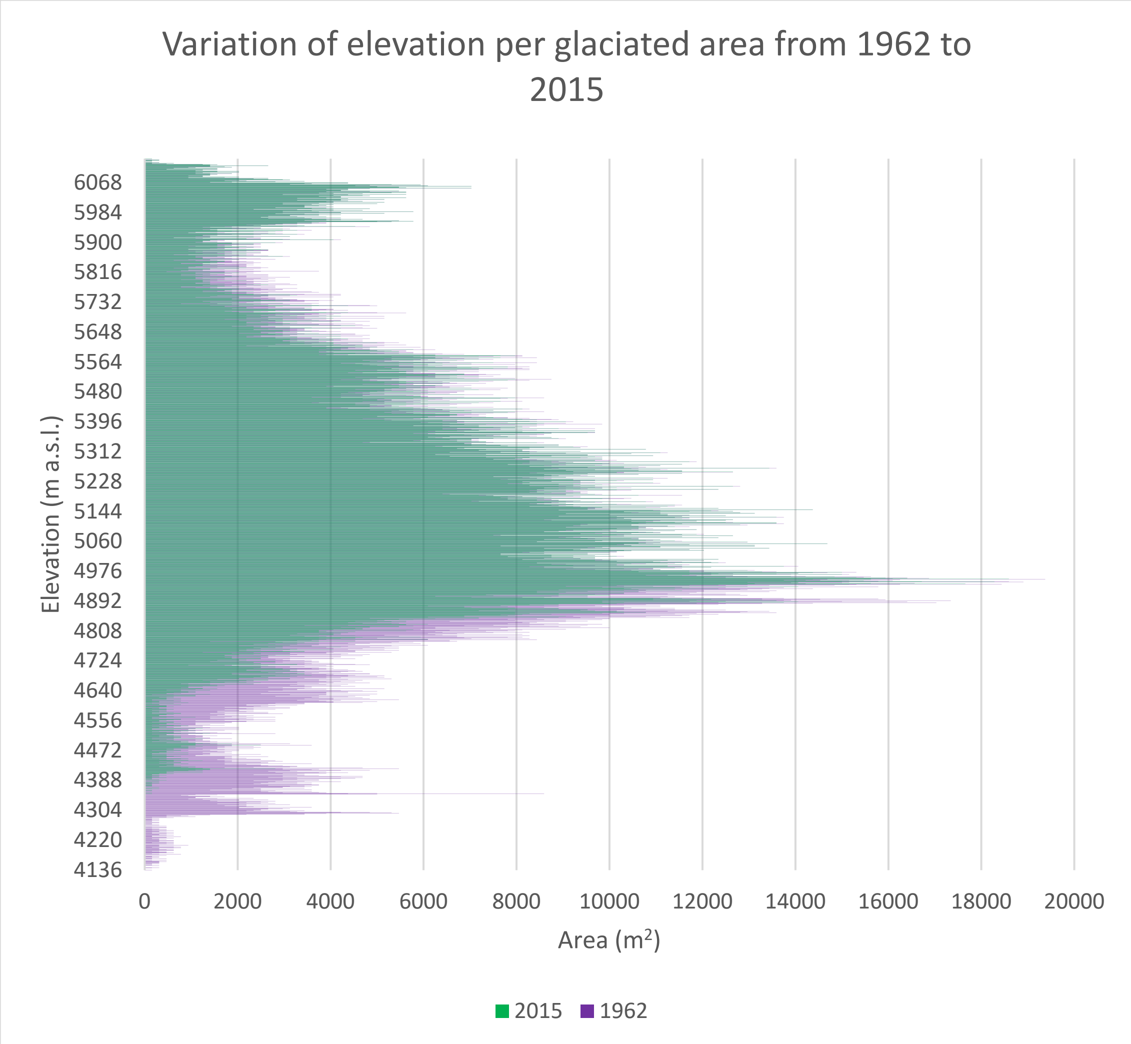

Figure 17. Comparison of the elevation value distribution per glaciated area between 1962 (purple) and 2015 (green).

Table 9. Values of the 6 defined elevation categories of area and percentage of area from the total comparing the glaciated area in 1962 and 2015.

Categories of Elevation (m a.s.l.)	Area 1962 (m^2)	Area 2015 (m^2)	1962 % per total area	2015 % per total area	2015% - 1962%
4136 - 4385	309219	3125	2.9	0.0	-2.9
4386 - 4635	595156	146562.5	5.6	1.7	-4.0
4636 - 4885	1525625	983437.5	14.5	11.2	-3.2
4886 - 5135	2925000	2769375	27.7	31.6	+3.9
5136 - 5385	2250313	2221406	21.3	25.4	+4.0
5386 - 5635	1524531	1405156	14.4	16.0	+1.6
5636 - 5885	699688	514375	6.6	5.9	-0.8
5886 - 6135	724219	712343.8	6.9	8.1	+1.3
Sum:	10553750	8755781	100	100	

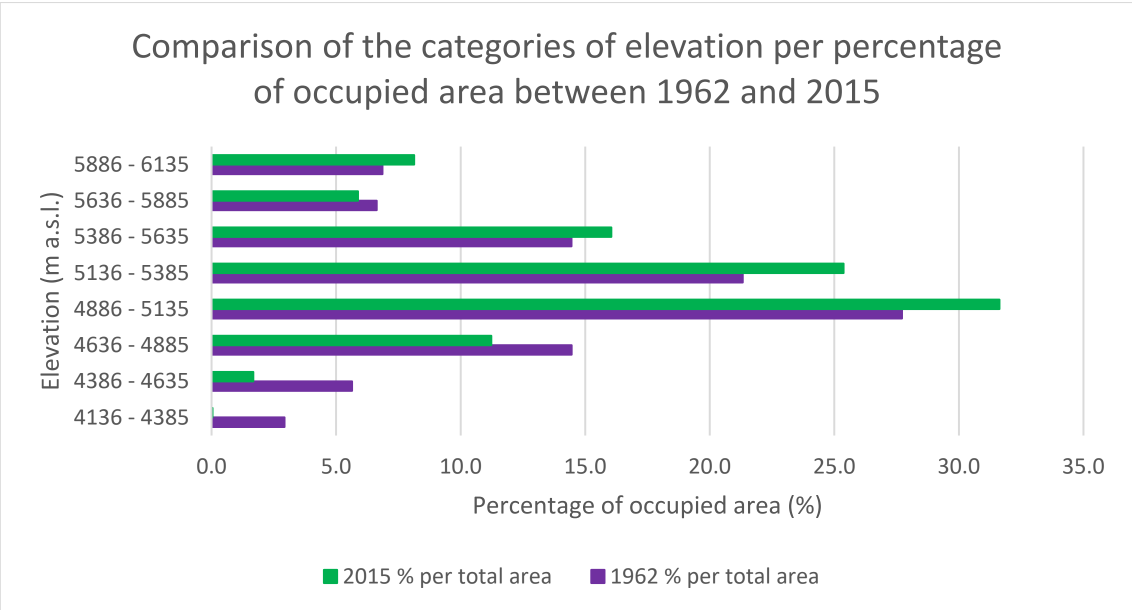

Figure 18. Comparison of the elevation categories distribution in percentage of area occupied between 1962 (purple) and 2015 (green).

Looking now at the reduction of the different elevation values compared to the values present in 1962, it is shown in Figure 19 that the reduced areas have mostly been at altitudes lower than

5000 m a.s.l., which coincides with glacier shrinkage due to warming. The glacier occupying almost 100% of the very low altitudes and 75% of the low altitudes have disappeared. On the other hand, the glacier at an altitude of about 5700 m decreased with 27%, which will be explained looking at the spatial distribution map shown in Figure 22.

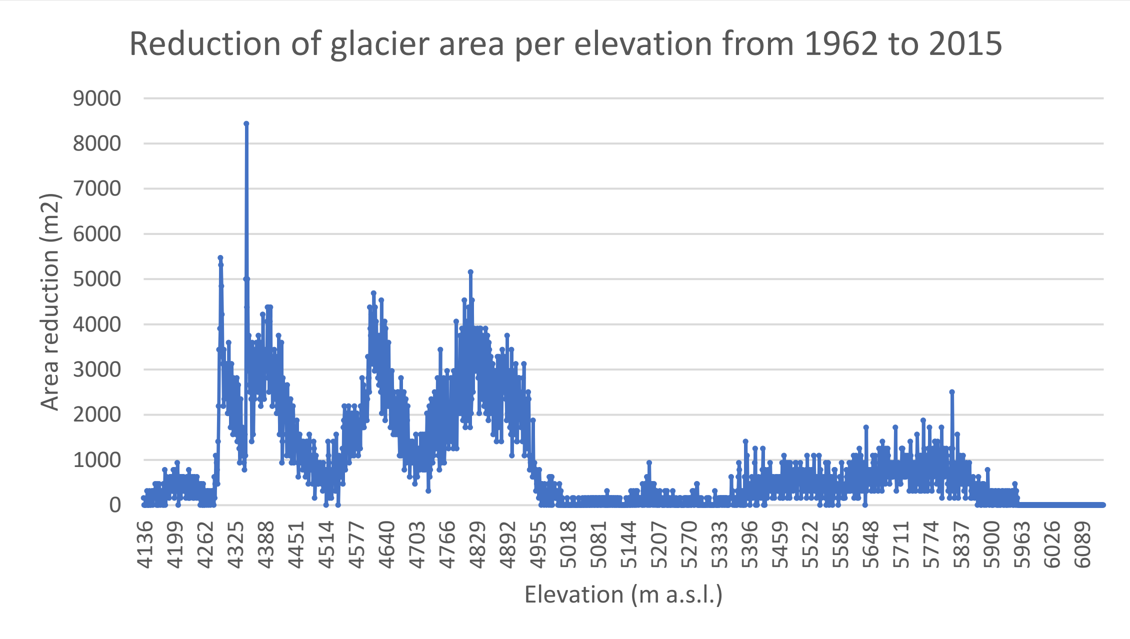

Figure 19. The reduction of glaciated area according to the elevation values from 1962 to 2015.

Table 10. Values of the 6 defined elevation categories of retreated area and percentage of area retreated from the area in 1962, until 2015.

Categories of Altitude (m a.s.l.)	Retreated area (1962 -2015) (m^2)	Retreated percentage from 1962
4136 - 4385	306094	99.0
4386 - 4635	448594	75.4
4636 - 4885	542188	35.5
4886 - 5135	155625	5.3
5136 - 5385	28906	1.3
5386 - 5635	119375	7.8
5636 - 5885	185313	26.5
5886 - 6135	11875	1.6

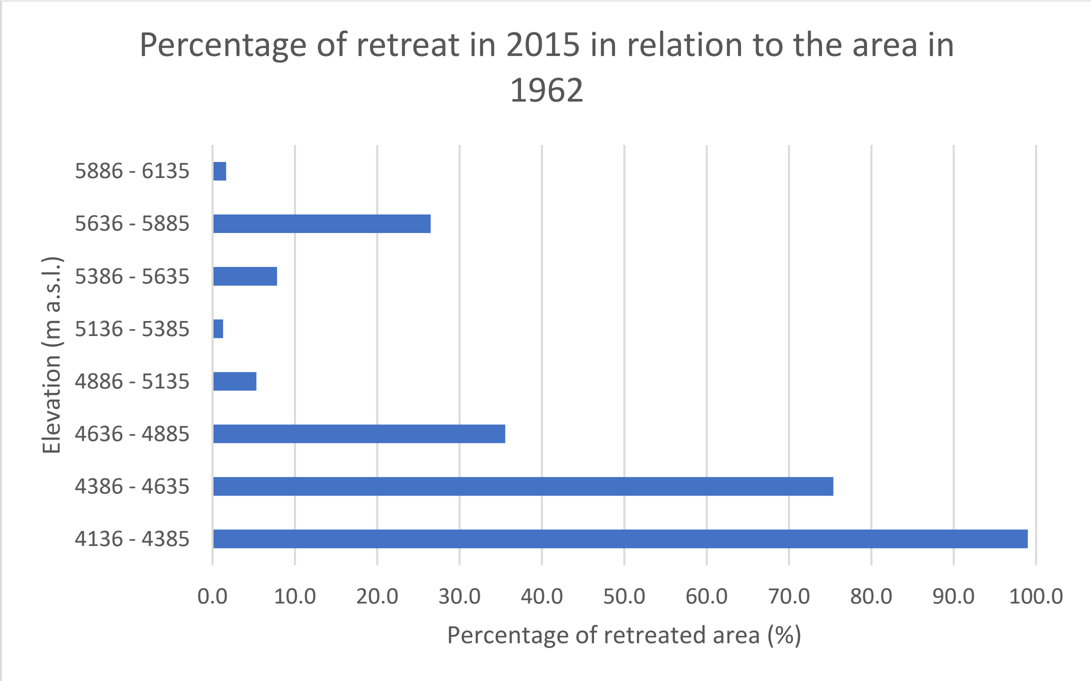

Figure 20. The percentage of retreated area in relation to the area glaciated in 1962 according to the categories of elevation defined.

The spatial distribution of the glacier retreat according to altitude is exhibited in Figure 22. The glacier has retreated from all the lower altitude areas. Additionally, there have been some reductions in higher areas which are explained by the slope values present.

3.1.3 3D Distance

The front line of the glacier has retreated to higher altitudes as it was previously explained. The distance that the glacier has retreated varies between 0 m and 1039 m with an average retreat of 306 m. The maximum of retreated distance has been in an area below the 4500 m that had as a result the formation of Laguna 513 as it is shown in Figure 23. It can also be seen other areas of glacier shrinkage at higher altitudes of the glacier which have not been considered for this study about the retreat distance.

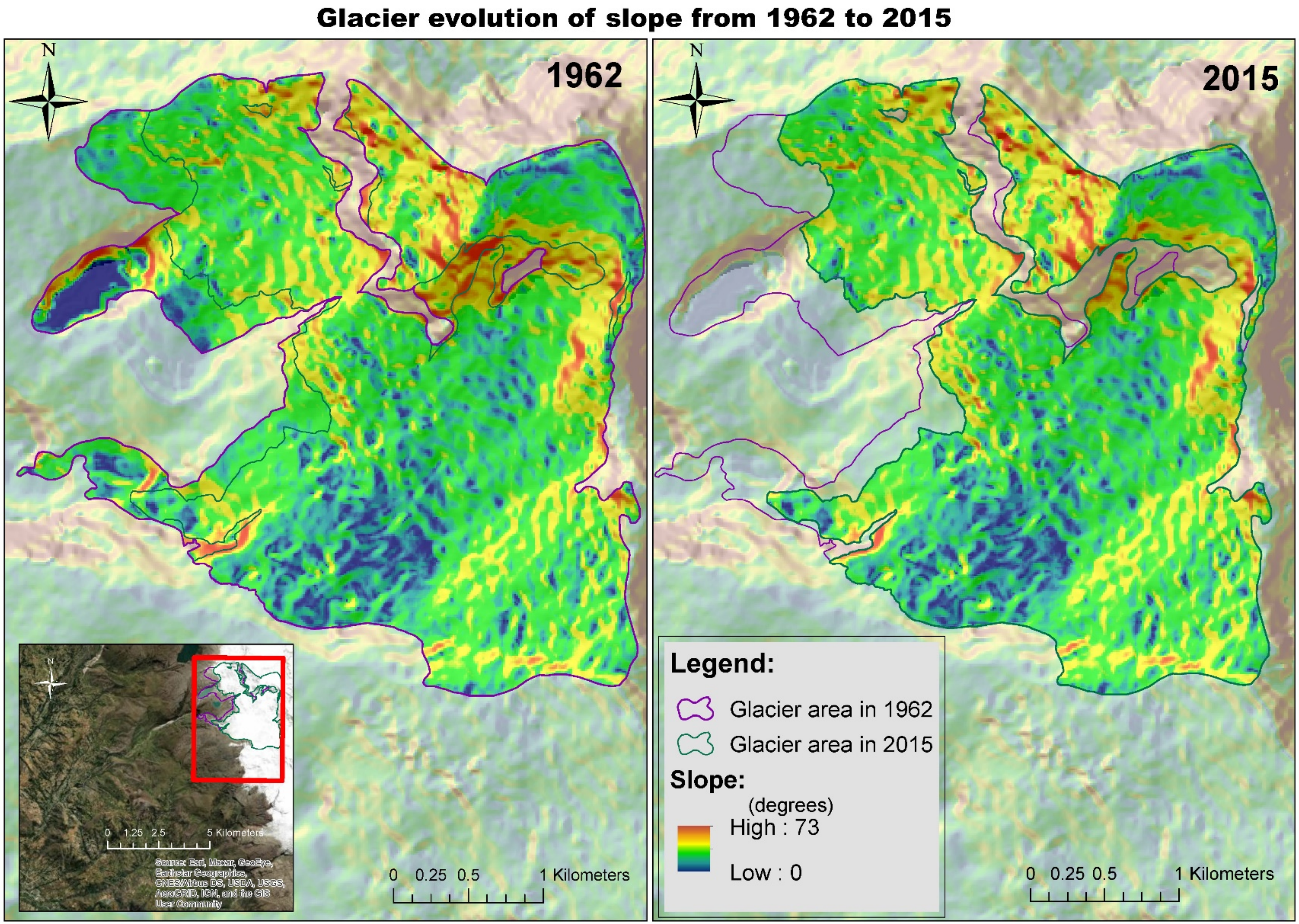

Figure 21. Map of the change in the glacier area according to slope from 1962 until 2015. Done in ArcGIS ArcMap.

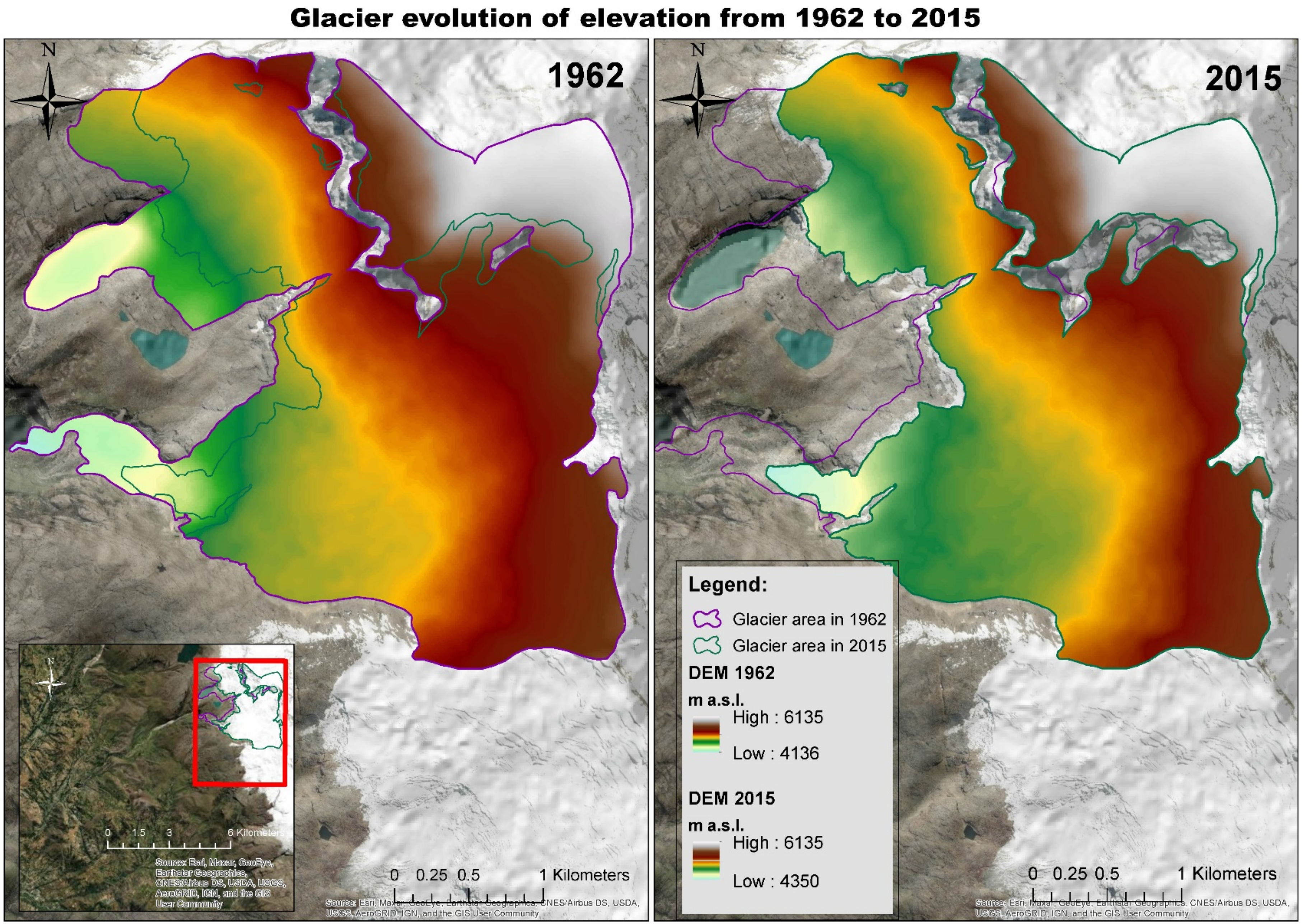

Figure 22. Map of the change of the glacier area according to altitude from 1962 until 2015. Done in ArcGIS ArcMap.

Retreated distance of the glacier from 1962 to 2015

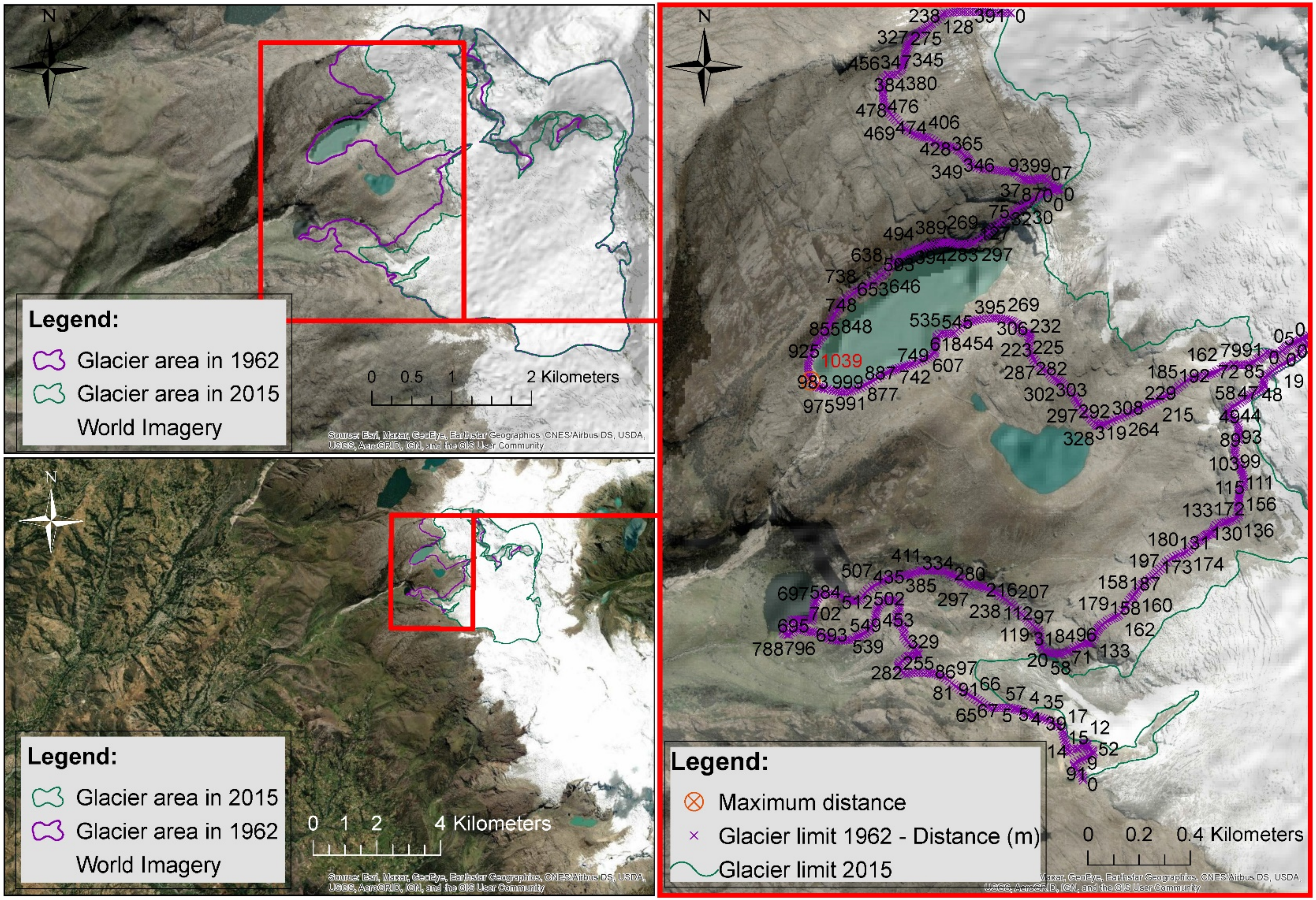

Figure 23. Map of the retreat of the glacier from 1962 to 2015, including the values of distance in meters and the greater retreat point. Done in ArcGIS ArcMap.

3.2 Climate data, scenarios

3.2.1 Historical data

The climate surrounding the lake and the glacier Cochca in mount Nevado Hualcán is a polar climate, a highland climate (H), according to Köppen classification (Aguado and Burt, 2014).

At an altitude of 4450 m a.s.l., where the lake is located, the yearly mean temperature is 4.7°C and the yearly average precipitation is 723 mm. The summer encompass from October to March, with an average temperature of 4.9°C, a mean maximum temperature of 13.3°C and a mean minimum of -3.5°C and a sum precipitation of 594 mm. The winter months, from April to September, have an average temperature of 4.5°C, a mean maximum temperature of 14.0°C and a mean minimum of -5.4°C and a sum precipitation of 132 mm. There are 10 months of humid period and 2 months of arid period in July and August. The climodiagram is represented below in Figure 24 and some additional information in Table 11.

In contrast to the strong seasonal variation in precipitation, the Peruvian Cordilleras are characterized by small seasonal temperature variability. During the dry season, the diurnal variation in air temperature is more pronounced and mean daily air temperatures are lower compared to the wet season (Schauwecker *et al.*, 2017).

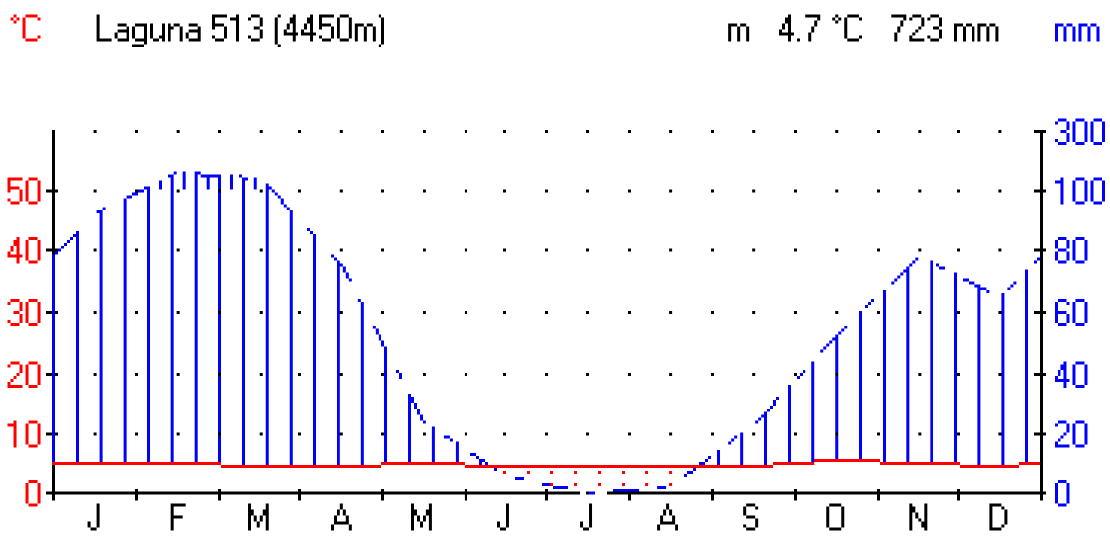

Figure 24. Climodiagram of the Lake Laguna 513 and surroundings, latitude 9.25° S and longitude 77.75° W for the time period 1961 a 2019 (58 years). Elaborated in Kima 0.9® with CRU data

Table 11. Monthly climate data of the Lake Laguna 513 and surroundings, latitude 9.25° S and longitude 77.75° W and altitude 4450 m, for the time period 1961 a 2019 (58 years). Elaborated in Kima 0.9® with CRU data.

Month	Tmax	Tmin	Precip	Tmean	Humidity
January	11.8	-2.1	92	4.8	humid
February	11.7	-2.0	164	4.8	humid
March	11.8	-2.4	142	4.7	humid
April	12.2	-2.8	75	4.7	humid
May	13.6	-3.7	24	5.0	humid
June	14.0	-5.4	6	4.3	humid
July	13.9	-5.3	0	4.3	arid
August	13.8	-4.8	2	4.5	arid
September	12.7	-4.1	23	4.3	humid
October	13.3	-2.8	52	5.3	humid
November	13.1	-3.4	78	4.8	humid
December	12.7	-3.5	65	4.6	humid

A closer view on the temperatures, according to the monthly distribution of temperatures (Figure 25), the maximum and the minimum values appear during the winter months, thus winter has a greater variability in temperatures with an inferior average temperature.

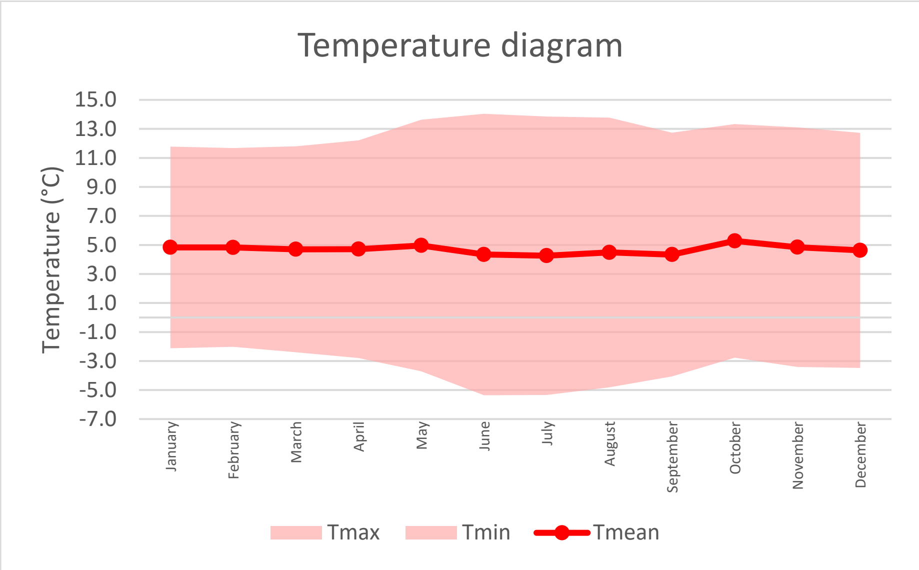

Figure 25. Temperature diagram with montly values of Tmean, Tmax and Tmin estimated for Laguna 513 for the time period 1961 a 2019 (58 years).

Trends:

From the year 1961 until 2019, it is shown that the trendline of temperatures and precipitation has a slight increase (Figure 26). For the annual temperature the increase is 0.13°C per decade, for the three temperature variables. For the summer temperature the increase is 0.12°C per decade. It is also represented that the mean temperatures are very similar for the summer and the annual temperatures, while the mean minimum temperatures present a larger variation between the summer and the annual ones. The annual precipitations have an increase of 25 mm per decade while the summer precipitation increases 27 mm per decade, which occurs in the rainy season.

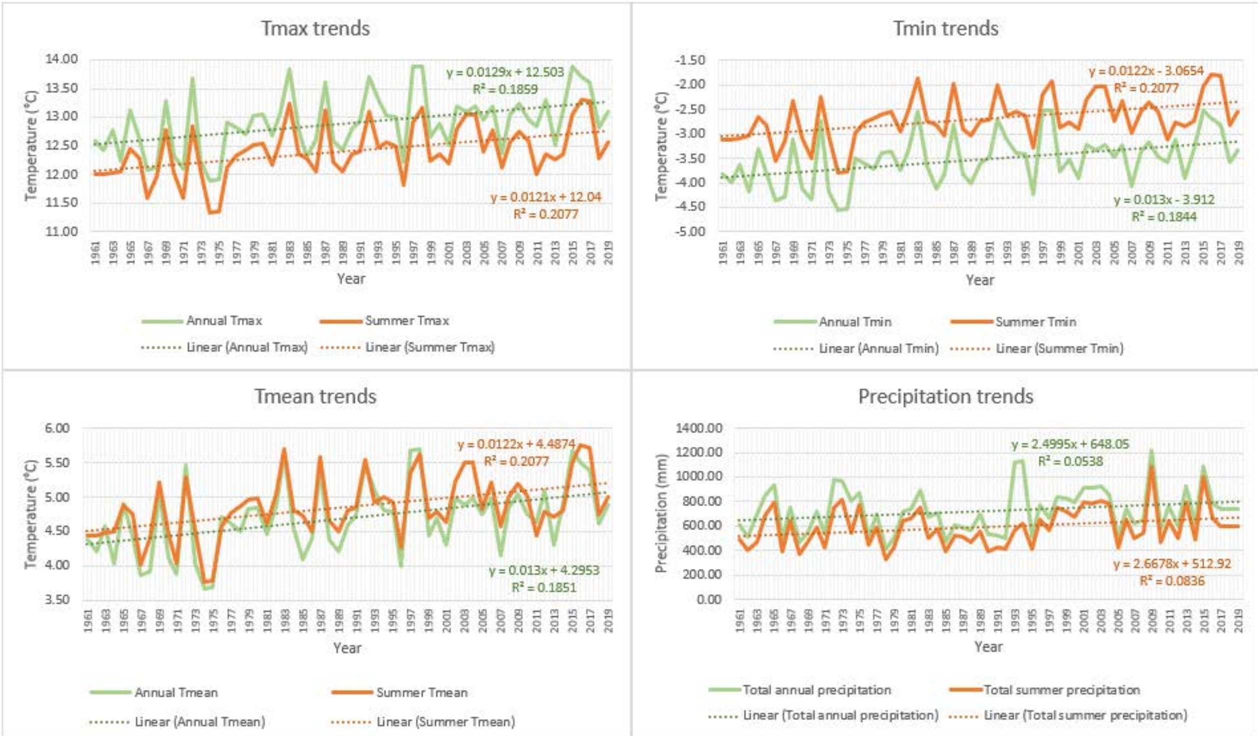

Figure 26. The annual and summer trends of the 4 studied variables for the period 1961 until 2019.

<u>Spatial variability:</u>

The spatial variability of the climatic variables is shown in Figure 27 and Figure 28. The grids 3, 5, 6 and 8 contain Cordillera Blanca, the highest mountain range of the area. These grids present the lower temperatures of all, both the Tmax and Tmin due to the high altitudes. The lowest temperature appears on the grid with the highest altitude, located South-east of the study area. On the west side the grids are in lower altitudes and in a closer distance to the coast, specially grids 1 and 4, being more influenced by the Pacific Ocean. These areas present the highest temperatures with the highest in the lowest altitude and decreasing with the elevation increase and the most scarce precipitations. On the East side of Cordillera Blanca an area with intermediate altitudes is located, very similar to the area South of the study area, with a similar altitude. These two areas present middle values of temperature, similar to each other but different average monthly precipitations values, presenting more abundant precipitations the area located more inland. The area with the most abundant precipitations is located East from the study area, containing part of the Cordillera Blanca and part of lower areas on the East side of this high mountain range.

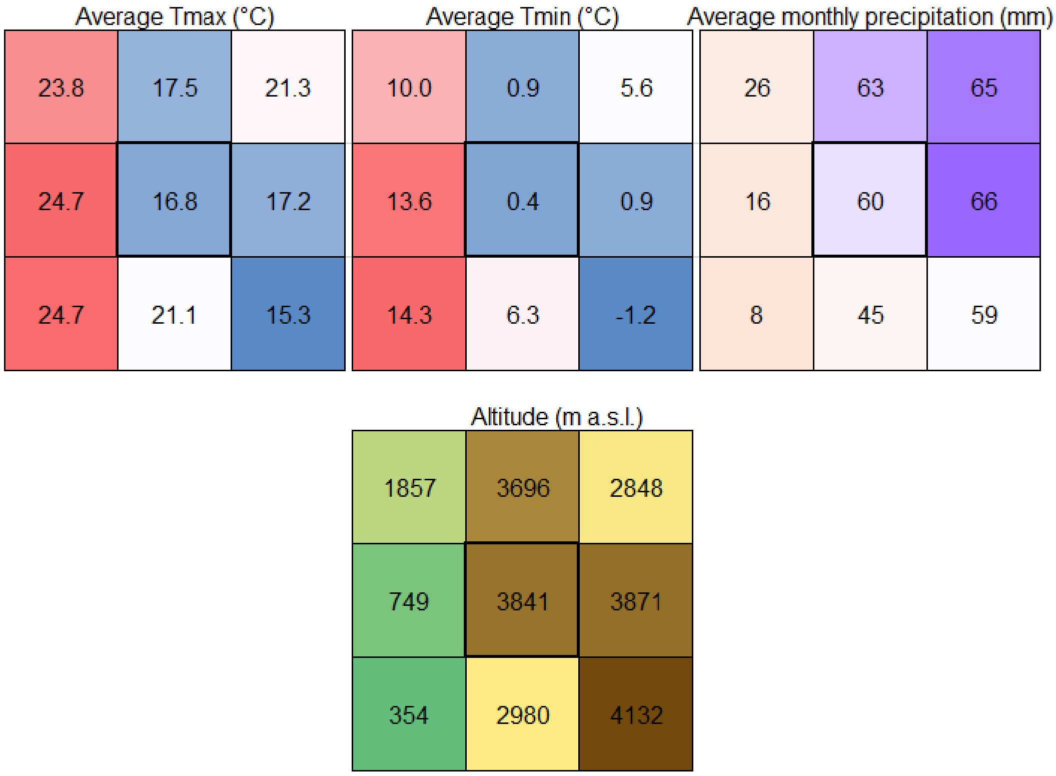

Figure 27. Spatial variability of Tmax, Tmin and Precipitation and altitude of these values organised in the 9 grids of CRU data.

Represenation of the 9 grids for CRU data

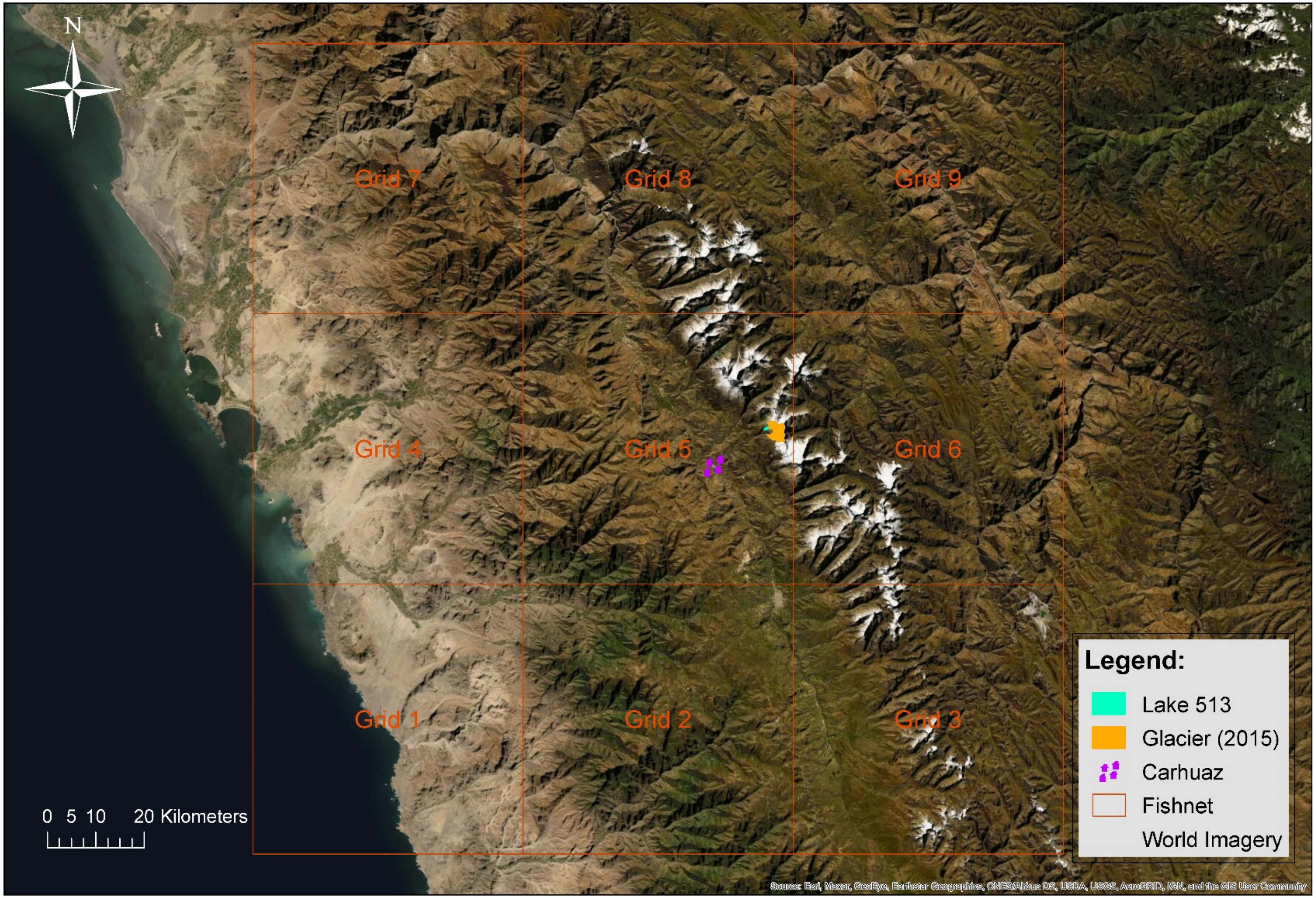

Figure 28. Map of the distribution of 9 grids from the coordinate values of the CRU data, the middle one contains the study area.

ENSO correlation:

The fluctuation of El Niño-Southern Oscillation affects the climate in the tropical zone including the area object of this study. To assess the extent of this interaction, a study of the correlation has been made. In Figure 29 it is shown the annual evolution of the mean temperatures together with the bimonthly ENSO Index. The positive and negative peaks are mostly correlated in the two variables. The extreme ENSO conditions increase bimonthly temperatures by 2 °C. To get a more quantitative insight into this relation, the data has been represented in a scatter graph (Figure 31) that shows the increasing trend in the data as well as a linear regression fit which provides a coefficient of determination R-square equal to 0.4514, this value can vary between 0 (no linear correlation between the variables) and 1 (complete correlation between them), in this case the coefficient shows a significant correlation between the temperature in the area with the El Niño phenomenon. Additionally, an analysis processed for the same time scale as ENSO data set has been performed. Figure 30 and Figure 32 show the corresponding results. In the second figure, the temperature has been represented as anomalies in relation to the average temperature of the time frame. In the case of both figures, the bimonthly data has a larger variability and hence presents a lower correlation of the two variables with a value of 0.3312.

Also, the correlation between the bimonthly data of both variables has been assessed by computing the Pearson correlation coefficient and the corresponding p-value. The result for the correlation coefficient R=0.5755 coincides with the result calculated by linear regression (R-squared=0.3312) and a p-value of $1.2*10^{-47}$ was obtained what indicates a strong evidence again the null hypothesis, thus confirming than the correlation is significant.

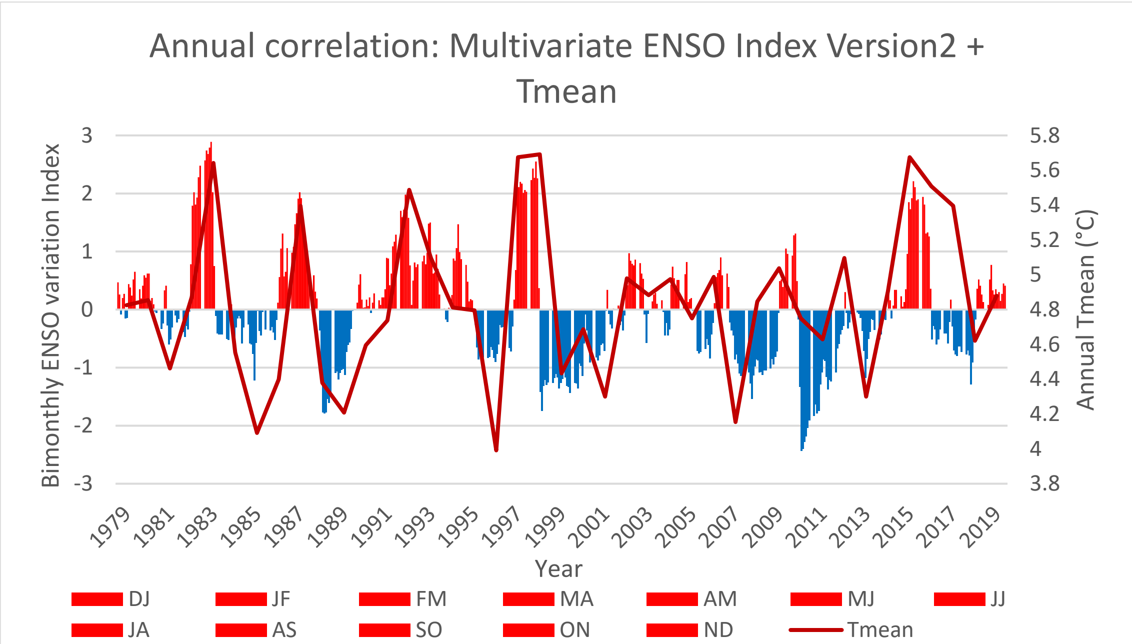

Figure 29. Comparison of the interconexion of the bimonthly Multivariate ENSO Index v2 and the annual average of mean temperature. Negative values of ENSO Index (La Niña) are represented in blue.

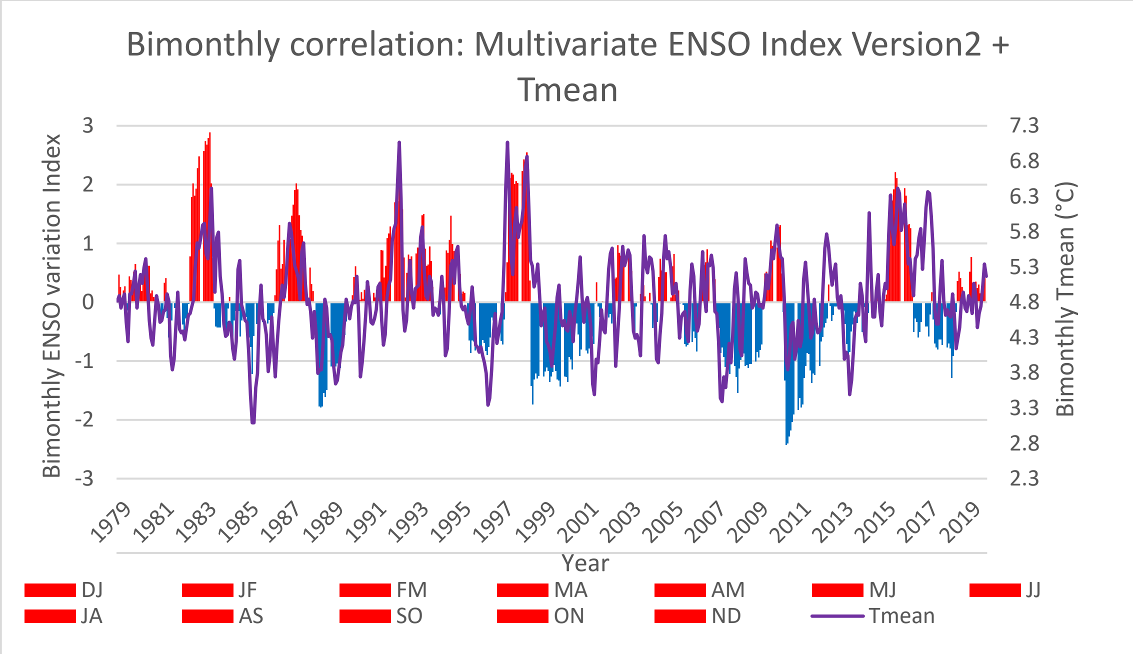

Figure 30. Comparison of the interconexion of the bimonthly Multivariate ENSO Index v2 and the bimonthly mean temperature. Negative values of ENSO Index (La Niña) are represented in blue.

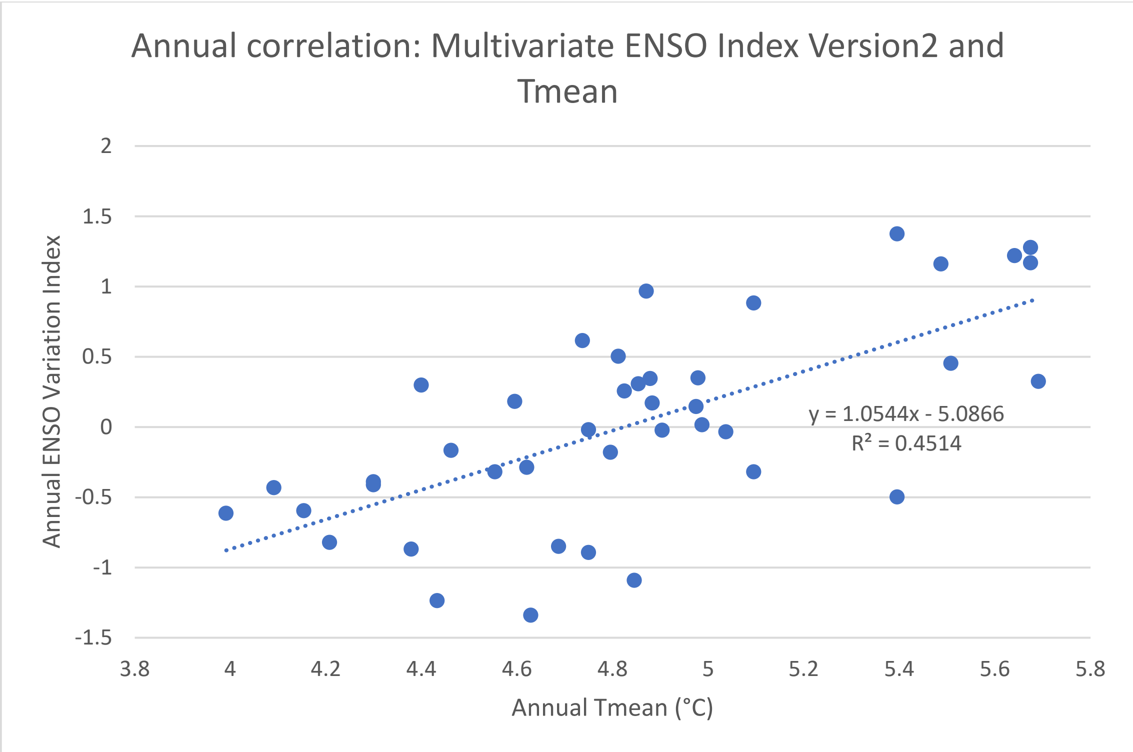

Figure 31. Annual Multivariate ENSO Index v2 versus the mean temperature after height correction of the study area, showing the correlation between the two variables. The trend is adjusted by a linear regression with a coefficient of determination R-square of 0,4514.

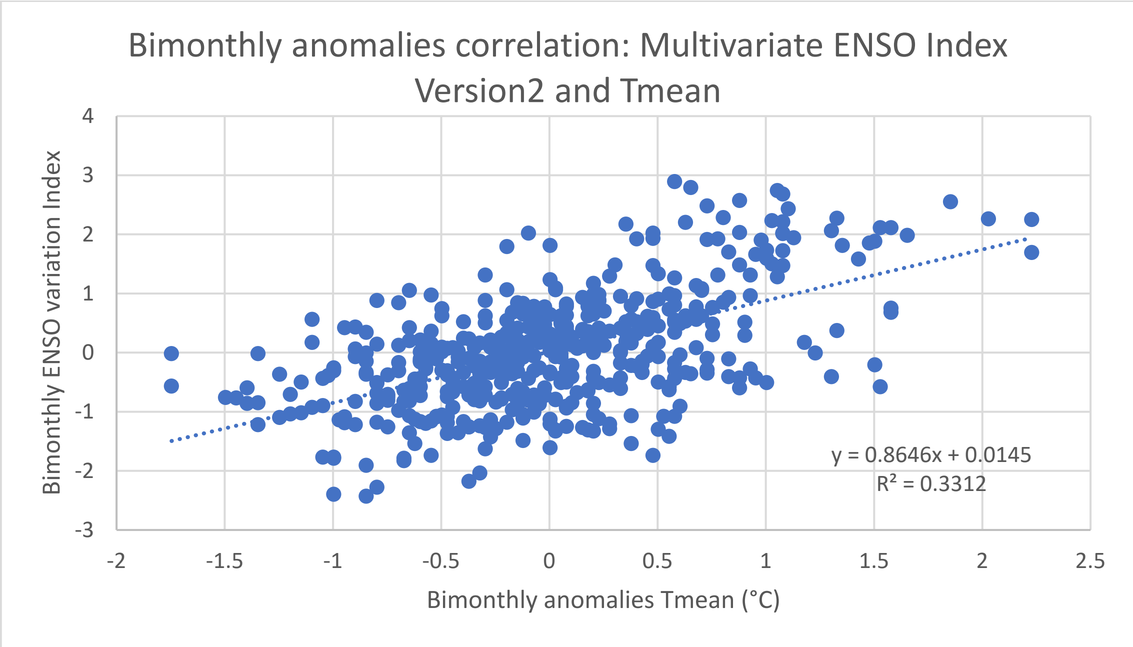

Figure 32. Bimonthly Multivariate ENSO Index v2 versus the anomalies in the mean temperature comparing with the average Tmean after height correction of the study area, showing the correlation between the two variables. The trend is adjusted by a linear regression with a coefficient of determination R-square of 0,3312.

Tropical glaciers are highly sensitive to temperature changes during the rainy season, this is because a shift in the snowline highly impacts the snow accumulation. This is even more relevant as in this area there is typically no variation in the temperature along the year, so the ENSO effect is even stronger than the seasonal cycle. To check this phenomenon, a bimonthly analysis of the summer months which correspond to the rainy season has been performed. The results are shown in Figure 33 and a more quantitative analysis in Figure 34. The results show a significant correlation between the two variables. The coefficient of determination R-square is 0.4471, which compared with the bimonthly analysis of the whole year in which the R-square was 0.3312, there is a stronger effect of ENSO in the temperature during the summer months (rainy season) than during the dry winter months, which can lead into a change in the snowline and consequently, snow accumulation.

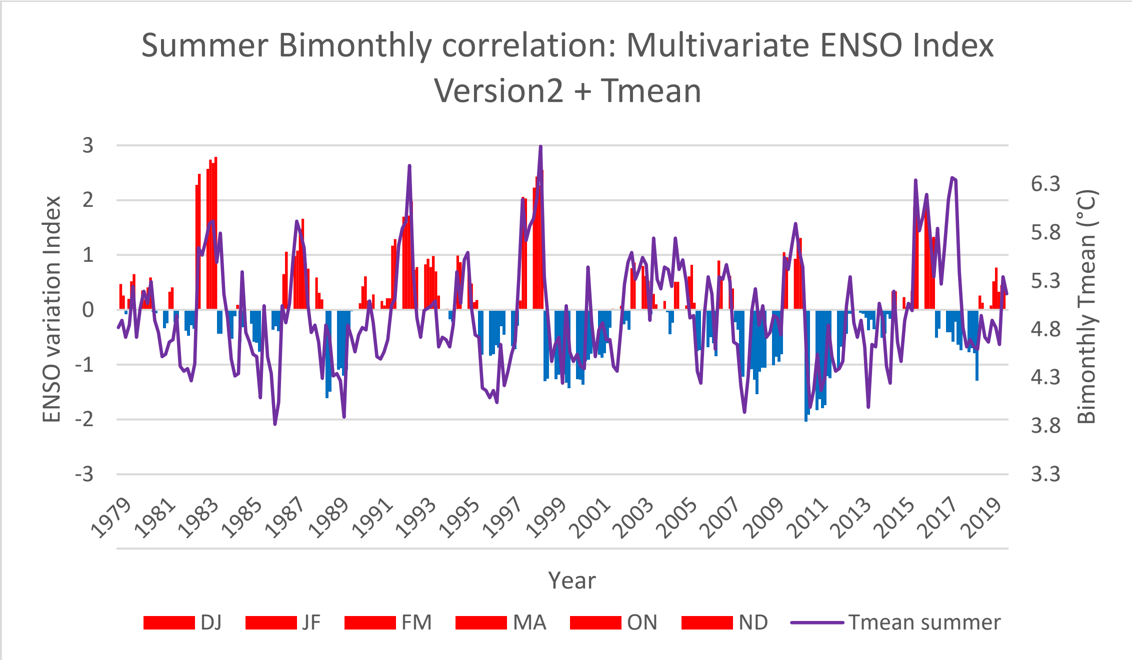

Figure 33. Comparison of the interconexion of the bimonthly Multivariate ENSO Index v2 and the bimonthly mean temperature during the summer months. Negative values of ENSO Index (La Niña) are represented in blue.

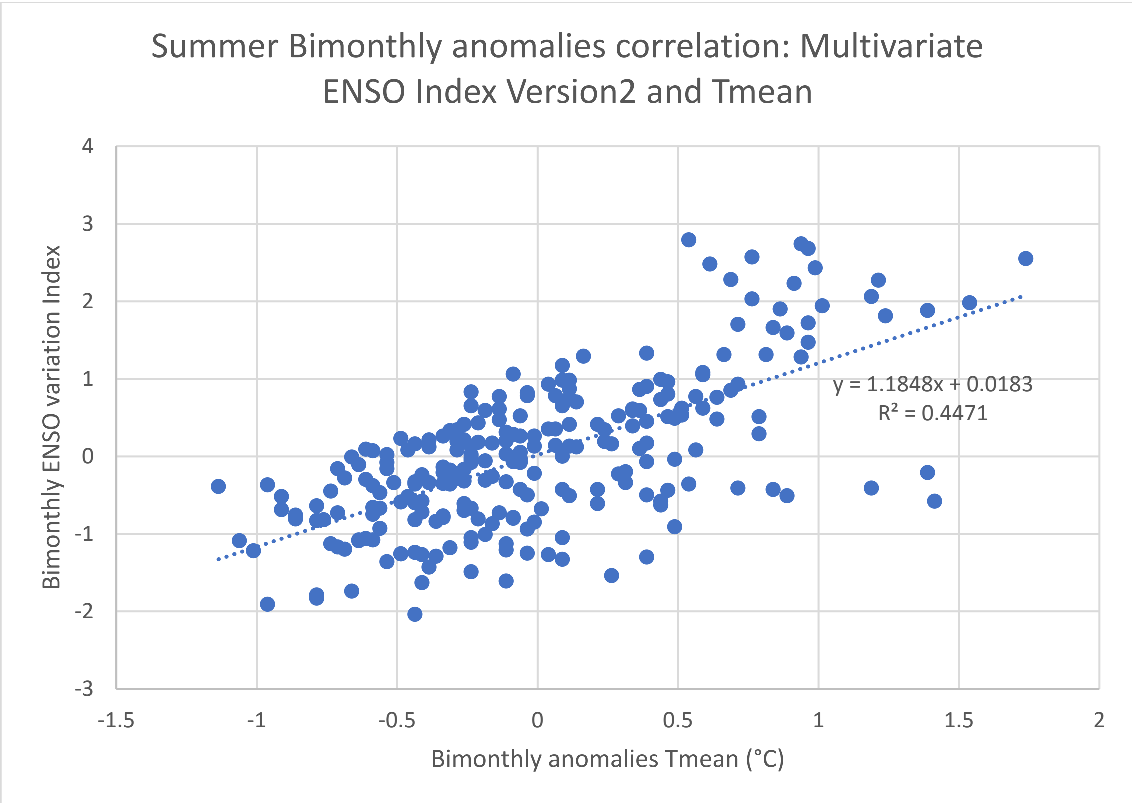

Figure 34. Bimonthly Multivariate ENSO Index v2 versus the anomalies in the mean temperature comparing with the average Tmean after height correction of the study area, showing the correlation between the two variables during the summer months. The trend is adjusted by a linear regression with a coefficient of determination R-square of 0,4471.

The bimonthly correlation with the precipitation is also performed. The results are shown in Figure 35 and Figure 36 and show no significant correlation between the two variables with a R-square value of 0.00007. A further analysis of the effect of ENSO during the summer months is also carried out and the results are shown in Figure 37 and Figure 38, which likewise do not show a correlation, with a R-square value of 0.0005. As a conclusion, there is no evidence of a significant correlation between ENSO and the precipitation in the study area.

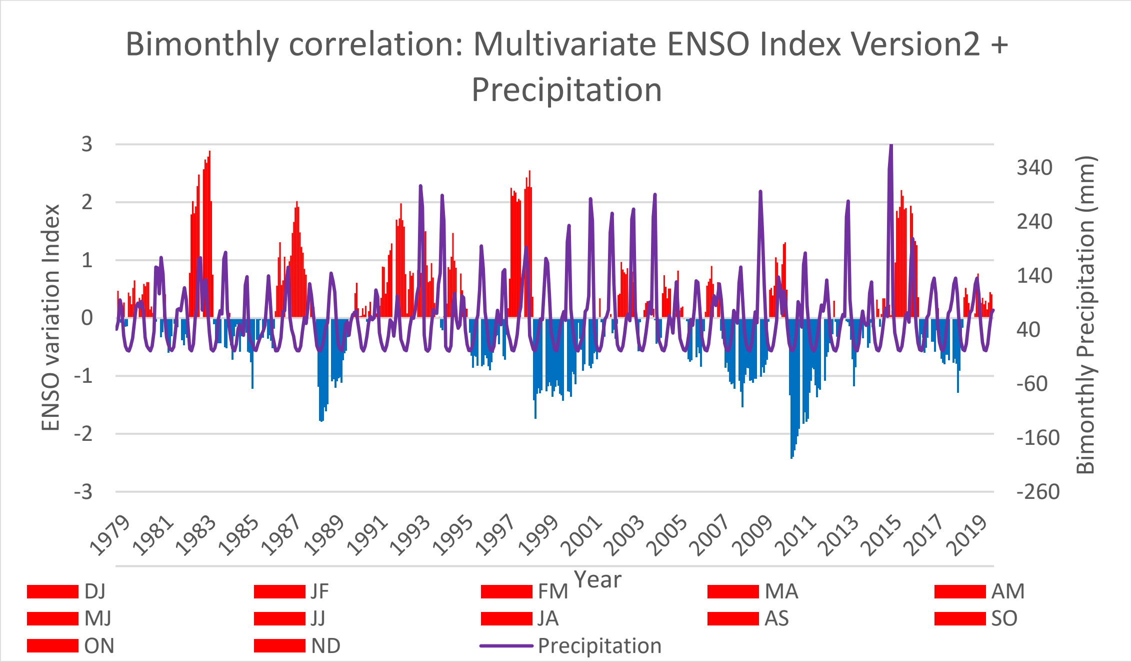

Figure 35. Comparison of the interconexion of the bimonthly Multivariate ENSO Index v2 and the bimonthly precipitation. Negative values of ENSO Index (La Niña) are represented in blue.

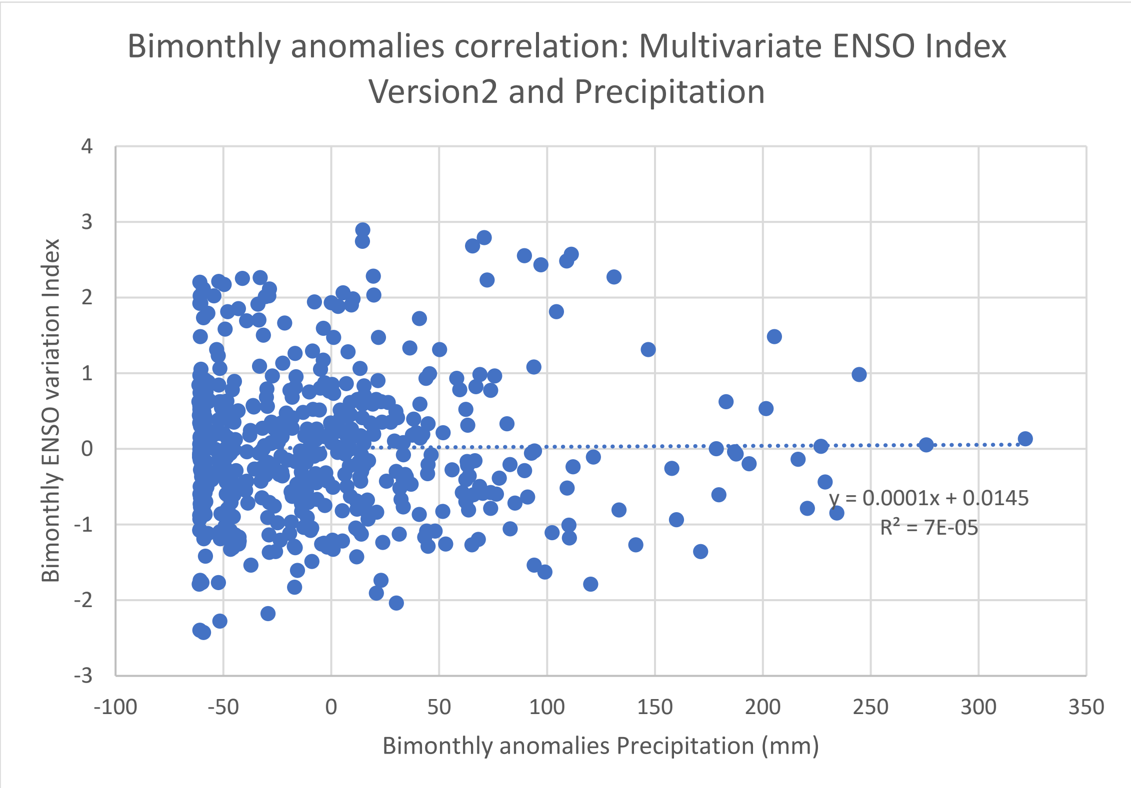

Figure 36. Bimonthly Multivariate ENSO Index v2 versus the anomalies in the precipitation, showing the correlation between the two variables. The trend is adjusted by a linear regression with a coefficient of determination R-square of 0,00007.

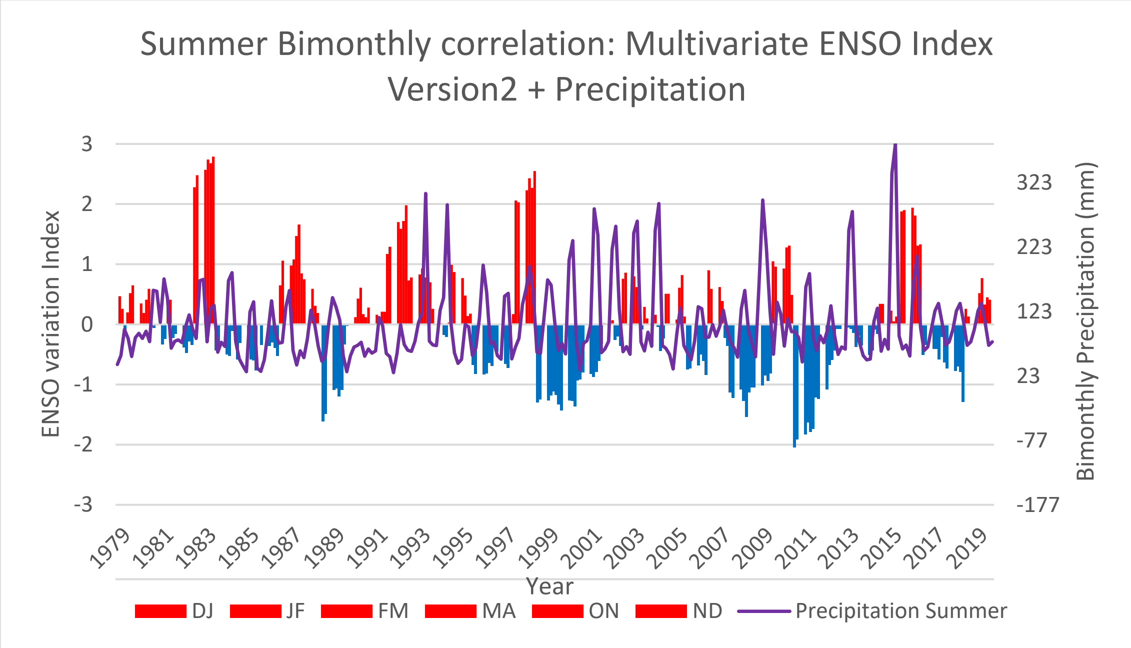

Figure 37. Comparison of the interconexion of the bimonthly Multivariate ENSO Index v2 and the bimonthly precipitation during the summer months. Negative values of ENSO Index (La Niña) are represented in blue.

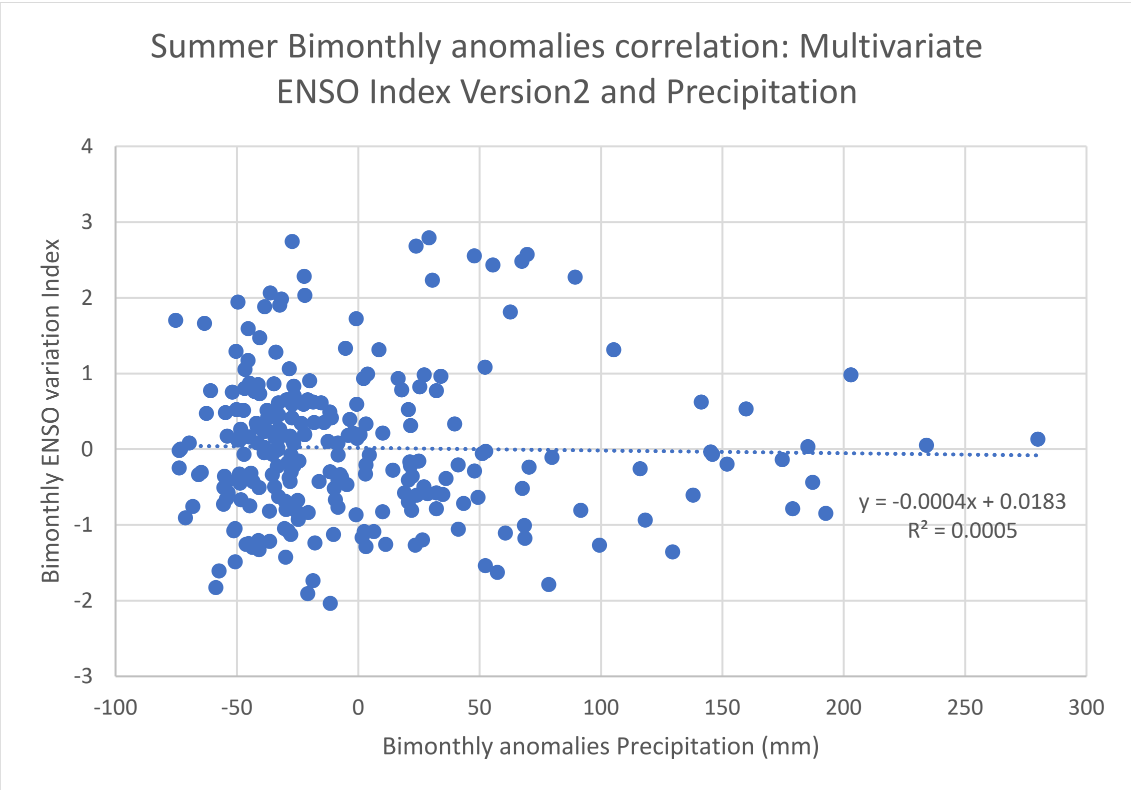

Figure 38. Bimonthly Multivariate ENSO Index v2 versus the anomalies in the precipitation showing the correlation between the two variables during the summer months. The trend is adjusted by a linear regression with a coefficient of determination R-square of 0,0005.

3.2.2 Future scenario projections

In order to evaluate future risks and an adequate resilience and adaptation, GCM projections constitute an advanced and adequate tool. However, they usually suffer from limitations that produce outputs different from the observed data and consequently need an adequate bias correction. Figure 39 displays projected values of monthly mean temperature and precipitation for Lake Laguna 513 and surroundings, during a period of 58 years, from 2020 until 2078 (as the climodiagram of observed data in Figure 24, to make them comparable). The projected data is the raw data together with their corrected values after height and bias correction (BC), taking as reference the CRU observed data after height correction (HC). The applied correction methods have been Linear Scaling (LS) for both temperature and precipitation. The results clearly show the need of bias correction as well as the acceptable performance of the correction.

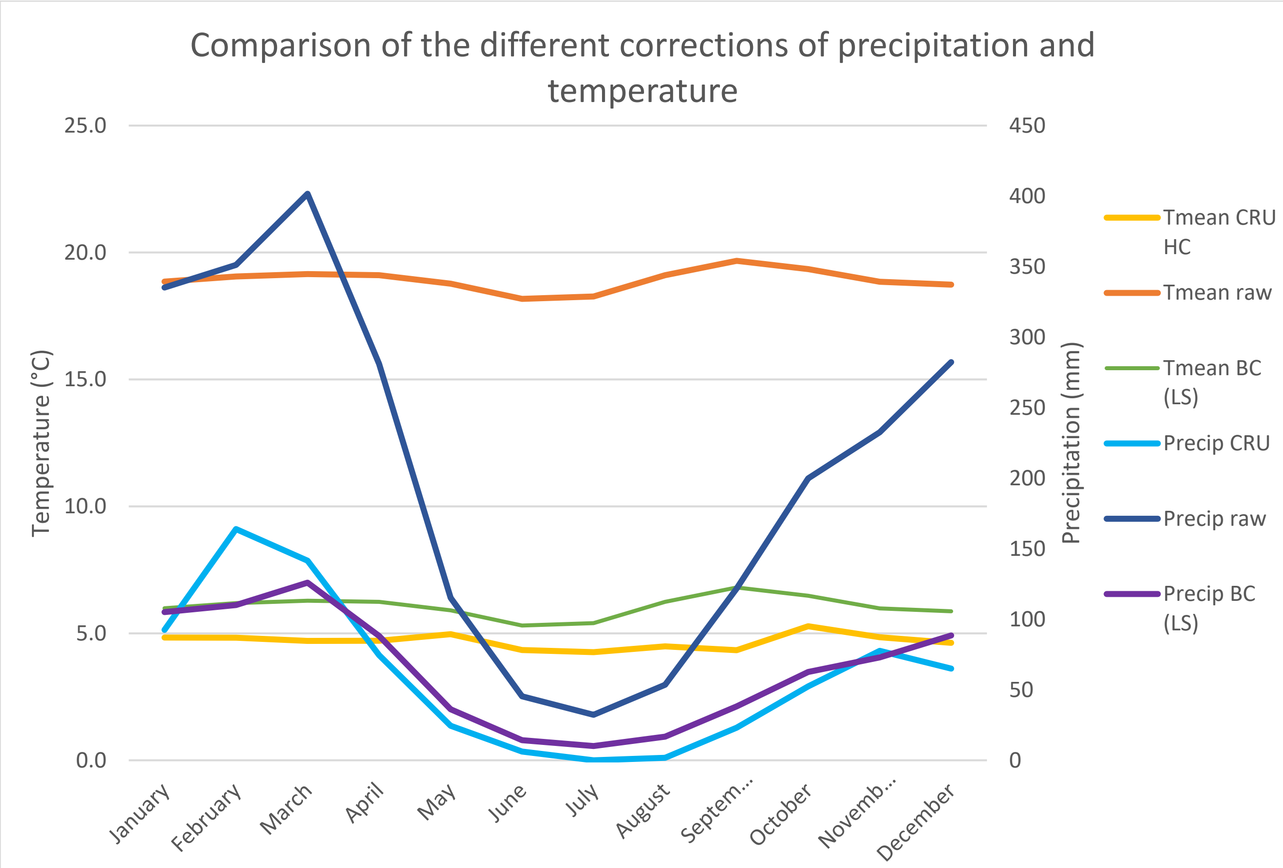

Figure 39. Bias correction of monthly mean temperature and precipitation using Linear Scaling (LS) correction for both variables together with the raw data and taking as reference the CRU observed data.

<u>Predictions:</u>

According to GCM future projections, it is expected an increase in the temperature and in the summer precipitation till 2100. The increase in the mean temperature is projected to be 2.5 °C for the scenario SSP245 and 5.9 °C for the scenario SSP585 per century, according to the Linear Scaling method (Figure 40). The precipitation in summer, the rainy season, is also expected to increase, with values of 14 mm per month for the scenario SSP245 and 28 mm per month for the scenario SSP585 per century (Figure 41).

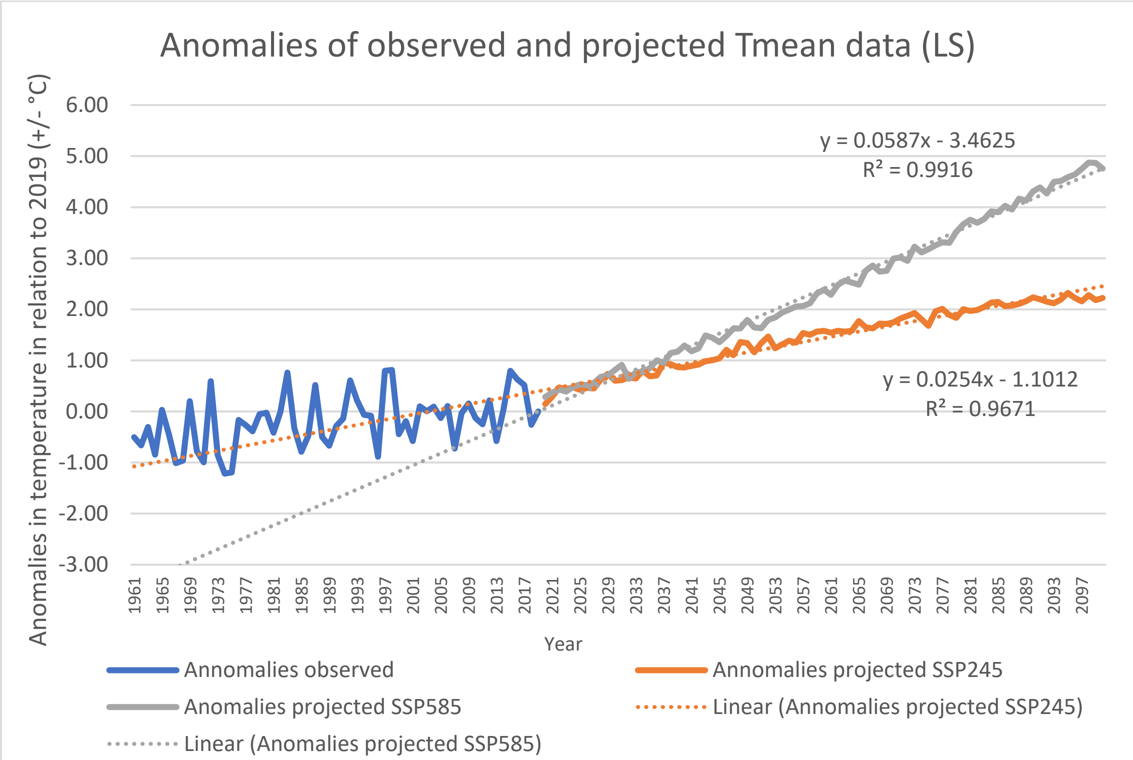

Figure 40. Anomalies of annual mean temperature values, in the periods from 1961 to 2019 (observed data) and from 2020 to 2100 (projected SSP245 and SSP585 data, corrected using Linear Scaling (LS) method).

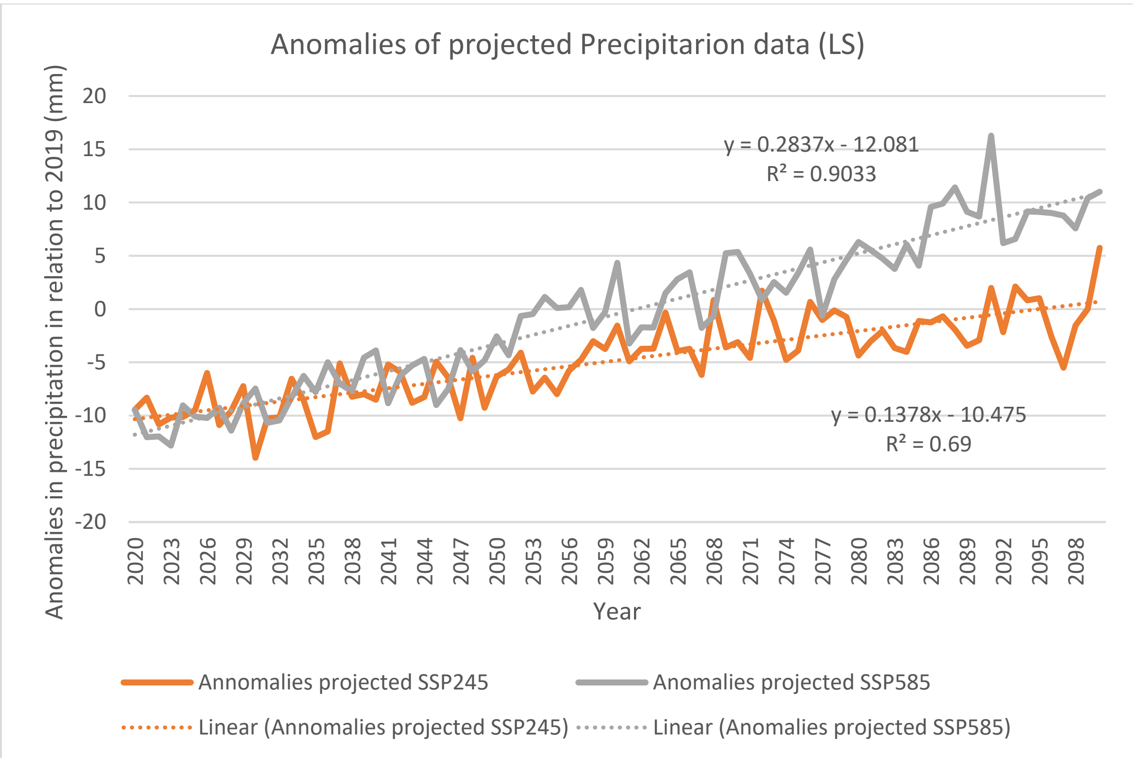

Figure 41. Anomalies of summer precipitation values [mm/month] from 2020 to 2100 (projected SSP245 and SSP585 data, corrected using Linear Scaling (LS) method)

3.3 Mass flow simulation of a GLOF event

3.3.1 Study area surface / Digital Elevation Model

The Digital Elevation Model of the study area utilized for the simulation is offered in Figure 42. It presents a resolution of 12.5 m, the lowest altitude of the study area is 2592 m a.s.l. and the highest it reaches is 6173 m a.s.l. The glacier Cochca covers almost all the highest altitudes and the city of Carhuaz is located in the lowest altitudes of the valley.

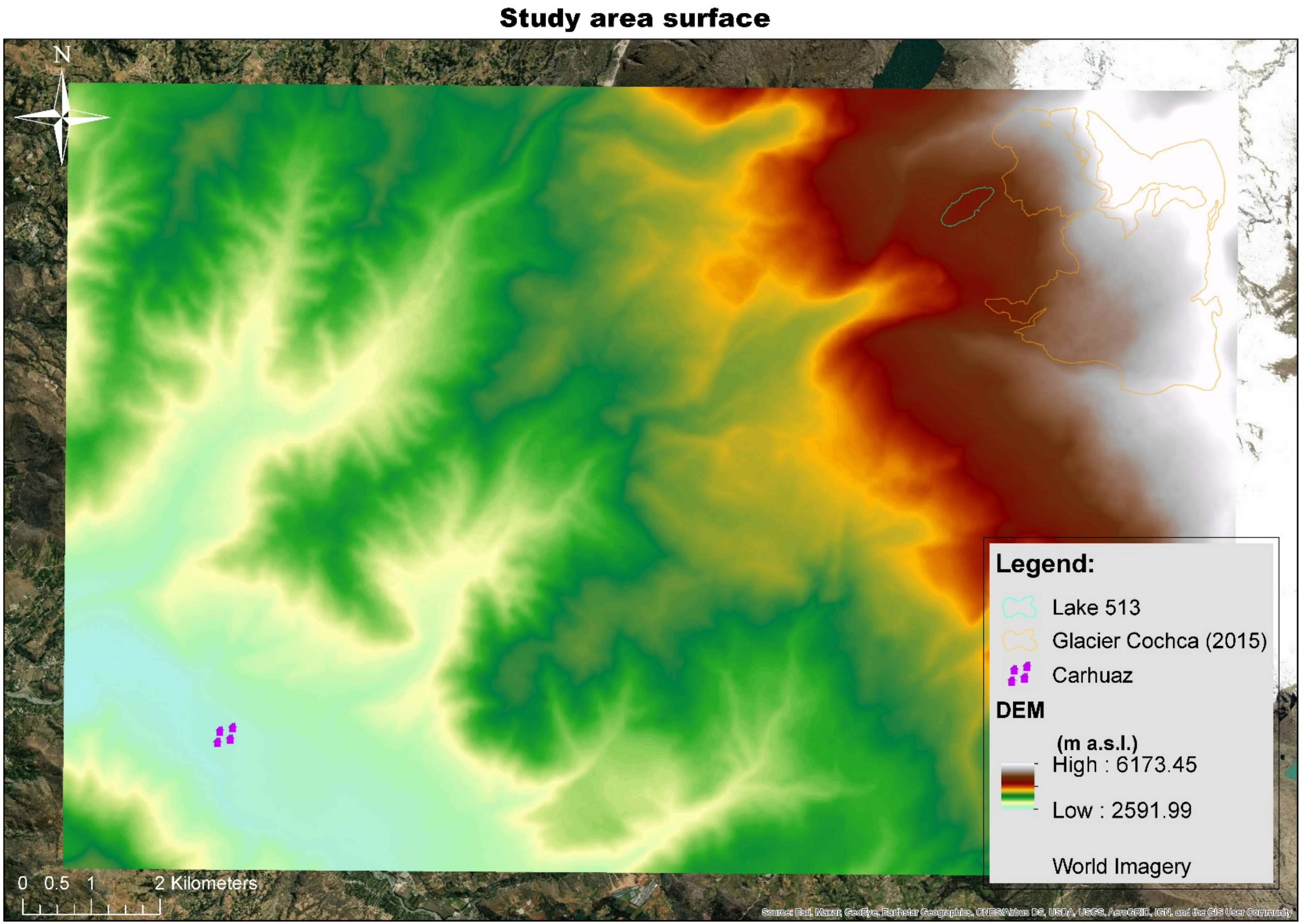

Figure 42. Map of the study area surface with a Digital Elevation Model, including the location of the lake Laguna 513, the glacier Cochca as it was in 2015, and the city of Carhuaz.

3.3.2 Lake´s volume scenarios / Fluid release area

Different lake´s volume scenarios are considered for this simulation. As explained in section 1.7 “Lake Laguna 513 history”, 4 tunnels were constructed in 1994. If maintain in a good state, these tunnels would considerably reduce the water level of the lake as it is shown in Figure 43 and Table 12.

The scenario 0 is a non-realistic scenario, showing the lake completely empty which would be very unlikely to happen in this location; however, it is used as control scenario to observe the difference of the water level and volume of the lake.

The scenario 1 exemplifies the lake when the lake is full of rain or glacier melt and the measures to reduce water level have worked perfectly. It keeps the water level until the drain of the first tunnel.

The scenario 2 shows the lake when it has been completely full, and the tunnels are not maintained in a well state with any kind of blockage that hamper the water evacuation. This scenario poses the highest hazard threat.

The difference between scenario 1 and 2 shows the importance of management measures and of maintaining of the current infrastructure, the tunnels, in an adequate state. As there is a considerable change in volume, more than 4 million m^3 considering the scenario of the tunnels are constructed and maintained.

Sediment deposits since the bathymetry was completed are not considered for the study.

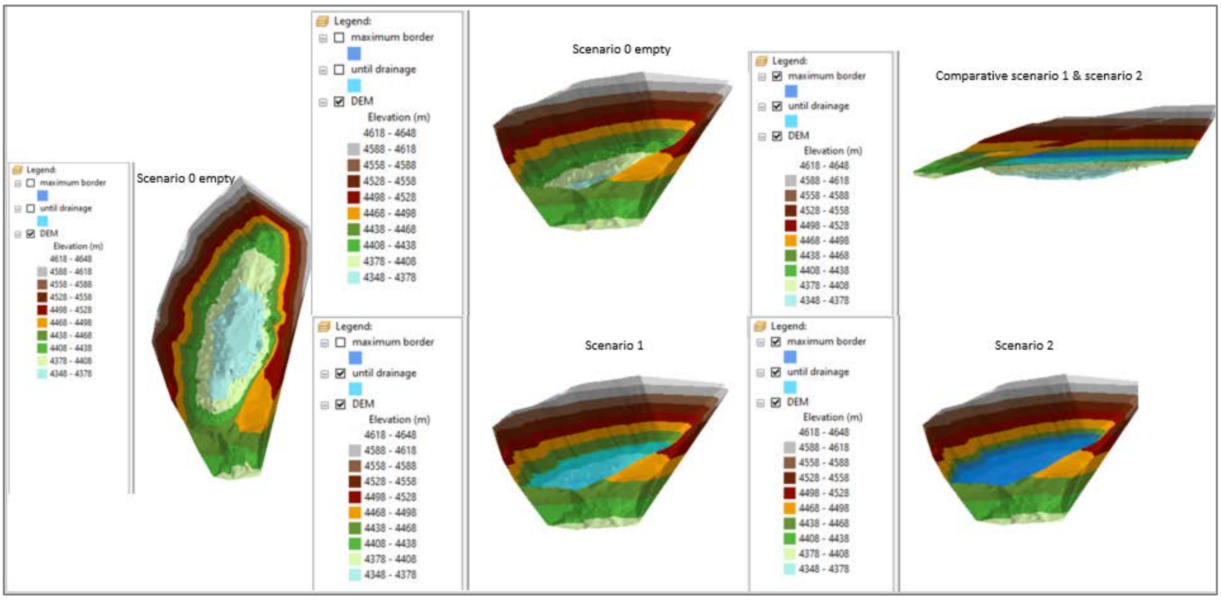

Figure 43. 3D representation of Laguna 513´s volume scenarios. Scenario 0 when the lake is empty, Scenario 1 when the water level reaches the 1st tunnel used for drainage and Scenario 2 when the water level reaches the verge of the lake and after that it overtops. Done in ArcGIS ArcScene®.

Table 12. The 3 Laguna 513´s volume scenarios with altitude, depth and volume data. Scenario 0 when the lake is empty, Scenario 1 when the water level reaches the 1st tunnel used for drainage and Scenario 2 when the water level reaches the verge of the lake and after that it overtops. Values calculated in ArcGIS ArcScene®.

Lake state scenarios	Altitude (m)	Depth (m)	Volume (m^3)
Scenario 0: empty	4347.9	0	0
Scenario 1: until drain	4431	83.1	9243368
Scenario 2: maximum, until verge	4450	102.1	13488862

3.3.3 Solid release area

Based on the study on glacier evolution in section 3.1 of slope, elevation and distance retreated, and previous GLOF events in the same location, the area selected from the glacier to simulate a GLOF event is represented in Figure 44. This solid release area from the glacier is actually formed by two parts, with high slope values located in the zone of the glacier that has retreated already, one bellow the non-glaciated area and one above.

These areas are not in the highest altitudes of the glacier as those will be less affected by climate change. Neither they are not located in the front line of the glacier retreat, which is closer to the lake and the area that will promptly melt, because it is less prone to cause catastrophic events as the kinetic energy would be remarkably higher coming from higher altitudes in a higher grading downhill.

The release materials from the glacier are rock and ice and the total volume is over a million cubic meters; the division of volume between the two phases is 50% rock and 50% ice as described in Table 13 bellow. The thickness of both materials to produce that volume are represented in Figure 44.

Table 13. Volume of rock and ice detaching from the glacier and falling into the lake. Calculated in r.avalow with data calculated in ArcGIS ArcMap.

Solid release area phase	Volume (m^3)
Phase 1: rock	652230
Phase 2: ice	652230
Total:	1304460

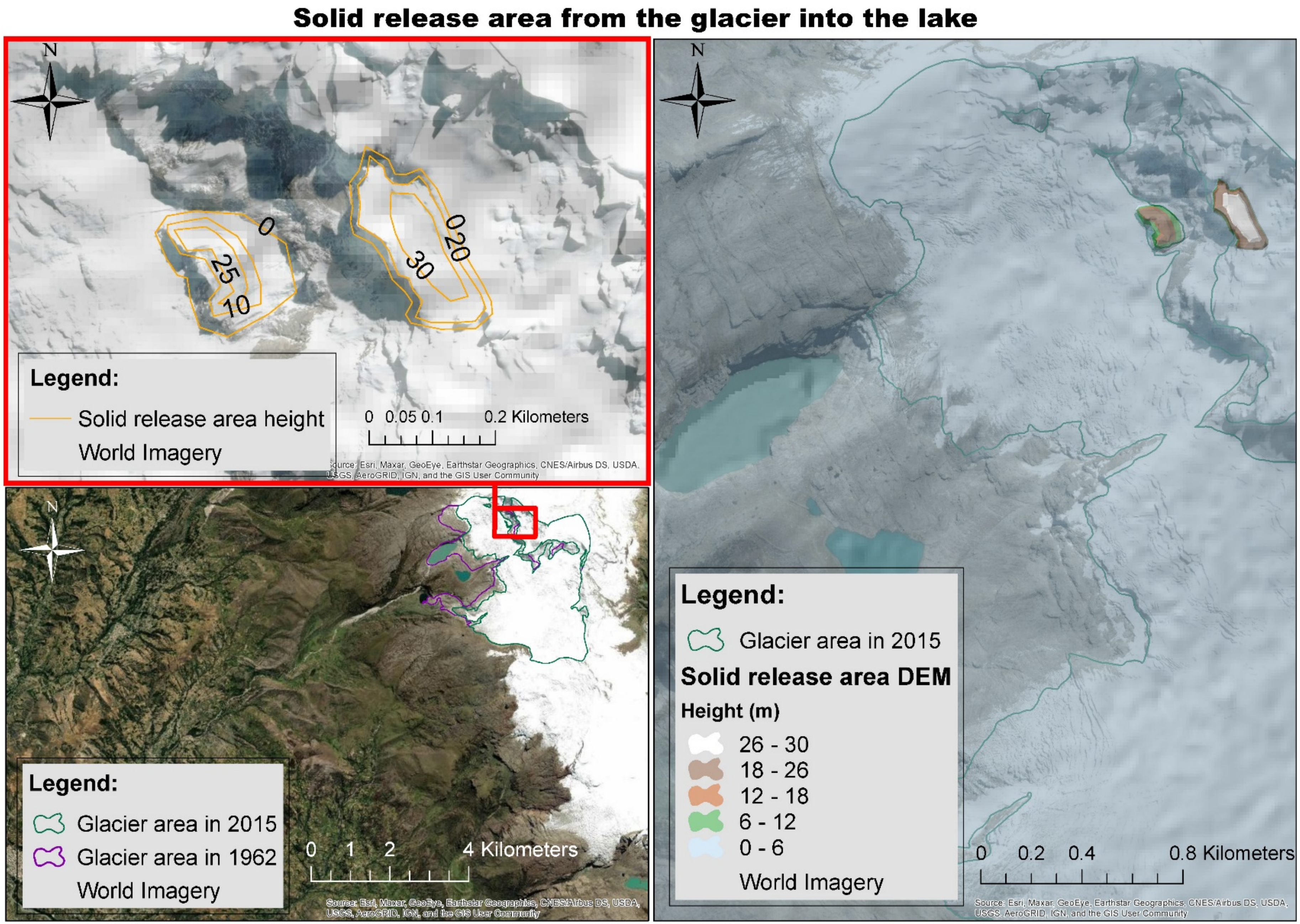

Figure 44. Map of the solid release area of the glacier including the estimated thickness of the selected area. Done in ArcGIS ArcMap.

3.3.4 Results of the simulation

The result simulation performed with *r.avaflow®* tools show physically plausible model parameters that represent a possible GLOF event in the study area. This simulation is predicting the possible behaviour of the mass flowing downstream from the glacier Cochca in a feasible GLOF event provoked by a detachment of rock and ice from the mentioned glacier. This simulation is applying the input data studied in the previous sections from the solid release area and the lake´s volume scenario 2. The simulation with the same parameters using lake´s volume scenario 1 is presented in Appendix 8.3, which entangles a significantly lower risk.

The results of the simulation appear in Figure 45 that shows the total area reached by the flood starting from the glacier until the city of Carhuaz. Values of maximum flow height, time of reach and flow kinetic energy can be seen together with Appendix Table 8.4-1, to know the exact values for each period of time.

The maximum velocity of the mass flow is predicted to be 71.64 m/s as shown in Appendix Table 8.4-1 (this velocity obtained from the summary file is more reliable that the ones present as V_{max} in the plots in Figure 46 as this extremely high velocity reflects some isolated numerical issues in the calculations).

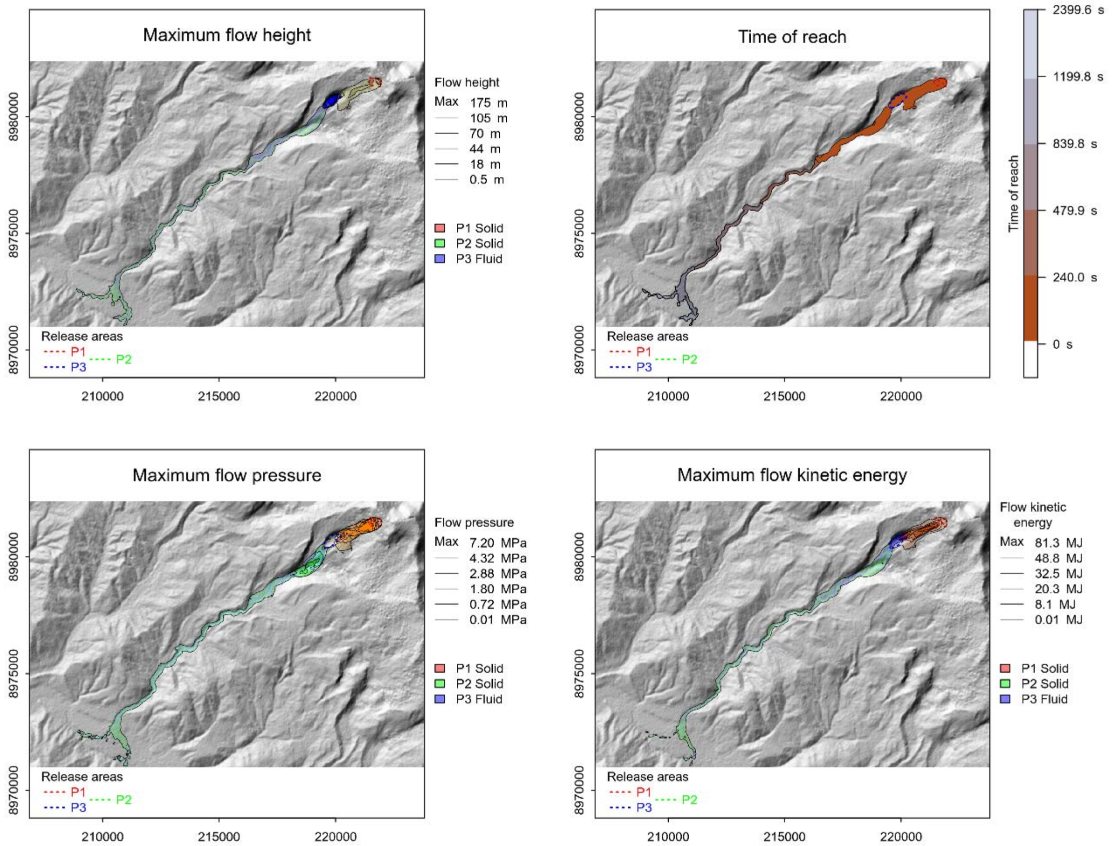

Figure 45. Maps of maximum flow height, time of reach, maximum flow pressure and maximum flow kinetic energy in the r.avaflow® simulation.

In Figure 46 the simulation in time steps is shown including the different stages of the GLOF event. Starting from the top-left image it can be seen the initial conditions of the event, the glacial area that is going to detach formed by rock (P1 Solid) and ice (P2 Solid) and the lake filled with water (P3 Fluid) under scenario 2. In the second image the glacial release area is detaching and in the third one, the mass has impacted on the lake and created a wave that propagates until it overtops the dam, and the flood propagates downstream. From the fourth image it can be seen the flood propagating in different stages of time. Around 15 minutes after the glacier detached, the mass flow reached the Río Santa river valley, where it floods some areas close to the city of Carhuaz, seen in image five, and afterwards converges with river Río Santa provoking a quick rise of the water level flowing which would become a flood in other areas of Carhuaz more west.

As it is not possible to simulate the flow of river Río Santa in this model, and due to small imprecisions of the study area DEM, the mass flow in the simulation does not flood these other areas of Carhuaz but there is a high confidence that the abrupt water level rise in the river Río Santa would be enough to provoke a flood in the west part of the city as the flow near Carhuaz shown in the simulation largely moves down the alluvial fan to the river Río Santa.

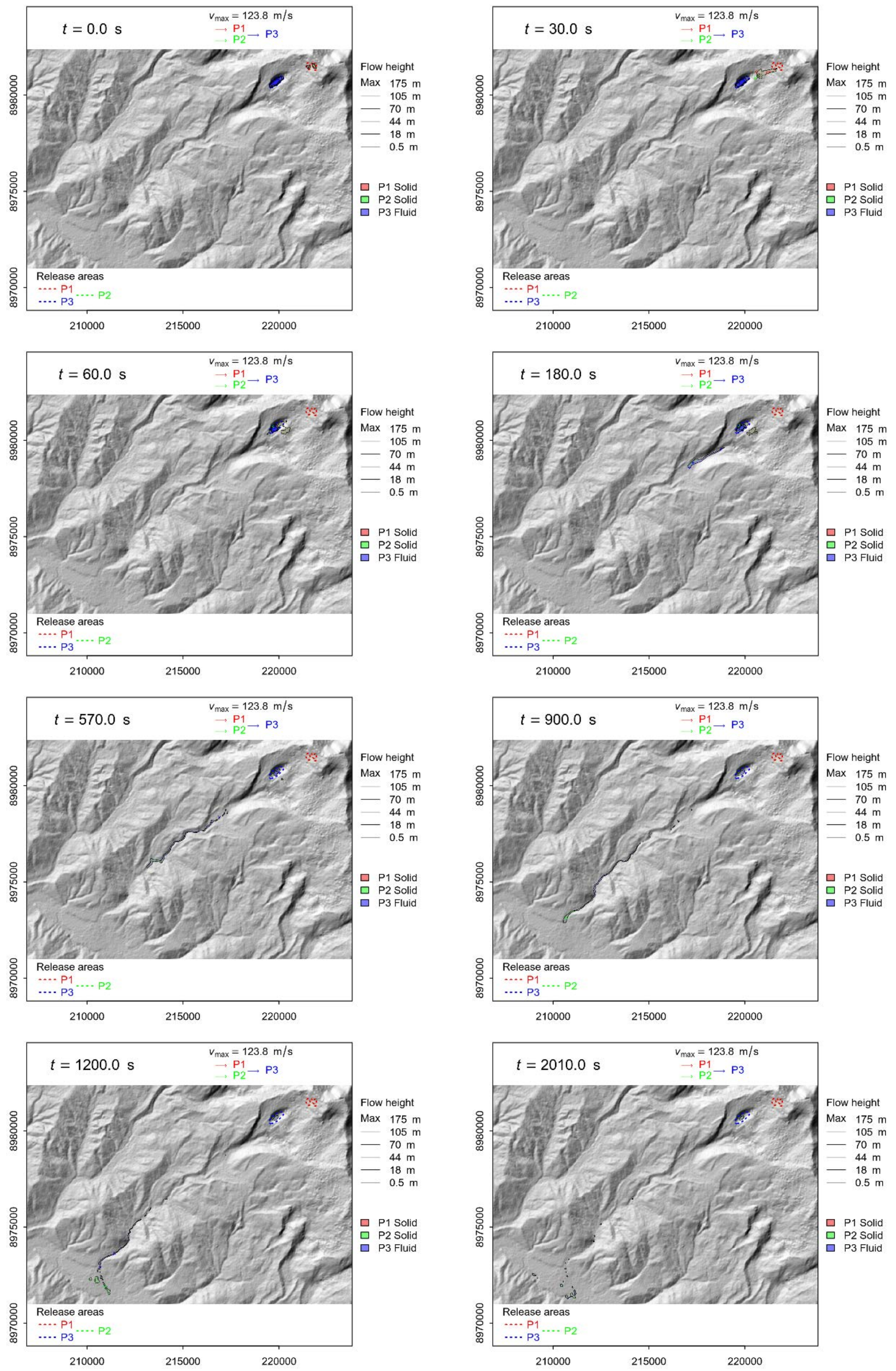

Figure 46. Time steps of the r.avaflow® simulation performed.

4 DISCUSSION

4.1 INTERPRETATION AND IMPLICATIONS OF FINDINGS

The results reveal that the studied glacier in Cordillera Blanca has been shrinking during the past decades. The most recent measure of the minimum altitude occupied by the glacier is 4350 m (in 2015) and has retreated to this higher altitude from 4136 m that was in 1962. The glacier has shifted specially from the lower areas and predominantly steep slopes to the higher altitudes of the glacier. The average distance retreated in the front line of the glacier has been 306 m from 1962 to 2015, with a maximum retreat of 1039 m in the area where lake Laguna 513 has formed.

The study demonstrates a correlation between ENSO phenomena and the temperatures in the study area, which explains the cyclic fluctuations in temperature in the region during the last decades. There is an even stronger correlation during the summer months/rainy season showing that the ENSO effect is even stronger than the seasonal cycle. There is no correlation found between ENSO and the precipitation.

This analysis supports the theory that there is a rising in the temperatures due to climate change which is inducing and will induce in the future a glacier retreat. Consequently, a cascade of processes that may lead to a potential disaster in the neighbouring populations, can be triggered.

The results indicate that there is a correlation or relationship among the glacier evolution and the climatological data, as it could be expected. There is an increase in temperature due to climate change and a reduction and retreat of the glacier to higher altitudes that go hand in hand. The increase of the observed annual temperature is 0.13°C per decade and a reduction of the glaciated area of 3.4 ha per year has been measured (for almost the same study period, i.e., 1961 to 2019 for the climate data and 1962 and 2015 for the glacier evolution). With a very simple correlation, without taking into account many factors, this would mean a reduction of the glacier of 261.5 ha per degree of warming at the altitude of the study, which in case of being continued, it would impose a high risk for the glacier. The future trends predicted for rising temperature of 2.5 °C for the scenario SSP245 and 5.9 °C for the scenario SSP585 per century, give an even more worrying perspective for the future glacier retreat in these areas.

The simulated scenarios of GLOF events in *r.avaflow®* suggest that if a large glacial avalanche falls from the glacier Cochca and impacts in the lake Laguna 513, a mass formed by solid and fluid materials would flow downstream, and converge with river Río Santa provoking a quick rise of the water level flowing which would become a flood. The simulated release from the glacier is formed by ice and rock with a total of over a million cubic meters of volume, that would impact the Laguna 513 simulated with two different scenarios of water level; with the scenario 2, in which this research is focused and shows the lake completely full, it would take around 15 to 25 minutes since the glacier detachment until it reaches the city.

Concerning the long-term water availability issue, this study does not provide enough evidence about the prospective state of water resources. Although the glacier is expected to shrink thus providing a smaller extent of fresh water that can likely lead to water scarcity, the future trend of summer precipitations for the next decades is increasing. There is not enough data from this study to assess which one of the two effects will have a larger influence on the water availability and whether the exhaustion of water supply, a widespread social fear, will become or not a reality.

The implications of this kind of studies for the local population are very important as these settlements are exposed to a risk due to climate change; they provide information and predictions that allow to take actions for adaptation and resilience against this glacier risk. Furthermore, it is a relevant investigation for the society in general as glacier shrinking is an indicator of climate change on a global scale.

4.2 STRENGTHS AND COMPARISON WITH OTHER STUDIES

This project combines both a climatological analysis and a glacier evolution study with a simulation of a GLOF event at a local scale. This is an innovative approach that includes a prior study to the mass flow simulation. This prior study incorporates the future state of the glacier which will most likely affect to a great extent the frequency of occurrence and magnitude of catastrophic events in the study area.

The past and future projections of the climatological data rely in a great extent to the available records, which are not very precise or abundant in this remote area, so the case is not comparable with other areas with abundance of climatic data. But with the available data, as part of this research, multiple studies have been performed using different methods and comparisons between observed and predicted values to verify the adequacy of the methodology. Despite the scarcity of data, these studies have been successfully completed and added value to this specific climatic research.

The mass flow simulation using the software *r.avaflow*® has reliably reproduce cascades of processes in GLOF with the advantage of combining the individual components and chain of processes in one integrated model, instead of coupling different simulation approaches. Two-phase and multi-phase flow models have been used; they consider not only the solid and the fluid phase separately but also phase interactions between them and therefore allow for considering more complex process interactions such as the impact of a landslide on a lake. This allowed a realistic reproduction of the corresponding events.

This methodology of the simulation can be compared with previous studies with similar characteristics. The research performed by Schneider *et al* (2014) was located on the same study area and simulated the last major event that occurred in 2010. The input information was similar as the one used for this study: satellite imagery, a DEM and a bathymetry of the lake. The purpose was different, instead of simulating future possible events, it modelled a past event that already occurred in the study area in 2010. The methodology consisted of (1) ice avalanche modelization with RAMMS -a numerical and physically based avalanche and debris flow model- (2) simulation of the impact wave propagation in the lake and dam overtopping with IBER -a hydrodynamic model for simulating turbulent free surface unsteady flow and environmental processes in river hydraulics- and (3) lake outburst flood and debris flow with RAMMS. But, single-phase models as this one do not describe the interactions between solid and fluid phase, or dynamic landslide–lake interactions, in an appropriate way, so that integrated approaches as *r.avaflow*® tools represent a significant improvement. The study from Schneider *et al* also recognises the existence of a hazard risk in the area, and additionally defines small, medium, and large scenarios according to avalanche volumes assigning hazard levels to them. Depending on these ice-avalanches volumes, the estimated durations of the mass movement vary. For scenario medium (avalanche of 1000000 m^3) and large (3000000 m^3) the estimated time to reach the upper fan area close to Carhuaz are 65 minutes and 35 minutes, both longer than the estimated time by this study of around 15 minutes. It is important to highlight the uncertainties in the modelling and the different cases modelled, as the RAMMS study reconstructs a past event and this current study is modelling future events.

The *r.avaflow*® software has been used in other areas, as mentioned in section 2.4 "Software justification"; the area closest to the area of study is Lake Palcacocha in Cordillera Blanca, studied by Mergili, Pudasaini, *et al.*(2020) with the reconstruction of a catastrophic event in 1941. The methodology of this research was performed with *r.avaflow*® tools using as input information (1)a DEM produced from stereo aerial photographs and airborne lidar, modifying it in order to obtain a DTM representing the situation before the modelled event in 1941 with the purpose of neglecting the possible error introduced by the effects of vegetation or buildings and focus on the effects of the lakes and of erosion, (2) a bathymetry of the lake, and (3) photographs to reconstruct the conditions in 1941, such as the moraine dam before the breach and the glacier. Different four scenarios were considered as the trigger of the sudden drainage of Lake Palcacocha was not clear, all of them using an integrated approach with a two-phase flow model, thus not considering ice as a separate phase, but considering the second phase either pure water or different mixtures of fine mud and water or fluid material. More complex simulations are performed, and the different scenarios have different behaviours of the mass flow and the error is estimated as the difference between simulated and reconstructed debris entrainment.

In conclusion, the innovative aspects of this research are:

- Prior to simulation: a glacial and climatological study
- Integrated approach methodology with *r.avaflow*® including phase interactions
- Three phases model considering ice as a separate phase
- Future projections of GLOF events instead of reconstruction of past events

4.3 LIMITATIONS AND OPEN ISSUES

In these remote areas, there exists a huge lack of available information and studies performed and therefore, there is considerable research that still needs to be conducted in these parts of the world. The information provided by the glacier inventories can not be compared with the studies performed in other parts of the world with a much higher availability of data, both past and present data that allow monitoring glacier area and volume changes accurately.

For the glacier evolution study, the DEM used has been the same for both periods of time (1962 and 2015) as there was no availability of a reliable DEM from 1962. It is foreseeable that the surface of the terrain has changed, especially on the area where the new lake has formed. Also, no intermediate information between 1962 and 2015 of the glacier conditions is available, so it had to be assumed a steady regression of the glacier, instead of, what could be predictable, small fluctuations on the glacier changes along the years with a general tendency of glacier area to decrease and with an accelerated trend of negative area in the last decades to years.

Another example of information paucity is the scarcity of thickness profiles available for the glaciers, so it is very problematic to quantify the ice volume, and hence the water volume, held in the world's mountain ranges. However, in general terms we can deduce that there is enough water reserve to contribute to short-term sea-level rise within the next century if the current rate of mountain glacier retreat remains or accelerates (Meier *et al.*, 2007; Bahr *et al.*, 2009; Thompson *et al.*, 2011).

The climatological data in the area are not very abundant, with a very low number of meteorological stations that provide reliable data, which makes the study very dependent on downscaling data from a bigger scale to the local scale of the study; these data can suffer from shortcomings, for example failing to take into account relevant factors which makes them less reliable or precise.

Another limitation of the study is the lack of in-situ data of the terrain, lake and glacier collected in the study area. This data measured in the actual location can provide a more precise information, adapted to the individual study if necessary. There are limitations to obtain this kind of data in terms of financial resources, but also in terms of accessibility to high mountain investigation sites such as this area of study.

As it is mentioned before, the software *r.avaflow*® is a very reliable method to simulate mass flows and process chains; but there still exist some open questions on the use of this software that include the proper understanding of wave generation as a response to landslides impacting the high-mountain lakes and, as a consequence, the quantification of indispensable parameters for example the volume of overtopping water and the discharge (Westoby, Glasser, Brasington, *et al.*, 2014). Moreover, in high-energy mass flows, the physical characteristics of the processes involved are not always understood at the required level of detail (Mergili, Frank, *et al.*, 2018). Also, three-phase flow models (rock, ice, and fluid) and the phase transitions among them need further research in order to improve the representation of the melting of glacier ice and a more suitable consideration of deposition of debris flow material along the channel (Mergili, Jaboyedoff, *et al.*, 2020). As a consequence of this, the quantitative data obtained from the simulation are subject to model uncertainties and possible threshold effects, therefore more studies are necessary to better predict the glacier and mass flow behaviour.

5 CONCLUSIONS

This study included the following main components: (i) analysis of the glacier Cochca evolution from 1962 to 2015 including the variations of slope and elevation and the distance retreated during this time period, (ii) study of the climate on the study area including the past temperature and precipitation trends, the spatial variability of temperature and precipitation and the correlation of the temperature with ENSO phenomenon (iii) the evaluation of the trends of future climate projection following different methods and SSPs and RCPs scenarios and (iv) simulating a scenario of a cascade of mass flow outburst flood from the glacier Cochca into the lake Laguna 513 that affects the city of Carhuaz.

Component (i) was important to assess the glacier retreat and obtain an idea for future predictions of glacier retreat. The climatic analysis in component (ii) was necessary to assess the temporal and spatial evolution of the climate in the past 58 years, supplemented with the future climatic analysis in component (iii) that predicted the future trends which will also influence the evolution of the glacier. The plausible assumptions of the modelization in component (iv) was necessary to simulate different scenarios of GLOF events and assess if there is a considerable risk for the populations.

Highlights of the main accomplishments and findings of this research are following:

- glacier Cochca in Cordillera Blanca retreated during the studied period and according to future temperature trends, it is expected to continue retreating
- the glacial areas of major retreat have been identified as those of lower attitude and steep slopes
- the climate in the area is determined by a strong seasonal variation in precipitation with the rainy season in summer and a small seasonal temperature variability with a yearly mean temperature of 4.7°C at the elevation of lake Laguna 513
- there is a correlation between the ENSO phenomenon and the temperature in the area, specially during the rainy season
- a warming is expected in the area according to future predictions; the extent of the temperature increase varies under climate scenarios driven by RCP4.5 and RCP8.5 between 2.5 °C and 5.9 °C per century
- precipitations during the rainy season are predicted to increase and the extent of the precipitation increase varies under climate scenarios driven by RCP4.5 and RCP8.5 between 14 and 28 mm/month per century
- if an event of the studied dimensions happens, it would pose a high risk for the population downstream
- according to the *r.avaflow*® simulation performed, the GLOF event would take a short time to reach the city of Carhuaz that would entail a significant risk

In conclusion, with effects of climate change rising all around the world, we need to put our attention to the most vulnerable areas to climate change effects, like regions around tropical glaciers. Supposing that we can predict where and in which extent the next GLOF disasters are going to happen, would mean that we can protect the populations from them. Is it possible that we can adapt and be more resilient to this natural hazard risk that is getting increased by climate change?

6 PERSPECTIVES

This chapter is focused on the applications and implications of this study, the next steps that can be developed in the matter, possible improvements in methodology and employed tools, future work for professional involvement and recommendations on good practices.

The methodology used for this project can also be extrapolated to other glacier lakes in the Cordillera Blanca mountain range or even to other areas worldwide. It can be used to study past major events related to GLOFs or to predict future behaviour and dangers of glacier meltdown due to climate change. Cordillera Blanca contains several recent glacier lakes with the same conditions as Laguna 513 that possess considerable risk to the populations downstream and can benefit of an integrated study of glacier behaviour and GLOF simulations; future studies could further address this matter. Also, the results can be improved adding some scientific studies as well as practical actions to produce better simulations, that can be used by the competent authorities to prevent or reduce disasters.

For this study scenarios mid-range SSP245 and high-emission SSP585 were used, but depending on the objective of the study other projection scenarios or new scenarios of radiative forcing that may appear in the future to replace the current ones, could also be used.

In case of extrapolation of this methodology to areas with availability of historical data, a more exhaustive climatological and glacier evolution study can be done. For example, by analysing the glacier evolution in different periods of time it can be assessed if there was a steady glacier retreat or was a slower retreat at the beginning and accelerated in the past years. Another example is the prediction of the retreat in area or volume of the glacier per degree of warming.

The precision of the simulations can be improved with a higher resolution DEM. There are multiple high resolution DEMs available like Pleiades or SPOT with resolutions smaller than 3 meters. For example, for this study it was considered PerúSAT-1, which obtains satellite images with stereoscopic pair (two photographs with sufficient overlap from different angles or viewpoints). This high quality images were requested to the Spatial Agency of Peru - Comisión Nacional de Investigación y Desarrollo Aeroespacial (CONIDA) - and through the software *Geomatica Banff®,* a DEM of 0.7 m pixel size can be created, instead of the 12.5 m DEM used for this project. PerúSAT-1 is a very-high-resolution Earth observation satellite system built for the government and the Space Agency of Peru. It must be taken into account that the use of data with higher resolution would have a larger processing time, so an equilibrium between time and precision of the data should be found, which can be adjusted in the *r.avaflow®* script. The satellite PerúSAT-1 is the first of its kind operated by Peru and was launched in September 2016 (Airbus S.A.S., 2020). The process to convert the high-resolution satellite images into a high-resolution Digital Elevation Model was explored for this project but the images couldn´t be obtained from CONIDA due to COVID-19 delays.

R.avaflow® simulations will be focused on the future towards the improvement of three-phase flow models (rock, ice, and fluid), like the one in this project, including enhancing the phase transitions in order to better capture the dynamics of complex landslides in glacierized environments, where ice – and melting of ice – are considered in a more explicit way. For example, an option to set the ice density lower than the liquid water density which is currently not possible.

A thickness profile of the glacier and observation of the glacier dynamics in the area would give much value to the investigation. Also, including a monitoring of the evolution of the thickness over decades to assess the climate change impact, not just in the area of reduction, would be recommended.

An in-situ study of the topography including the roughness of the terrain in the area possibly affected by the event would increase the quality of the simulation. Local-scale data, including topography data which would be hardly extrapolated from a global scale, are typically scarce, particularly in remote mountain regions.

To develop new projects and initiatives in these areas, international programs can play a critical role, but local authorities are also required to be convinced to invest into these long-term, high-effort-needed activities. Large international funding agencies and programs could play a significant role in these lines of work. They have the potential to support local-scale monitoring and the creation and maintenance of data services in a way they currently do at the global scale; it is needed they commence to develop these services for climate data at more regional scales. As a consequence, there is also a need for new techniques and methods in snow and glacier measuring procedures that allow to work in a systematic way to reduce monitoring efforts of these processes and evaluate the runoff changes in more efficient ways.

Social aspects and communication can also be successfully included in the study. An important concern in these areas is the acceptance by the population of the measures undertaken. This issue can be exemplified by the destruction of one of the EWS stations accomplished by local inhabitants in 2016. The adaptation and mitigation measures can not be imposed by the authorities, but there is instead a need of engaging stakeholders in effective communication and decision-making processes. Additionally, a participatory approach is recommended to be taken, incorporating the local practices, so the measures have a much better chance of being properly planned, broadly accepted and consistently maintained between the inhabitants of the area. This process involving engagement rather than a "top-down" process imposed from outside without consultation or interaction with the population must also be focused on long term strategic thinking to deal with the future challenges. This is complementary with clear environmental education of people around glaciers and their dangers, creating an understanding of their own vulnerability, a sense of responsibility to solve the problem and a willingness to engage in adaptation planning.

Additionally, socio-economic aspects have to be taken into account for the future studies, like changes in distribution in the population of Carhuaz since the event in 2010, as well as the mitigation measures conducted to reduce future glacier risks - both the development of new measures and the maintaining of the current infrastructure, e.g., the tunnels, in an adequate state.

All these complementary or additional studies together would give a much closer approximation to the future foreseen events in the area of study and of their consequences, which would have importance on a global scale too. All this data and recommendations of good practices could be applicable for professional activity as well as to implement measures by the competent authorities of the area in order to reduce the risk.

7 References

7.1 Software

Autodesk Inc (2020) *AutoCAD Civil 3D version 2019.* Available at: https://www.autodesk.com/products/civil-3d/

Environmental Systems Research Institute (ESRI) (2020) *ArcGIS Desktop: ArcMap and ArcScene Release 10.7.1*. Redlands, CA. Available at: https://desktop.arcgis.com/

ET Spatial Techniques. *ET GeoWizards version 12*. South Africa. Available at: https://www.ian-ko.com/

Google LLC (2020). *Google Earth Pro version 7.3*. Available at: https://www.google.com/earth/

Mergili, M., Pudasaini, S.P., (2014-2020) *R.avaflow - The mass flow simulation tool and r.avaflow tool r.lakerefill*. Available at: https://www.avaflow.org

Tobias Thrierer (1999). *Klima 0.9 for Windows. pHreaX.* Available at: http://www.phreax.net

7.2 Cartography and Data

Autoridad Nacional del Agua (ANA) and Unidad de Glaciología y Recursos Hídricos (UGRH) (2011) *Batimetría de la Laguna 513 en junio 2011.* Proyecto CRYOPERU.

Climatic Research Unit (CRU) (2020) *Data: High-resolution gridded datasets (and derived products)*. University of East Anglia, UK. Available at: https://crudata.uea.ac.uk/cru/data/hrg/ Accessed [20/08/2020]

Dataset ASF DAAC (2011) *ALOS PALSAR_Radiometric_Terrain_Corrected_high_resolution, AP_27249_FBS_F7000_RT1.dem.tif*; Includes Material ©JAXA/METI (2011). Accessed through ASF DAAC [04/05/2020]. Registration and login required. https://asf.alaska.edu/doi/10-5067-z97hfcnkr6va/

Physical Science Laboratory (2020) *Multivariate ENSO Index Version 2 (MEI.v2)* Available at: https://www.psl.noaa.gov/enso/mei/ Accessed [15/06/2020]

Ronald Concha (2020). *Avance al mapa geomorfológico de formas fluvioglaciares al oeste del Nevado Hualcán* (Cordillera Blanca, Perú). Proyecto CRYOPERU.

7.3 Literature

Aguado, E. and Burt, J. E. (2014) *Understanding Weather and Climate*, *Boston Columbus Indianapolis New York*. Available at: https://www.cambridge.org/core/product/identifier/CBO9781107415324A009/type/book_part.

Airbus S.A.S. (2020) *PerúSAT-1 Mission*. Available at: https://www.airbus.com/space/earth-observation/perusat.html (Accessed: 20 July 2020).

Allen, S. K., Ballesteros-Canovas, J., Randhawa, S. S., Singha, A. K., Huggel, C. and Stoffel, M. (2018) 'Translating the concept of climate risk into an assessment framework to inform adaptation planning: Insights from a pilot study of flood risk in Himachal Pradesh, Northern India', *Environmental Science and Policy*, 87(September 2017), pp. 1–10.

https://doi.org/10.1016/j.envsci.2018.05.013.

Allen, S. K., Linsbauer, A., Randhawa, S. S., Huggel, C., Rana, P. and Kumari, A. (2016) 'Glacial lake outburst flood risk in Himachal Pradesh, India: an integrative and anticipatory approach considering current and future threats', *Natural Hazards*.Springer Netherlands, 84(3), pp. 1741–1763. https://doi.org/10.1007/s11069-016-2511-x.

Almazroui, M., Saeed, F., Saeed, S., Nazrul Islam, M., Ismail, M., Klutse, N. A. B. and Siddiqui, M. H. (2020) 'Projected Change in Temperature and Precipitation Over Africa from CMIP6', *Earth Systems and Environment*.Springer International Publishing, 4(3), pp. 455–475. https://doi.org/10.1007/s41748-020-00161-x.

Ancey, C. and Bain, V. (2015) 'Dynamics of glide avalanches and snow gliding', *Reviews of Geophysics*, 53(3), pp. 745–784. https://doi.org/10.1002/2015RG000491.

Arnaud, Y., Muller, F., Vuille, M. and Ribstein, P. (2001) 'El Niño-Southern Oscillation (ENSO) influence on a Sajama volcano glacier (Bolivia) from 1963 to 1998 as seen from Landsat data and aerial photography', *Journal of Geophysical Research Atmospheres*, 106(D16), pp. 17773–17784. https://doi.org/10.1029/2001JD900198.

Bahr, D. B., Dyurgerov, M. and Meier, M. F. (2009) 'Sea-level rise from glaciers and ice caps: A lower bound', *Geophysical Research Letters*, 36(3), pp. 2–5. https://doi.org/10.1029/2008GL036309.

Barbadillo Jorge, B. (2020) *Análisis preliminar del riesgo por GLOFs en las lagunas glaciares de la Cordillera Blanca, Perú*.Universidad Complutense de Madrid.

Benn, D. I., Bolch, T., Hands, K., Gulley, J., Luckman, A., Nicholson, L. I., Quincey, D., Thompson, S., Toumi, R. and Wiseman, S. (2012) 'Response of debris-covered glaciers in the Mount Everest region to recent warming, and implications for outburst flood hazards', *Earth-Science Reviews*.Elsevier B.V., 114(1–2), pp. 156–174. https://doi.org/10.1016/j.earscirev.2012.03.008.

Boelens, R. (2014) 'Cultural politics and the hydrosocial cycle: Water, power and identity in the Andean highlands', *Geoforum*.Elsevier Ltd, 57, pp. 234–247. https://doi.org/10.1016/j.geoforum.2013.02.008.

Bouma, M. J., Kovats, R. S., Goubet, S. A., Cox, J. S. H. and Haines, A. (1997) 'Global assessment of El Nino's disaster burden', *Lancet*, 350(9089), pp. 1435–1438. https://doi.org/10.1016/S0140-6736(97)04509-1.

Bradley, R. S., Keimig, F. T., Diaz, H. F. and Hardy, D. R. (2009) 'Recent changes in freezing level heights in the Tropics with implications for the deglacierization of high mountain regions', *Geophysical Research Letters*, 36(17). https://doi.org/10.1029/2009GL037712.

Bradley, R. S., Vuille, M., Diaz, H. F. and Vergara, W. (2006) 'Threats to Water Supplies in the Tropical Andes', *Science*, 312(23 June 2006), pp. 1755–1757.

Buckel, J., Otto, J. C., Prasicek, G. and Keuschnig, M. (2018) 'Glacial lakes in Austria - Distribution and formation since the Little Ice Age', *Global and Planetary Change*.Elsevier, 164(August 2017), pp. 39–51. https://doi.org/10.1016/j.gloplacha.2018.03.003.

Burns, P. and Nolin, A. (2014) 'Using atmospherically-corrected Landsat imagery to measure glacier area change in the Cordillera Blanca, Peru from 1987 to 2010', *Remote Sensing of Environment*.Elsevier B.V., 140, pp. 165–178. https://doi.org/10.1016/j.rse.2013.08.026.

Carey, M., Baraer, M., Mark, B. G., French, A., Bury, J., Young, K. R. and McKenzie, J. M. (2014)

‘Toward hydro-social modeling: Merging human variables and the social sciences with climate-glacier runoff models (Santa River, Peru)’, *Journal of Hydrology*.Elsevier B.V., 518(PA), pp. 60–70. https://doi.org/10.1016/j.jhydrol.2013.11.006.

Carey, M., Huggel, C., Bury, J., Portocarrero, C. and Haeberli, W. (2012) ‘An integrated socio-environmental framework for glacier hazard management and climate change adaptation: Lessons from Lake 513, Cordillera Blanca, Peru’, *Climatic Change*, 112(3–4), pp. 733–767. https://doi.org/10.1007/s10584-011-0249-8.

Carey, M., Molden, O. C., Rasmussen, M. B., Jackson, M., Nolin, A. W. and Mark, B. G. (2017) ‘Impacts of Glacier Recession and Declining Meltwater on Mountain Societies’, *Annals of the American Association of Geographers*, 107(2), pp. 350–359. https://doi.org/10.1080/24694452.2016.1243039.

Carrivick, J. L. and Tweed, F. S. (2016) ‘A global assessment of the societal impacts of glacier outburst floods’, *Global and Planetary Change*.Elsevier B.V., 144(July), pp. 1–16. https://doi.org/10.1016/j.gloplacha.2016.07.001.

Chen, C. C., McCarl, B. A. and Adams, R. M. (2001) ‘Economic implications of potential ENSO frequency and strength shifts’, *Climatic Change*, 49(1–2), pp. 147–159. https://doi.org/10.1023/A:1010666107851.

Christensen, J. H., Carter, T. R. and Giorgi, F. (2002) ‘PRUDENCE employs new methods to assess european climate change’, *Eos*, 83(13), p. 147. https://doi.org/10.1029/2002EO000094.

Christie, D. A., Lara, A., Barichivich, J., Villalba, R., Morales, M. S. and Cuq, E. (2009) ‘El Niño-Southern Oscillation signal in the world’s highest-elevation tree-ring chronologies from the Altiplano, Central Andes’, *Palaeogeography, Palaeoclimatology, Palaeoecology*.Elsevier B.V., 281(3–4), pp. 309–319. https://doi.org/10.1016/j.palaeo.2007.11.013.

Clague, J. J. and Evans, S. G. (2000) ‘A review of catastrophic drainage of moraine-dammed lakes in British Columbia . Quaternary Science Reviews A review of catastrophic drainage of moraine-dammed lakes in British Columbia’, *Quaternary Science Reviews*, 19, pp. 1763–1783. https://doi.org/10.1016/S0277-3791(00)00090-1.

Collins, M., An, S. Il, Cai, W., Ganachaud, A., Guilyardi, E., Jin, F. F., Jochum, M., Lengaigne, M., Power, S., Timmermann, A., Vecchi, G. and Wittenberg, A. (2010) ‘The impact of global warming on the tropical Pacific Ocean and El Nĩo’, *Nature Geoscience*, 3(6), pp. 391–397. https://doi.org/10.1038/ngeo868.

Coudrain, A., Francou, B. and Kundzewicz, Z. W. (2005) ‘Glacier shrinkage in the Andes and consequences for water resources’, *Hydrological Sciences Journal*, 50(6), pp. 925–932. https://doi.org/10.1623/hysj.2005.50.6.925.

David A. Randall, R. A. W. (2007) ‘Climate Models and Their Evaluation’, *Evaluation*, 323(January), pp. 589–662. Available at: http://scholar.google.com/scholar?hl=en&btnG=Search&q=intitle:Climate+Models+and+Their+Evaluation#0.

Emmer, A. and Cochachin, A. (2013) ‘The causes and mechanisms of moraine-dammed lake failures in the cordillera blanca, North American Cordillera, and Himalayas’, *Acta Universitatis Carolinae, Geographica*, 48(2), pp. 5–15. https://doi.org/10.14712/23361980.2014.23.

Emmer, A., Klimeš, J., Mergili, M., Vilímek, V. and Cochachin, A. (2016) ‘882 lakes of the Cordillera Blanca: An inventory, classification, evolution and assessment of susceptibility to outburst floods', *Catena*, 147, pp. 269–279. https://doi.org/10.1016/j.catena.2016.07.032.

Emmer, A., Merkl, S. and Mergili, M. (2015) 'Spatiotemporal patterns of high-mountain lakes and related hazards in western Austria', *Geomorphology*.Elsevier B.V., 246, pp. 602–616. https://doi.org/10.1016/j.geomorph.2015.06.032.

Emmer, A. and Vilímek, V. (2013) 'Review article: Lake and breach hazard assessment for moraine-dammed lakes: An example from the Cordillera Blanca', *Natural Hazards and Earth System Sciences*, 13(6), pp. 1551–1565. https://doi.org/10.5194/nhess-13-1551-2013.

Emmer, A. and Vilímek, V. (2014) 'New method for assessing the susceptibility of glacial lakes to outburst floods in the Cordillera Blanca, Peru', *Hydrology and Earth System Sciences*, 18(9), pp. 3461–3479. https://doi.org/10.5194/hess-18-3461-2014.

Evans, S. G. and Delaney, K. B. (2015) 'Chapter 16: Catastrophic mass flows in the mountain glacial environment', in *Snow, and Ice-Related Hazards, Risks, and Disasters*.[Haeberli, W. and C. Whitemann (eds.)]. Elsevier, Amsterdam, pp. 563–606.

Fang, G. H., Yang, J., Chen, Y. N. and Zammit, C. (2015) 'Comparing bias correction methods in downscaling meteorological variables for a hydrologic impact study in an arid area in China', *Hydrology and Earth System Sciences*, 19(6), pp. 2547–2559. https://doi.org/10.5194/hess-19-2547-2015.

Fell, R. (1994) 'Landslide risk assessment and acceptable risk', *Canadian Geotechnical Journal*.

Fell, R., Chapman, T. G. and Maguire, P. K. (1991) 'A model for prediction of piezometric levels in landslides', in *Slope stability engineering developments and applications*.Londo, UK., pp. 37–42.

Fischer, L., Purves, R. S., Huggel, C., Noetzli, J. and Haeberli, W. (2012) 'On the influence of topographic , geological and cryospheric factors on rock avalanches and rockfalls in high-mountain areas', pp. 241–254. https://doi.org/10.5194/nhess-12-241-2012.

Francou, B., Ribstein, P., Saravia, R. and Tiriau, E. (1995) 'Monthly balance and water discharge of an inter-tropical glacier: Zongo Glacier, Cordillera Real, Bolivia, 16' S', *Journal of Glaciology*, 41(137).

Francou, B., Vuille, M., Favier, V. and Cáceres, B. (2004) 'New evidence for an ENSO impact on low-latitude glaciers: Antizana 15, Andes of Ecuador, 0°28'S', *Journal of Geophysical Research Atmospheres*, 109(18), pp. 1–17. https://doi.org/10.1029/2003JD004484.

Francou, B., Vuille, M., Wagnon, P., Mendoza, J. and Sicart, J. E. (2003) 'Tropical climate change recorded by a glacier in the central Andes during the last decades of the twentieth century: Chacaltaya, Bolivia, 16°S', *Journal of Geophysical Research: Atmospheres*, 108(5), pp. 1–12. https://doi.org/10.1029/2002jd002959.

Frey, H., Haeberli, W., Linsbauer, A., Huggel, C. and Paul, F. (2010) 'A multi-level strategy for anticipating future glacier lake formation and associated hazard potentials', *Natural Hazards and Earth System Science*, 10(2), pp. 339–352. https://doi.org/10.5194/nhess-10-339-2010.

Gao, J. (2019) 'Global Population Projection Grids Based on Shared Socioeconomic Pathways (SSPs), Downscaled 1-km Grids, 2010-2100'.Palisades, NY: NASA Socioeconomic Data and Applications Center (SEDAC). Available at: https://doi.org/10.7927/H44747X4.

Gardelle, J., Arnaud, Y. and Berthier, E. (2011) 'Contrasted evolution of glacial lakes along the

Hindu Kush Himalaya mountain range between 1990 and 2009', *Global and Planetary Change*, 75(1–2), pp. 47–55. https://doi.org/10.1016/j.gloplacha.2010.10.003.

Garreaud, R. D. and Aceituno, P. (2001) 'Interannual rainfall variability over the South American Altiplano', *Journal of Climate*, 14(12), pp. 2779–2789. https://doi.org/10.1175/1520-0442(2001)014<2779:IRVOTS>2.0.CO;2.

Geoscience Division Pacific Community (SPC) (2016) *Pacific Coordinate Systems: EPSG:32718*. Available at: http://pacificprojections.spc.int/32718 (Accessed: 10 July 2020).

Glaciology Unit (2009) *Inventario de glaciares Cordillera Blanca. Autoridad Nacional del Agua. Unidad de Glaciología. Peru*.

Haeberli, W. (1983) 'Frequency an Characteristics of Glacier Floods in the Swiss Alps', *Annals of Glaciology*, 4, pp. 7–12.

Haeberli, W. (2013) 'Mountain permafrost - research frontiers and a special long-term challenge', *Cold Regions Science and Technology*, 96(December 2013), pp. 71–76. https://doi.org/10.1016/j.coldregions.2013.02.004.

Haeberli, W., Kääb, A., Mühll, D. V. and Teysseire, P. (2001) 'Prevention of outburst floods from periglacial lakes at Grubengletscher, Valais, Swiss Alps', *Journal of Glaciology*, 47(156), pp. 111–122. https://doi.org/10.3189/172756501781832575.

Haeberli, W., Noetzli, J., Arenson, L., Delaloye, R., Gärtner-Roer, I., Gruber, S., Isaksen, K., Kneisel, C., Krautblatter, M. and Phillips, M. (2011) 'Mountain permafrost: Development and challenges of a young research field', *Journal of Glaciology*, 56(200), pp. 1043–1058. https://doi.org/10.3189/002214311796406121.

Hausfather, Z. (2018) 'Explainer: How "Shared Socioeconomic Pathways" explore future climate change', *Carbon Brief*. Available at: https://www.carbonbrief.org/explainer-how-shared-socioeconomic-pathways-explore-future-climate-change.

Hock, R., Rasul, G., Adler, C., Cáceres, B., Gruber, S., Hirabayashi, Y., Jackson, M., Kääb, A., Kang, S., Kutuzov, S., Milner, A., Molau, U., Morin, S., Orlove, B. and Steltzer, H. I. (2019) 'High Mountain Areas', in H.-O. Pörtner, D.C. Roberts, V. Masson-Delmotte, P. Zhai, M. Tignor, E. Poloczanska, K. Mintenbeck, A. Alegría, M. Nicolai, A. Okem, J. Petzold, B. Rama, N.M. Weyer (eds.) (ed.) *IPCC Special Report on the Ocean and Cryosphere in a Changing Climate*, pp. 131–202.

Holmgren, M., Scheffer, M., Ezcurra, E., Gutiérrez, J. R. and Mohren, G. M. J. (2001) 'El Niño effects on the dynamics of terrestrial ecosystems', *Trends in Ecology and Evolution*, 16(2), pp. 89–94. https://doi.org/10.1016/S0169-5347(00)02052-8.

Huggel, C., Cochachin, A., Drenkhan, F., Fluixá-sanmartín, J., Frey, H., Hernández, J. G., Jurt, C., Muñoz, R., Price, K. and Vicuña, L. (2020) 'Glacier Lake 513, Peru: Lessons for early warning service development', 69, pp. 45–52.

Huggel, C., Haeberli, W., Kääb, A., Bieri, D. and Richardson, S. (2004) 'An assessment procedure for glacial hazards in the Swiss Alps', *Canadian Geotechnical Journal*, 41(6), pp. 1068–1083. https://doi.org/10.1139/T04-053.

Huggel, C., Kääb, A., Haeberli, W., Teysseire, P. and Paul, F. (2002) 'Remote sensing based assessment of hazards from glacier lake outbursts: A case study in the Swiss Alps', *Canadian Geotechnical Journal*, 39(2), pp. 316–330. https://doi.org/10.1139/t01-099.

Hungr, O., Morgan, G. C. and Kellerhals, R. (1984) 'Quantitative analysis of debris torrent hazards for design of remedial measures.', *Canadian Geotechnical Journal*, 21(4), pp. 663–677. https://doi.org/10.1139/t84-073.

Instituto Nacional de Estadística e Informática (National Institute of Statistics and Informatics of Peru) (2018) *Áncash: censo de población resultados definitivos (population census definitive results)*, *Censos económicos*. Available at: http://www.inr.pt/uploads/docs/recursos/2013/20Censos2011_res_definitivos.pdf.

IPCC (2007) *Climate Change 2007: The Physical Science Basis. Contribution of Working Group I to the Fourth Assessment Report of the Intergovernmental Panel on Climate Change, [Solomon, S., D. Qin, M. Manning, Z. Chen, M. Marquis, K.B. Averyt, M. Tignor and H.L. Miller (eds.)]. Cambridge University Press, Cambridge, United Kingdom and New York, NY, USA, 996 pp.* https://doi.org/10.1256/wea.58.04.

Iribarren Anacona, P., Mackintosh, A. and Norton, K. P. (2015) 'Hazardous processes and events from glacier and permafrost areas: Lessons from the Chilean and Argentinean Andes', *Earth Surface Processes and Landforms*, 40(1), pp. 2–21. https://doi.org/10.1002/esp.3524.

Jones, B. and Neill, B. C. O. (2016) 'Spatially explicit global population scenarios consistent with the Shared Socioeconomic Pathways Spatially explicit global population scenarios consistent with the Shared Socioeconomic Pathways'.IOP Publishing.

Kafle, J., Pokhrel, P. R., Khattri, K. B., Kattel, P., Tuladhar, B. M. and Pudasaini, S. P. (2016) 'Landslide-generated tsunami and particle transport in mountain lakes and reservoirs', *Annals of Glaciology*, 57(71), pp. 232–244. https://doi.org/10.3189/2016aog71a034.

Lliboutry, L., Arnao, B. M., Pautre, A. and Schneider, B. (1977) 'Glaciological Problems Set by the Control of Dangerous Lakes in Cordillera Blanca, Peru', *Journal of Glaciology*, 19(81), pp. 673–674. https://doi.org/10.3189/s0022143000029610.

Loriaux, T. and Casassa, G. (2013) 'Evolution of glacial lakes from the Northern Patagonia Icefield and terrestrial water storage in a sea-level rise context', *Global and Planetary Change*.Elsevier B.V., 102, pp. 33–40. https://doi.org/10.1016/j.gloplacha.2012.12.012.

Markert, K. N., Chishtie, F., Anderson, E. R., Saah, D. and Griffin, R. E. (2018) 'Results in Physics On the merging of optical and SAR satellite imagery for surface water mapping applications', *Results in Physics*.The Authors, 9, pp. 275–277. https://doi.org/10.1016/j.rinp.2018.02.054.

McDowell, G., Huggel, C., Frey, H., Wang, F. M., Cramer, K. and Ricciardi, V. (2019) 'Adaptation action and research in glaciated mountain systems: Are they enough to meet the challenge of climate change?', *Global Environmental Change*.Elsevier Ltd, 54(June 2018), pp. 19–30. https://doi.org/10.1016/j.gloenvcha.2018.10.012.

McDowell, G. and Koppes, M. (2017) 'Robust adaptation research in high mountains: Integrating the scientific, social, and ecological dimensions of glacio-hydrological change', *Water (Switzerland)*, 9(10). https://doi.org/10.3390/w9100739.

Meier, M. F., Dyurgerov, M. B., Rick, U. K., O'Neel, S., Pfeffer, W. T., Anderson, R. S., Anderson, S. P. and Glazovsky, A. F. (2007) 'Glaciers dominate eustatic sea-level rise in the 21st century', *Science*, 317(5841), pp. 1064–1067. https://doi.org/10.1126/science.1143906.

Mergili, M., Emmer, A., Juřicová, A., Cochachin, A., Fischer, J. T., Huggel, C. and Pudasaini, S. P. (2018) 'How well can we simulate complex hydro-geomorphic process chains? The 2012 multi-lake outburst flood in the Santa Cruz Valley (Cordillera Blanca, Perú)', *Earth Surface*

Processes and Landforms, 43(7), pp. 1373–1389. https://doi.org/10.1002/esp.4318.

Mergili, M., Fischer, J. T., Krenn, J. and Pudasaini, S. P. (2017) 'R.avaflow v1, an advanced open-source computational framework for the propagation and interaction of two-phase mass flows', *Geoscientific Model Development*, 10(2), pp. 553–569. https://doi.org/10.5194/gmd-10-553-2017.

Mergili, M., Frank, B., Fischer, J. T., Huggel, C. and Pudasaini, S. P. (2018) 'Computational experiments on the 1962 and 1970 landslide events at Huascarán (Peru) with r.avaflow: Lessons learned for predictive mass flow simulations', *Geomorphology*.The Authors, 322, pp. 15–28. https://doi.org/10.1016/j.geomorph.2018.08.032.

Mergili, M., Jaboyedoff, M., Pullarello, J. and Pudasaini, S. P. (2020) 'Back calculation of the 2017 Piz Cengalo-Bondo landslide cascade with r.avaflow: What we can do and what we can learn', *Natural Hazards and Earth System Sciences*, 20(2), pp. 505–520. https://doi.org/10.5194/nhess-20-505-2020.

Mergili, M., Pudasaini, S. P., Emmer, A., Fischer, J. T., Cochachin, A. and Frey, H. (2020) 'Reconstruction of the 1941 GLOF process chain at Lake Palcacocha (Cordillera Blanca, Peru)', *Hydrology and Earth System Sciences*, 24(1), pp. 93–114. https://doi.org/10.5194/hess-24-93-2020.

Morgan, G. C., Rawlings, G. E. and Sobkowicz, J. C. (1992) 'Evaluating total risk to communities from large debris flows', in BiTech Publishers Ltd (ed.) *Geotechnique and Natural Hazards*.Vancouver, British Columbia Canada, pp. 225–236.

Mostyn, G. R. and Li, K. S. (1993) 'Probabilistic slope analysis - state of play', in K.S. Li and S.C.R. Lo. A.A. Balkema, Rotterdam, T. N. (ed.) *Probabilistic Methods in Geotechnical Engineering*.Canberra, Australia: Taylor and Francis, pp. 89–110.

Narama, C., Daiyrov, M., Tadono, T., Yamamoto, M., Kääb, A., Morita, R. and Ukita, J. (2017) 'Seasonal drainage of supraglacial lakes on debris-covered glaciers in the Tien Shan Mountains, Central Asia', *Geomorphology*.Elsevier B.V., 286, pp. 133–142. https://doi.org/10.1016/j.geomorph.2017.03.002.

Nesje, A. (2014) 'Reconstructing Paleo ELAs on Glaciated Landscapes', *Reference Module in Earth Systems and Environmental Sciences, Elsevier*.Elsevier. https://doi.org/https://doi.org/10.1016/B978-0-12-409548-9.09425-2.

Paul, F. and Mölg, N. (2014) 'Hasty retreat of glaciers in northern Patagonia from 1985 to 2011', *Journal of Glaciology*, 60(224), pp. 1033–1043. https://doi.org/10.3189/2014JoG14J104.

Portocarrero Rodríguez, C. A., The Mountain Institute and Engility Corporation Washington DC (2014) *Reducing risk from dangerous galcier lakes in the Coordillera Blanca, Peru. Technical report: The glacier lake handbook*.

Pudasaini, S. P. (2012) 'A general two-phase debris flow model', *Journal of Geophysical Research: Earth Surface*, 117(3), pp. 1–28. https://doi.org/10.1029/2011JF002186.

Quadros, N., Collier, P. and Fraser, C. (2008) 'Integration of bathymetric and topographic Lidar: a preliminary investigation', *The International Archives of the Photogrammetry Remote Sensing and Spatial Information Sciences Beijing 2008*, XXXVII(B8), pp. 1299–1304.

Ribstein, P., Tiriau, E., Francou, B. and Saravia, R. (1995) 'Tropical climate and glacier hydrology: a case study in Bolivia', *Journal of Hydrology*, 165(1–4), pp. 221–234. https://doi.org/10.1016/0022-1694(94)02572-S.

Schauwecker, S., Rohrer, M., Huggel, C., Endries, J., Montoya, N., Neukom, R., Perry, B., Salzmann, N., Schwarb, M. and Suarez, W. (2017) ‘The freezing level in the tropical Andes, Peru: An indicator for present and future glacier extents’, *Journal of Geophysical Research*, 122(10), pp. 5172–5189. https://doi.org/10.1002/2016JD025943.

Schneider, D., Huggel, C., Cochachin, A., Guillén, S. and García, J. (2014) ‘Mapping hazards from glacier lake outburst floods based on modelling of process cascades at Lake 513, Carhuaz, Peru’, *Advances in Geosciences*, 35(April 2010), pp. 145–155. https://doi.org/10.5194/adgeo-35-145-2014.

Singh, V. P. ., Singh, P. and Haritashya, U. K. (2011) *Encyclopedia of Snow, Ice and Galciers*.Springer.

Solomina, O., Jomelli, V., Kaser, G., Ames, A., Berger, B. and Pouyaud, B. (2007) ‘Lichenometry in the Cordillera Blanca, Peru: “Little Ice Age” moraine chronology’, *Global and Planetary Change*, 59(1–4), pp. 225–235. https://doi.org/10.1016/j.gloplacha.2006.11.016.

Somos-Valenzuela, M. A., Chisolm, R. E., Rivas, D. S., Portocarrero, C. and McKinney, D. C. (2016) ‘Modeling a glacial lake outburst flood process chain: The case of Lake Palcacocha and Huaraz, Peru’, *Hydrology and Earth System Sciences*, 20(6), pp. 2519–2543. https://doi.org/10.5194/hess-20-2519-2016.

Swiss Agency for Development and Cooperation (SDC), CARE Peru, Zurich University, Centre de recherche sur l’environnement alpin (CREALP) and École Polytechnique Fédérale de Lausanne (EPLF) (2020) *Proyecto Glaciares+*. Available at: http://www.proyectoglaciares.pe.

Thompson, L. G., Mosley-Thompson, E., Brecher, H., Davis, M., León, B., Les, D., Lin, P. N., Mashiotta, T. and Mountain, K. (2006) ‘Abrupt tropical climate change: Past and present’, *Proceedings of the National Academy of Sciences of the United States of America*, 103(28), pp. 10536–10543. https://doi.org/10.1073/pnas.0603900103.

Thompson, L. G., Mosley-Thompson, E., Davis, M. E. and Brecher, H. H. (2011) ‘Tropical glaciers, recorders and indicators of climate change, are disappearing globally’, *Annals of Glaciology*, 52(59), pp. 23–34. https://doi.org/10.3189/172756411799096231.

Trenberth, K. E. and Caron, J. M. (2000) ‘The southern oscillation revisited: Sea level pressures, surface temperatures, and precipitation’, *Journal of Climate*, 13(24), pp. 4358–4365. https://doi.org/10.1175/1520-0442(2000)013<4358:TSORSL>2.0.CO;2.

Vaidya, R. A., Shrestha, M. S., Nusrat Nasab, D. R., Gurung, N. K., Pradhan, N. S. and Wasson, R. J. (2019) ‘Disaster Risk Reduction and Building Resilience in the Hindu Kush Himalaya’, in Wester, P. A. Mishra, A. M. and A. B. S. (eds. . (ed.) *The Hindu Kush Himalaya Assessment. Mountains, Climate Change, Sustainability and People*.Springer International Publishing, pp. 389–419. https://doi.org/10.1007/978-3-319-92288-1_7.

Vuille, M., Bradley, R. S. and Keimig, F. (2000) ‘Climate variability in the Andes of Ecuador and its relation to tropical Pacific and Atlantic Sea Surface temperature anomalies’, *Journal of Climate*, 13(14), pp. 2520–2535. https://doi.org/10.1175/1520-0442(2000)013<2520:CVITAO>2.0.CO;2.

Westoby, M. J., Glasser, N. F., Brasington, J., Hambrey, M. J., Quincey, D. J. and Reynolds, J. M. (2014) ‘Modelling outburst floods from moraine-dammed glacial lakes’, *Earth-Science Reviews*.Elsevier B.V., 134, pp. 137–159. https://doi.org/10.1016/j.earscirev.2014.03.009.

Westoby, M. J., Glasser, N. F., Hambrey, M. J., Brasington, J., Reynolds, J. M. and Hassan, M. A.

A. M. (2014) ‘Reconstructing historic glacial lakeoutburst floods through numerical modelling and geomorphological assessment: Extreme events in the himalaya’, *Earth Surface Processes and Landforms*, 39(12), pp. 1675–1692. https://doi.org/10.1002/esp.3617.

Wolter, K. and Timlin, M. S. (2011) ‘El Niño/Southern Oscillation behaviour since 1871 as diagnosed in an extended multivariate ENSO index (MEI.ext)’, *International Journal of Climatology*, 31(7), pp. 1074–1087. https://doi.org/10.1002/joc.2336.

Worni, R., Huggel, C., Clague, J. J., Schaub, Y. and Stoffel, M. (2014) ‘Coupling glacial lake impact , dam breach , and flood processes : A modeling perspective Geomorphology Coupling glacial lake impact , dam breach , and fl ood processes : A modeling perspective’, *Geomorphology*.Elsevier B.V., 224(November 2017), pp. 161–176. https://doi.org/10.1016/j.geomorph.2014.06.031.

Xenarios, S., Gafurov, A., Schmidt-Vogt, D., Sehring, J., Manandhar, S., Hergarten, C., Shigaeva, J. and Foggin, M. (2019) ‘Climate change and adaptation of mountain societies in Central Asia: uncertainties, knowledge gaps, and data constraints’, *Regional Environmental Change*.Regional Environmental Change, 19(5), pp. 1339–1352. https://doi.org/10.1007/s10113-018-1384-9.

Xiong, S., Muller, J. P. and Li, G. (2017) ‘The application of ALOS/PALSAR InSAR to measure subsurface penetration depths in deserts’, *Remote Sensing*, 9(6), pp. 1–19. https://doi.org/10.3390/rs9060638.

Zemp, M. *et al.* (2015) ‘Historically unprecedented global glacier decline in the early 21st century’, *Journal of Glaciology*, 61(228), pp. 745–762. https://doi.org/10.3189/2015JoG15J017.

Zhang, G., Yao, T., Xie, H., Wang, W. and Yang, W. (2015) ‘An inventory of glacial lakes in the Third Pole region and their changes in response to global warming’, *Global and Planetary Change*.Elsevier B.V., 131, pp. 148–157. https://doi.org/10.1016/j.gloplacha.2015.05.013.

8 APPENDICES

8.1 APPENDIX 8.1: GLOBAL CIRCULATION MODELS AVAILABLE IN THE AREA OF STUDY

Appendix Table 8.1-1. List of Global circulation Models available with the corresponding vertical and horizontal resolution. Adapted from (Almazroui *et al.*, 2020)

	GCMs	Latitude	Longitude	Deg y	Deg x	Km y	Km x	Selected
01)	ACCESS-CM2_ssp245_r1i1p1f1_gn	144	192	1.25	1.88	138.94	208.41	
02)	ACCESS-ESM1-5_ssp245_r1i1p1f1_gn	145	192	1.24	1.88	137.98	208.41	
03)	CanESM5_ssp245_r1i1p1f1_gn	64	128	2.81	2.81	312.61	312.61	
04)	CNRM-CM6-1_ssp245_r1i1p1f2_gr	128	256	1.41	1.41	156.3	156.3	
05)	CNRM-ESM2-1_ssp245_r1i1p1f2_gr	128	256	1.41	1.41	156.3	156.3	
06)	**EC-Earth3_ssp245_r1i1p1f1_gr**	**256**	**512**	**0.7**	**0.7**	**78.15**	**78.15**	**Sel (1)**
07)	EC-Earth3-Veg_ssp245_r1i1p1f1_gr	256	512	0.7	0.7	78.15	78.15	
08)	GFDL-ESM4_ssp245_r1i1p1f1_gr1	180	288	1	1.25	111.15	138.94	
09)	INM-CM4-8_ssp245_r1i1p1f1_gr1	120	180	1.5	2	166.73	222.3	
10)	INM-CM5-0_ssp245_r1i1p1f1_gr1	120	180	1.5	2	166.73	222.3	
11)	IPSL-CM6A-LR_ssp245_r1i1p1f1_gr	144	143	1.25	2.52	138.94	279.82	
12)	MIROC6_ssp245_r1i1p1f1_gn	128	256	1.41	1.41	156.3	156.3	
13)	**MPI-ESM1-2-HR_ssp245_r1i1p1f1_gn**	**192**	**384**	**0.94**	**0.94**	**104.2**	**104.2**	**Sel (2)**
14)	MPI-ESM1-2-LR_ssp245_r1i1p1f1_gn	96	192	1.88	1.88	208.41	208.41	
15)	NorESM2-LM_ssp245_r1i1p1f1_gn	96	144	1.88	2.5	208.41	277.88	
16)	**MRI-ESM2-0_ssp245_r1i1p1f1_gn**	**160**	**320**	**1.13**	**1.13**	**125.04**	**125.04**	**Sel (3)**
17)	UKESM1-0-LL_ssp245_r1i1p1f2_gn	144	192	1.25	1.88	138.94	208.41	
18)	**AWI-CM-1-1-MR_ssp245_r1i1p1f1_gn**	**192**	**384**	**0.94**	**0.94**	**104.2**	**104.2**	**Sel (4)**
19)	**BCC-CSM2-MR_ssp245_r1i1p1f1_gn**	**160**	**320**	**1.13**	**1.13**	**125.04**	**125.04**	**Sel (5)**
20)	CESM2_ssp245_r4i1p1f1_gn	192	288	0.94	1.25	104.2	138.94	
21)	CESM2-WACCM_ssp245_r1i1p1f1_gn	192	288	0.94	1.25	104.2	138.94	
22)	CMCC-CM2-SR5_ssp245_r1i1p1f1_gn	192	288	0.94	1.25	104.2	138.94	
23)	**CNRM-CM6-1-HR_ssp245_r1i1p1f2_gr**	**360**	**720**	**0.5**	**0.5**	**55.58**	**55.58**	**Sel (6)**
24)	FGOALS-g3_ssp245_r1i1p1f1_gn	80	180	2.25	2	250.09	222.3	
25)	GFDL-CM4_ssp245_r1i1p1f1_gr1	180	288	1	1.25	111.15	138.94	
26)	GFDL-CM4_ssp245_r1i1p1f1_gr2	90	144	2	2.5	222.3	277.88	
27)	HadGEM3-GC31-LL_ssp245_r1i1p1f3_gn	144	192	1.25	1.88	138.94	208.41	
28)	KACE-1-0-G_ssp245_r1i1p1f1_gr	144	192	1.25	1.88	138.94	208.41	
29)	MIROC-ES2L_ssp245_r1i1p1f2_gn	64	128	2.81	2.81	312.61	312.61	
30)	NESM3_ssp245_r1i1p1f1_gn	96	192	1.88	1.88	208.41	208.41	
31)	NorESM2-MM_ssp245_r1i1p1f1_gn	192	288	0.94	1.25	104.2	138.94	

8.2 Appendix 8.2: Parameters of the simulation

The parameters, as explained by Mergili, M. and Pudasaini, S.P. in their website, that were defined for the simulation are the following:

Cell size: the same as the input data, 12.5 m.

Phases: as it is mentioned before, it is a multi-phase (P1: solid, P2: solid, P3: fluid) that can be defined with the code s,s,f. Being s=solid (plastic behaviour, frictional, non-viscous) and f=fluid (viscosity-dominated viscoplastic, non-frictional, viscous). The interactions between the three phases are being considered by the software.

Density:

- Rock 2700 kg/m^3. It is the solid material density (grain density) (Mergili *et al.*, 2017)
- Ice 1000 kg/m^3 (even though the ice density is lower, for the simulation is 1000 because the density of phase 2 must be higher than the density of the phase 3, as well as the density of phase 1 has to be higher that the density of phase 2).
- Water 1000 kg/m^3

Friction: Internal friction and base friction angle associated to each phase

- Internal friction angle of P1: the internal friction can not be lower than the basal friction, 35 degrees.
- Basal friction angle of P1: 20 degrees
- Internal friction angle of P2: This value has to be set zo zero for purely viscous material. The internal friction can not be lower than the basal friction. 15 degrees
- Basal friction angle of P2: This value has to be set zo zero for purely viscous material. 12 degrees
- Internal friction angle of P3: This value is neglected for fluid material. 0 degrees
- Basal friction angle of P3: This value is neglected for fluid material. 0 degrees

Viscosity: viscosities of the three phases

- Kinematic viscosity of P1: The logarithm with base 10 of the viscosity. Very low values have to be used for purely frictional materials. This parameter is neglected for solid material. -9999 m^2/s
- Yield strength of P1: The yield strength of the material. This parameter is neglected for solid material. If -9999 is provided for fine solid, the yield strength is computed automatically. -9999 Pa
- Kinematic viscosity of P2: The logarithm with base 10 of the viscosity. Very low values have to be used for purely frictional materials. Ice viscosity: -12 m^2/s
- Yield strength of P2: The yield strength of the material. If -9999 is provided, the yield strength is computed automatically. -9999 Pa
- Kinematic viscosity of P3: The logarithm with base 10 of the viscosity. -3 m^2/s
- Yield strength of P3: The yield strength of the material. 0 Pa

Ambient: Parameters governing the interaction of the flow with the atmosphere and the basal surface

- Ambient drag coefficient: Coefficient to be multiplied with the frontal surface and the velocity of the flow to derive air resistance. 0.01

- Fluid friction coefficient: Manning's N is used as the fluid friction coefficient, to consider the effects of roughness of the basal surface. Only applies to fluid phases. 0.075
- Entrainment coefficient: Coefficient multiplied with the total kinetic energy of the flow (entrainment=1 in the parameter control) or the total flow momentum (entrainment=2) to derive the entrainment rate of basal material. The logarithm with base 10 of the entrainment coefficient has to be entered, except for 0 which means no entrainment. -7.0
- Stopping criterion: If the values 4 or 5 are provided for stopping (parameter control), the threshold of the total flow kinetic energy (stopping=4) or the total flow momentum (stopping=5) has to be provided. In both cases, this threshold has to be expressed as fraction of the maximum value reached during the flow (i.e. 0.05 would mean 5 per cent of the maximum). If stopping has been deactivated or set to 1, a value of 0 should be entered. 0.0

Controls: Control parameters

- Conversion between depths and heights: Conversion of release heights (measured in vertical direction) into release depths (measured perpendicular to the local topography), and reconversion of computed flow, entrainment and deposition depths to heights for output. 1
  - 0 = no conversion of flow heights to flow depths;
  - 1 = basic conversion of flow heights to flow depths (multiplication with the cosine of the slope);
  - 2 = advanced conversion of flow heights to flow depths (considering the pixel neighbourhoods, not available for the multi-phase model).
- Diffusion control: If activated, the flow only propagates from a source pixel to a target pixel if the flow has propagated far enough within source pixel to allow reaching the target pixel with the given velocity. This function helps to avoid excessive diffusion imposed by the numerical scheme. However, it is still experimental and, in most cases, not recommended to be used. Particularly for highly viscous flows, it might produce unexpected results. 1 for avoiding the numerical disappearance of the lake
  - 0 = no diffusion control;
  - 1 = diffusion control
- Surface control and non-hydrostatic model: This function is important for the interaction between landslides and reservoirs, i.e. the formation and propagation of impact waves. Careful balancing of the forces is important to reduce numerical oscillations on the water surface and along shorelines, but can have negative effects on simulations in other circumstances (e.g. for highly viscous flows). Further, the consideration of non-hydrostatic effects leads to a more realistic representation of such effects. 0
  - 0 = non-hydrostatic effects are neglected, and no surface control is applied (recommended for all simulations without landslide-reservoir interactions);
  - 1 = non-hydrostatic effects are neglected, but surface control is applied;
  - 2 = non-hydrostatic effects are considered, and surface control is applied.
- Entrainment: If activated, the flow is allowed to entrain material from its basal surface. 0
  - 0 = no entrainment;
  - 1 = entrainment coefficient multiplied with flow kinetic energy;
  - 2 = entrainment coefficient multiplied with flow momentum.

- Stopping: If activated, a criterion is defined which decides at each time step whether the flow continues or stops and deposits. 0
    - 0 = no stopping;
    - 1 = the flow stops as soon as the shear resistance (computed by a Mohr-Coulomb criterion) exceeds the sum of the static and dynamic shear forces. The dynamic shear force for each pixel is the force needed to bring the mass to rest. It is approximated through the momentum divided by the travel time between two pixels. The simulation is terminated once the entire flow has stopped and the flow depth at the time of stopping is added to the depth of deposition. Stopping only applies to decelerating flows;
    - 4 = the flow stops if the flow kinetic energy is lower than the threshold value given in the ambient parameters;
    - 5 = the flow stops if the flow momentum is lower than the threshold value given in the ambient parameters.
    - 7 = the flow stops when there is no raster cell at which the dynamic flow pressure is larger than the threshold value for flow pressure given in the thresholds parameter.

Thresholds: threshold parameters

- Minimum flow height for display: Flow heights below this value will not be displayed in the map layouts. The value specified has no influence on the simulation itself. 0.5 m
- Minimum flow kinetic energy for display: Flow kinetic energies below this value will not be displayed in the map layouts. The value specified has no influence on the simulation itself. 10000 J
- Minimum flow pressure for display: Flow pressures below this value will not be displayed in the map layouts. The value specified has no influence on the simulation itself. 10000 Pa
- Minimum flow height for simulation: Only flow heights above this value will be considered in the simulation. Equal or lower values are set to 0 in order not to compromise numerical stability. 0.01 m

Time: Time interval for output and end time. Two comma-separated numbers. The first number indicates the real-time interval in seconds at which output information is displayed. The second number indicates the real time in seconds after which the simulations stops. 30, 2400

8.3 APPENDIX 8.3: SIMULATION SCENARIO 1

For lake´s volume scenario 1 with a volume of 9243368 m^3, compared to scenario 2 with a volume of 13488862 m^3, the simulation performed does not reach the city of Carhuaz, it stops just a few kilometers after overtopping the dam. This shows the importance of adequate maintaining measures of the current infrastructure for flood prevention that need to be clean and remove the rocks present.

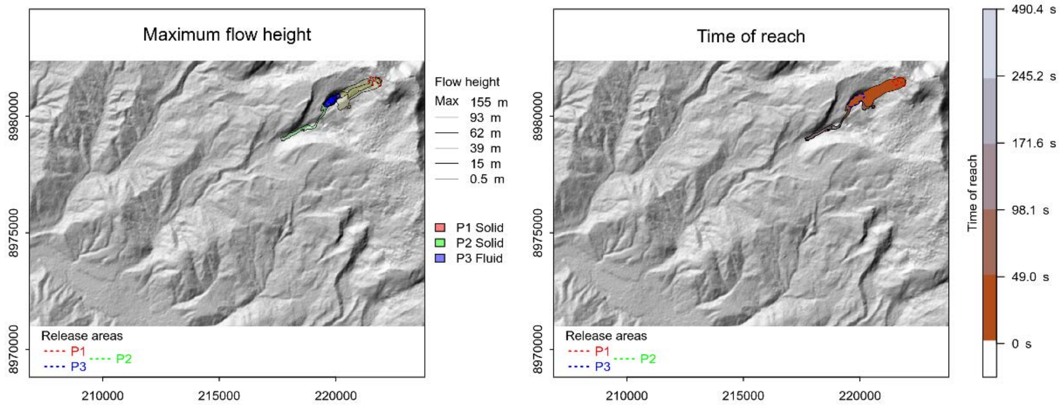

Appendix Figure 8.3-1. Maps of maximum flow height and time of reach in the r.avaflow® simulation for scenario 1

8.4 Appendix 8.4: Summary of the simulation values

Appendix Table 8.4-1. Values of the simulation including: $Time_{sum}$: time passed since start of the flow (s); $Depth_{max}$: maximum flow depth at time step (m); $Veloc_{max}$: maximum flow velocity at time step (m/s); Volume: flow volume at time step (cubic metres in the summary file; 1000s of cubic metres on the screen output in Figure 39 and Figure 40); Ekin: kinetic energy summed up over the entire flow (J in the summary file; MJ on the screen output Figure 39 and Figure 40). Numbers at the end of the headers indicate the phase the column refers to (1: rock, 2: ice and 3: water). First row is showing the initial conditions of the simulation.

$Time_{sum}$	$Depth1_{max}$	$Veloc1_{max}$	$Depth2_{max}$	$Veloc2_{max}$	$Depth3_{max}$	$Veloc3_{max}$	Volume1	Volume2	Volume3	Ekin
-----	*18.0	-----	*18.0	-----	*101.0	-----	*652230	*652230	*13014438	-----
0	17	0	17	0	101	0	652230	652230	13014438	-----
30.1	9	71.35	9.4	71.64	84.9	26.99	678121	678898	10284109	3.24333E+12
60	24.1	65.11	21.1	64.49	103.4	34.69	857231	867510	7877071	1.13655E+12
90.1	19.8	14.68	14.4	60.36	85.4	51.1	730209	808369	6261620	3.84808E+11
120.1	13.2	12.44	9.3	47.23	63.1	35.8	603877	742059	4854904	1.69025E+11
150.2	11.1	11.18	8.1	27.3	56.9	36.98	531372	724141	4266227	1.64729E+11
180	9.4	9.83	7.2	25.58	52.9	25.51	476269	692525	3819279	1.06319E+11
210.1	8.3	8.87	6.4	24.12	49.2	23.63	428409	660733	3408540	57901153873
240.2	7.5	9.77	6.7	20.59	46.1	21.18	387234	626617	3060571	39318787713
270.1	6.7	9.3	6.9	16.97	43.3	17.61	350819	592244	2760459	26385932933
300	6.1	10.24	7.2	19.48	40.7	19.63	318816	557719	2502617	22111785861
330.1	5.6	9.42	7.5	17.17	38.3	21.17	290514	522745	2278161	23022883366
360.1	5.1	8.11	7.4	24.13	36.1	20.23	265245	493510	2083914	30529151253
390.1	4.8	9.21	7	30.37	34.1	22.71	242924	467946	1915041	38448894291
420.2	4.4	8.83	6.7	30.98	32.1	24.18	222632	447325	1764274	52018672106
450.1	4.1	10.3	6.9	34.89	30	35.02	203300	436177	1637481	85367124698
480.1	3.8	8.95	7.1	36.89	28	26.18	184950	430882	1519392	73438376715
510.2	3.6	8.45	5	31.48	26.1	24.45	168434	413304	1410915	81332621448
540.1	3.3	9.3	4.5	30.11	24.3	23.65	153831	400750	1312667	85981444871

570.1	3.2	8.14	5	30.19	22.6	20.41	140822	389240	1225678	63048264092
600.2	3	8.98	3.9	27.78	21.1	21.75	129154	376160	1150093	66607862421
630.2	2.9	9.34	3.8	30.64	19.6	22.45	118744	364286	1079467	67474511468
660.1	2.7	6.43	3.8	27.02	18.7	18.49	110750	355129	1028479	48502823828
690.2	2.6	7.04	4.5	23.83	17.8	16.61	103879	346135	985182	40116893386
720.1	2.5	7.33	4.4	26.05	17	17.11	97735	342368	945352	43496844585
750.2	2.4	5.87	4.9	22.43	16.2	17.41	91933	338426	908800	32659196839
780.3	2.3	5.91	6.8	22.63	15.5	18.51	86692	333877	878429	26622947176
810	2.2	6.02	6.8	21.45	14.8	18.24	81905	327255	848924	18661957925
840.2	2.2	6.63	5.6	18.78	14.1	17.82	77263	319730	822487	30654571381
870.1	2.1	5.86	4	22.16	13.6	19.5	73097	314077	797019	38010702145
900.2	2	6.73	4.1	23.26	13	18.07	69139	308845	772157	38089719354
930.3	1.9	4.47	4	26.27	12.5	14.89	65432	304347	746960	32664454999
960.3	1.8	4.87	4.6	22.72	12	13.42	61991	301002	723483	19456185343
990	1.7	5.08	4	23.45	11.4	12.54	58683	297578	700674	17666054989
1020.2	1.6	5.23	3.7	20.17	10.9	12.11	55443	292219	677880	13250228022
1050.3	1.6	5.53	3.6	14.32	10.4	12.33	52338	287079	654696	12361851440
1080	1.5	5.87	3.5	13.26	9.9	11.68	49449	282063	631994	11687699839
1110.3	1.4	4.39	3.5	19.4	9.7	11.38	46951	277566	612965	11017035469
1140.2	1.3	4.5	3.4	19.83	9.4	10.95	44731	273197	596772	11831132088
1170.1	1.3	4.88	3.4	22.01	9.1	10.6	42610	269130	580958	12910327505
1200.3	1.2	3.55	3.4	21.71	8.8	10.4	40599	265084	565312	10093994626
1230.1	1.2	3.93	3.3	17.35	8.6	10.1	38866	261752	552592	6721832951
1260.2	1.1	4.12	3.2	9.12	8.4	9.92	37202	259429	540615	5134646688

1290.2	1.1	2.68	3.3	9.05	8.2	9.66	35660	256906	529303	4773329906
1320.3	1	2.86	3.3	8.21	7.9	9.45	34187	254252	517787	4282077502
1350.3	1	2.64	3	7.75	7.7	9.21	32724	251945	506341	3928591716
1380.3	0.9	2.79	3.1	8.01	7.5	8.89	31284	249717	495337	3720007465
1410.3	0.9	2.9	3.3	7.72	7.2	8.61	29885	247436	484144	3494138465
1440.3	0.8	3.38	3.1	9.92	6.8	8.3	28299	244185	469478	3574012256
1470.3	0.8	2.76	2.6	13.9	6.6	8.46	26732	240682	454779	3561300186
1500.3	0.8	2.73	2.6	7.5	6.3	8.51	25249	237155	440103	3119945124
1530	0.7	2.13	2.4	7.36	6.1	8.84	23855	233408	425991	2893748940
1560.2	0.7	2.14	2.4	6.53	5.9	8.5	22456	229479	412230	2743895975
1590.1	0.7	2.25	2.3	7.61	5.6	8.67	21122	225787	399020	2726631131
1620.1	0.6	1.51	2.3	7.05	5.4	8.74	19829	221985	386268	2863897630
1650.1	0.6	1.69	2.2	18.45	5.2	9.58	18537	218173	374040	3273118397
1680.2	0.6	1.49	2.2	14.02	5.1	8.99	17469	214227	363722	2866748327
1710.3	0.6	0.47	2.2	7.33	5	8.94	16444	204307	353701	2478171768
1740.2	0.5	0.49	2.2	7.3	5	8.38	15453	197806	343339	2088655278
1770.3	0.5	0.39	2.3	7.82	5.3	8.15	14649	193092	334591	1702283585
1800.4	0.5	0.32	2.4	8.6	5.5	8.09	13899	189978	327557	1531571590
1830.4	0.5	0.22	2.5	7.42	5.7	7.68	13187	187952	321247	1387915027
1860.4	0.5	0	2.5	6.02	5.6	7.55	12449	185833	314904	1268819037
1890.2	0.5	0	2.4	6.21	5.6	7.49	11746	183508	308764	1183174865
1920.1	0.4	0	2.3	8.39	5.5	7.43	11014	180719	302315	1298675554
1950.1	0.4	0	2.2	7.49	5.3	8.34	10310	178168	295992	1369307811
1980.3	0.4	0	2.1	5.57	5.1	8.26	9659	176249	290554	1253998674

2010.1	0.4	0	2.1	5.63	4.9	7.75	9035	174369	285549	1139876570
2040.3	0.4	0	2	5.74	4.7	7.84	8467	172462	280587	1069526007
2070	0.4	0	2	5.66	4.9	7.95	7991	170513	275682	1022454706
2100.3	0.4	0	2	5.48	5.3	7.74	7560	168424	270778	965621954
2130.1	0.3	0	2	5.47	5.7	7.87	7123	166238	265957	927729663
2160.2	0.3	0	2	5.55	6	7.88	6664	163952	261166	891845722
2190	0.3	0	2	5.61	6.2	7.85	6288	161694	256402	868652049
2220.3	0.3	0	2	5.67	6.4	7.87	5993	159416	251576	838116948
2250.3	0.3	0	2.2	5.74	6.4	7.89	5703	156910	246638	800746649
2280.2	0.3	0	2.2	5.81	6.5	7.9	5434	154474	241701	769447864
2310.3	0.3	0	2.2	5.14	6.6	7.5	5180	152008	236835	722679787
2340.3	0.2	0	2.2	5.34	6.4	7.66	4905	149138	231466	782186589
2370.3	0.2	0	2.2	5.4	6.5	7.6	4635	146060	225689	746666577
2400.2	0.2	0	2.2	4.9	6.5	7.67	4376	143025	219997	726071741